Microfabrication and microstructuring of hydrogel materials

Mytnyk, Serhii

DOI
10.4233/uuid:e62593a6-5118-4eb7-a638-d4091e6ce6eb

Publication date
2019

Document Version
Final published version

Citation (APA)
Mytnyk, S. (2019). *Microfabrication and microstructuring of hydrogel materials*. [Dissertation (TU Delft), Delft University of Technology]. https://doi.org/10.4233/uuid:e62593a6-5118-4eb7-a638-d4091e6ce6eb

Important note
To cite this publication, please use the final published version (if applicable).
Please check the document version above.

Microfabrication and microstructuring of hydrogel materials

Serhii Mytnyk

Microfabrication and microstructuring of hydrogel materials

Dissertation

for the purpose of obtaining the degree of doctor
at Delft University of Technology
by the authority of the Rector Magnificus prof. dr. ir. T. H. J. J. van der Hagen
chair of the Board of Doctorates
to be defended publicly on

Tuesday, 22nd of January 2019 at 12:30 o'clock

by

Serhii MYTNYK

Master of Science in Chemistry,
Taras Shevchenko National University of Kyiv, Ukraine
born in Cherkasy, Ukraine

This dissertation has been approved by the

Promotor:	Prof. dr. J.H. van Esch
Second promotor:	Dr. habil. E. Mendes

Composition of the doctoral committee:

Rector Magnificus	Delft University of Technology	chairman
Prof. dr. J.H. van Esch.	Delft University of Technology	promotor
Dr. habil. E. Mendes	Delft University of Technology	promotor

Independent members

Prof. dr. rer. nat. C. Stubenrauch	University of Stuttgart, Germany
Prof. dr. E.J.R. Sudhölter	Delft University of Technology
Prof. dr. S.J. Picken	Delft University of Technology
Dr.ir. M. Ottens	Delft University of Technology

The work described in this thesis was carried out in the Advanced Soft Matter group at Delft University of Technology. This research was funded by EC 7th Framework Programme Marie Curie Actions *via* the European ITN SMARTNET No. 316656

ISBN: 978-94-6323-484-9

Cover design: Serhii Mytnyk

Printed by: Gildeprint - Enschede

Table of contents

To my loving wife Kateryna
I am infinetely grateful for your support and endless patience

Chapter 1

Introduction

If it looks like a gel it must be a gel.
D.J. Lloyd, 1926

Hydrogels

Hydrogels are omnipresent in our everyday life, most commonly as various foods (jelly, mayonnaise), personal care products (hair gels, diapers) and medical treatments (contact lenses, wound dressings). Hydrogels are solid-like, easily deformable soft materials that can contain up to 99% water but do not spontaneously flow. They owe these properties to their internal structure formed by a three-dimensional cross-linked network of polymeric chains and/or colloidal aggregates entrapping a high volume fraction of water.[1] Lately, due to the similarity of their mechanical properties to human tissues, hydrogels started playing an important role in advanced biomedical research, most often forming a basis of many medical treatments and diagnostic tools. For example, hydrogels serve as scaffolds that provide structural support for artificially grown tissues and organoids in regenerative medicine and personalized drug discovery research. Furthermore, hydrogel micro- and nano-particles are widely employed for sustained, targeted or environmentally sensitive (triggered) release of loaded drug molecules.[2]

Hydrogels are broadly divided into chemically and physically cross-linked (**Figure 1**).[2,3] The hydrogels of the first group, also known as "permanent", are formed through covalent chemical bonds between entangled polymeric chains (e.g. poly(acrylamide)), thus locking them in place and leading to a permanently cross-linked network. Such structure gives these hydrogels higher mechanical strength but makes them susceptible to rupture under stress. Some of their applications include coatings, soft robotics and as drug delivery vehicles. On the other hand, physically cross-linked, or "reversible", hydrogels form through weaker, non-covalent forces, such as electrostatic complexation, hydrophobic interactions or hydrogen bonding.[3] Most common examples of physical hydrogels are agar, gelatin, alginate and starch-based hydrogels. Physical hydrogels span a broad range of mechanical strengths, and due to the reversible nature of physical cross-linking, can display a variety of useful properties, such as being self-healing and injectable. These features find use in hydrogel coatings and lubricants, as well as in the design of so-called smart materials, imbuing them with responsiveness and adaptiveness. Some of these hydrogels are applied in a form of wound dressings, cell-culturing matrices and triggered drug release formulations.

A special group of physically cross-linked hydrogels are low-molecular weight hydrogels (LMWHs), formed through self-assembly of small molecules into supramolecular fibrils, which then form an entangled 3D-network (**Figure 1c**).[4] Whereas the properties of polymeric hydrogels are mostly defined by the length of the polymer used for their formation, interactions in self-assembled LMWHs can be tuned to a larger extent, thus making them more flexible choice for various applications. Even though first examples of such gels have been discovered a long time ago, recently, LMWHs started attracting attention as a tool for mimicking natural molecular self-assembly processes, such as lipids assembly, in design of novel responsive materials.

Most biomedical applications of hydrogels strongly rely on the structure, texture and morphology of a given hydrogel material at various length scales. For instance, shape of a hydrogel actuator can define the extent and type of its deformation upon exposure to a stimulus.[1] At the same time, adjusting the microstructure of a hydrogel, such as porosity, can be used to alter mechanical response of the material and its permeability to various solutes. Finally, controlling the gel composition and arrangement on the molecular level allows to adjust its interaction with, among other things, biological objects, such as proteins and cells.

However, even though much has been done to understand and control these separate

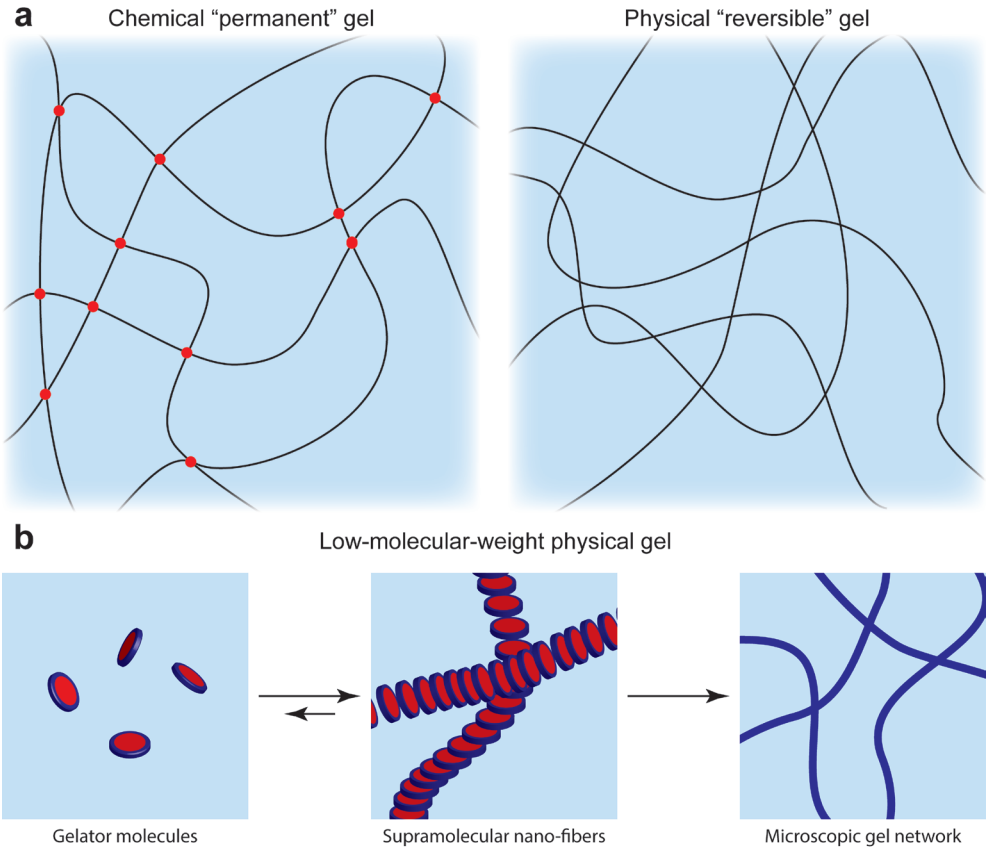

Figure 1. (**a**) Schematic illustration of network structure of chemical and physical hydrogels. While chemical cross-links (red circles) are permanent and act as knots in a fishing net, physical cross-links are generally weak and reversible, thus allowing such bonds to continuously break and reform. (**b**) Low-molecular-weight hydrogels (LMWH) form *via* self-assembly of small gelator molecules into fibrillary structures, followed by their entanglement into a physically cross-linked gel network.

aspects of hydrogel architecture, the challenge of bridging molecular, mesoscopic and macroscopic length scales using current technology remains to be addressed. Therefore, there is a need in development of novel approaches for controlling hydrogel structuring and formulation at multiple levels in order to modulate performance of such materials.

In general, hydrogel fabrication and structuring techniques can be broadly divided into macro- and microscopic. The first group focuses on formation of objects and features on the scale of hundreds of micrometers and above, whereas microscopic methods operate on the scale of tens of micrometers and below. Additionally, fabrication and structuring techniques are classified as "top-down" or "bottom-up", depending on the strategy they employ to manufacture the desired structures. Top-down approaches rely on direct modification of the material on the micro- and macro-scale using sophisticated equipment. Bottom-up approaches, on the other hand, aim to construct complex micro-structures from nano- and microscopic building blocks by manipulating their interactions. In order to better explain advantages and limits of most common hydrogel fabrication and structuring strategies, remainder of this chapter aims to provide the reader with an overview of current state of

microfabrication techniques, followed by a review of emerging micro-structuring approaches.

Microfabrication of hydrogels

Many potential applications of hydrogels can greatly benefit from the ability to produce them in variable shapes and with controlled macroscopic architectures. To meet this growing demand a whole range of top-down microfabrication techniques have been developed. Most commonly, they involve one or a combination of such approaches as photo-lithography, micromolding, 3D-printing and microfluidics (**Figure 2**).

Photo-lithography is a well-established and accessible method that is based on photo-activated conversion of a pre-gel solution into a gel of desired shape and size through controlling the pattern of illumination with a physical or digital photo-mask. Both approaches have been successfully used for producing two- and three-dimensional cell-laden hydrogel environments either by using multi-layer conventional photolithography[5] or digital stereo-lithography[6]. For example, Malachowski *et al.* used photo-lithography to create complex thermo-responsive hydrogel grippers for localized drug delivery, thereby enabling an impressive new direction in soft robotics.[7] Another advanced type of photo-lithography, called direct laser-writing, allows direct mask-less 2D- and 3D-fabrication using either conventional or multi-photon laser illumination, and has been shown to perform with a superior accuracy for constructing highly sophisticated 3D-structures within pre-formed hydrogels.[8,9] Main advantages of the first two approaches are their speed and flexibility while offering moderate resolution, though they typically require layer-by-layer production for the construction of 3D-architectures. At the same time multi-photon laser writing offers greater precision and structural complexity at the expense of long fabrication times, making the technique unsuitable for production of structures covering large areas. However, while optimized multi-photon fabrication approach

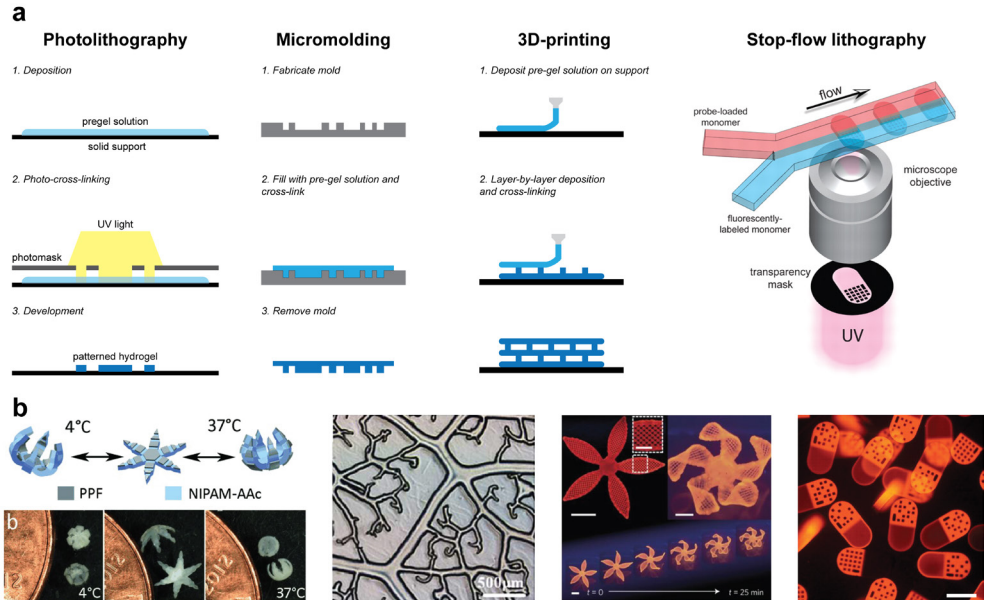

Figure 2. (**a**) Schematic representation of the steps involved in microfabrication of hydrogel objects using photo-lithography, micromolding, 3D-printing and microfluidic stop-flow lithography approaches; (**b**) examples hydrogel objects fabricated using above-mentioned techniques. Scalebars left to right: 500 µm, 5 mm, 100 µm. Images adapted from references 7, 11, 16, 24.

in non-aqueous media has been able to reach submicron spatial resolution, fabrication of hydrogel objects remains significantly less accurate (generally ~10 μm) due to the use of typically lower monomer and initiator concentrations, resulting in broader produced features caused by the diffusion of the components during cross-linking. In addition, surface tension of water leads to softening of the sharp edges of soft elastic hydrogels, leading to further decrease in attainable accuracy of fabricated features.[10]

Micromolding is a technique that uses a fabricated template to direct the formation of a hydrogel structure by acting as a mold during the gelation. Typically, it involves fabricating a suitable negative template, or mold, followed by casting and curing of a pre-gel solution and eventual separation of the mold and produced structure. While being very flexible, fast and easy-to-use, micromolding is generally limited to only two-dimensional patterning of hydrogels, with only thickness of the produced gel being controlled in z-dimension. For instance, He *et al.* have employed this approach to replicate natural venation network of a mulberry leaf in agarose hydrogel and used this vascularized material to guide the growth of endothelial cells.[11]

In the last two decades 3D-printing concepts have also been extended to fabrication of hydrogel objects. Due the primary focus of hydrogel 3D-printing on creating tissue-like constructs from cell-containing pre-gel solutions it is often referred to as bioprinting. Many successful examples of applying 3D-printing to formation of biologically relevant hydrogel materials have been reported recently.[13–15] Overall, based on the technology bioprinting can be classified into inkjet, micro-extrusion and laser-assisted bioprinting (LAB).[12] Inkjet-based printing relies on the controlled supply of picoliter droplets of pre-gel solution through a nozzle to generate patterns that are then cross-linked using light or temperature, thus forming a hydrogel object. Inkjet-based printers are the most accessible and popular since they offer ~50 μm resolution and high fabrication speed. Micro-extrusion is generally performed using solid-like source material, often a thermo-responsive gel, to generate desired architectures at higher resolution but at lower speed. Laser-assisted bioprinting (LAB), on the other hand, is a nozzle-free printing technique based on laser-induced transfer of soft biological materials from a thin transparent support film onto the substrate, approach also known as laser-induced forward transfer (LIFT). LAB offers good microscale resolution while maintaining medium production speed, however its limited flexibility and high cost are currently limiting the technique. Additionally, Gladman *et al.* have reported an impressive example of shape-morphing hydrogel objects in which they programmed the structure during 3D-printing and induced the shape-change by gels swelling in water.[16]

Microfluidics represents one of the youngest, but at the same time most rapidly developing among hydrogel microfabrication techniques. It is based on manipulation of flows of minute amounts of liquids inside micro-channels to produce micro-particles. Droplet microfluidics allows producing femtoliter droplets with an unmatched degree of precision by engineering the channel geometries and exploiting the interfacial phenomena arising between immiscible fluids. This emulsion-based approach have been extensively explored for production of spherical micro-hydrogels from a variety of gelling materials ranging from synthetic and natural polymers to colloids and self-assembling small molecules.[17–20] Alternatively, stop-flow lithography combines microfluidics with photo-lithography, thus significantly expanding the selection of attainable hydrogel shapes with micrometer dimensions – polygons, disks and even barcoded particles.[21–24]

Despite the variety of existing microfabrication techniques applicable for hydrogel

production, most of them are only able to reach resolutions of the order of 10-100 um. Furthermore, while microfabrication techniques rapidly advance, resolution and complexity of microfabricated hydrogels are inherently limited by interplay of capillary forces and elastic properties of such materials.[10,25] One potential way to mitigate some of these limitations is to complement the above-mentioned microfabrication techniques with advanced nano- and micro-structuring approaches, many of which belong to bottom-up strategies.

Microstructuring of hydrogels

Micro-structure of hydrogel materials seriously influences their properties and thus affects their performance in specific applications. By adjusting the average density of the network, for example, one can tune the microscopic mechanical properties of a hydrogel. Additionally, control of the porosity or introduction of distinct micro-domains are often needed to adjust local mechanical and diffusive properties of a given material. Finally, filling hydrogel network with aligned nano-structures (nanoparticles, clay sheets, polymer chains) has been shown to imbue hydrogel materials with anisotropic properties leading to specific shape changes in response to external stimuli, such as swelling-induced strain, temperature or light.[1] Therefore, the interest in the ability to control the micro-structure of hydrogel materials by design has significantly grown.

In their attempts to control the microstructure of hydrogel materials, researchers have reached practical limits of direct hydrogel modification with traditional top-down approaches. These limitations have been partially overcome by an elegant combination of top-down microfabrication methods and microscale interfacial phenomena (**Figure 3**). Most commonly, such approaches for hydrogel microstructuring are based on dispersion of one or multiple immiscible phases within a pre-gel solution, followed by gelation to capture the resulting structure. This leads to the formation of composite hydrogels with various micro-domains ranging from micro-droplets and solid particles to even gas bubbles.[26–29] If necessary, subsequent removal of such dispersed phases after gelation (e.g. salt leaching) can

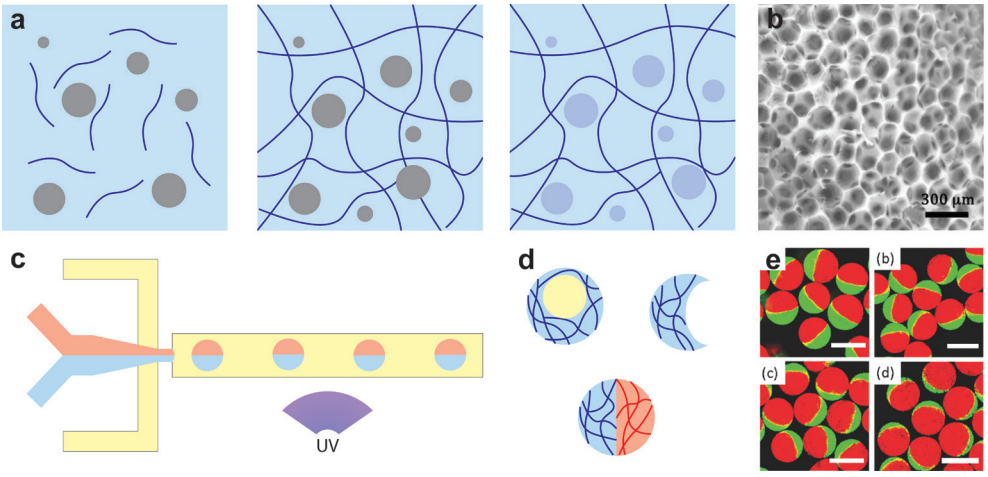

Figure 3. (**a**) Schematic illustration of controlling hydrogel micro-structure via (left to right) dispersion of porogens in a pre-gel solution, followed by gelation and porogen removal to afford micro-porous hydrogel. (**b**) Scanning electron micrograph displaying the structure of a hydrogel produced using gas foaming. Scale bar 300 µm. (**c-d**) Schematic illustration of microfluidic production of structured hydrogel particles resulting in core-shell, crescent-shaped and Janus particles depending on fabrication conditions. (**e**) Fluorescent micrographs of various Janus microhydrogels produced with microfluidics. Scale bars 100 µm. Images (**b**) and (**e**) adapted from references 32 and 36.

be employed to create controlled micro- and macro-porous hydrogels with pore sizes in the range of 10-200 μm.[30–32] Alternatively, microfluidic generation of multiple emulsion droplets have been used to engineer composite hydrogel micro-particles with core-shell and Janus-type architectures.[33–36] Above-mentioned methods are well-studied and offer decent degree of control over material structure, however they mostly fail to achieve the level of complexity of hydrogel matrices occurring in living organisms. Furthermore, it is often impossible to apply such strategies to bulk material structuring.

Nature-inspired bottom-up approaches aim to address the drawbacks of top-down strategies by exploiting the assembly of molecular, nano- and/or micro-scopic building units in solution into complex 3D architectures (**Figure 4**). While this field is only beginning to be explored, several directions of bottom-up structuring exist. For instance, molecular self-assembly field focuses on engineering low-molecular hydrogelators to direct their interactions and growth into nano-sized fibrillary structures, which further form an entangled network of microscopic bundles, eventually leading to bulk hydrogel formation.[37–39] Additionally, final hydrogel micro-architecture and bulk gel properties could be manipulated by adjusting the gelator's structure, changing the strength of molecular interactions or even by controlling the speed of gelation.[40,41] Assembly of pre-fabricated nano- and micro-hydrogels has also been used to produce micro-structured hydrogel composites for tissue engineering.[42,43] Furthermore, hydrogel structuring by introduction of various membrane-enclosed compartments has been recently reported. This approach mimics cellular organization and involves dispersing nano-scopic vesicles formed through self-assembly of lipids, surfactants or block-copolymers and containing various aqueous media isolated within such membranes from the bulk of the hydrogel. This concept has been applied to design hydrogels with triggered drug release properties and programmed hydrogel degradation.[44,45] Very recently, Yang *et al.* demonstrated an interesting approach to compartmentalization of supramolecular hydrogel using virus-like particles incorporated into the gel network *via* host-guest interactions, which they exploited to control the release of the drug encapsulated within the particles.[46]

However, so far, programming macroscale structure of the constructs using only bottom-up approaches remains unattainable, and the use of hybrid strategies – combination of top-down and bottom-up approaches – is one of the most promising future directions. So far only several examples of such hybrid strategies have been reported. For instance, Ziemecka *et al.* have controlled the orientation of self-assembled dibenzoyl-L-cystine fibers by inducing

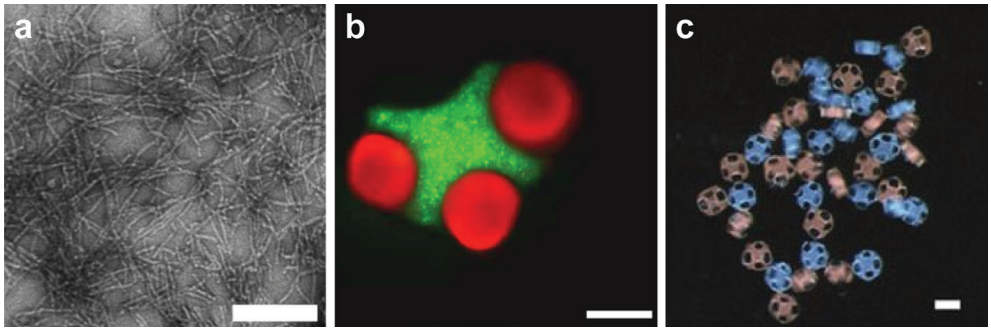

Figure 4. Hydrogel materials produced *via* bottom-up approaches across different length scales. (**a**) Electron microscopy micrograph of a hydrogel formed through small peptide self-assembly. Scale bar 250 nm. (**b**) Shape-driven assembly of polymeric micro-hydrogels. Scale bar 200 μm. (**c**) DNA-directed assembly of engineered hydrogel particles into a macroscopic network. Scale bar 1 mm. Images adapted from references 38, 43 and 42.

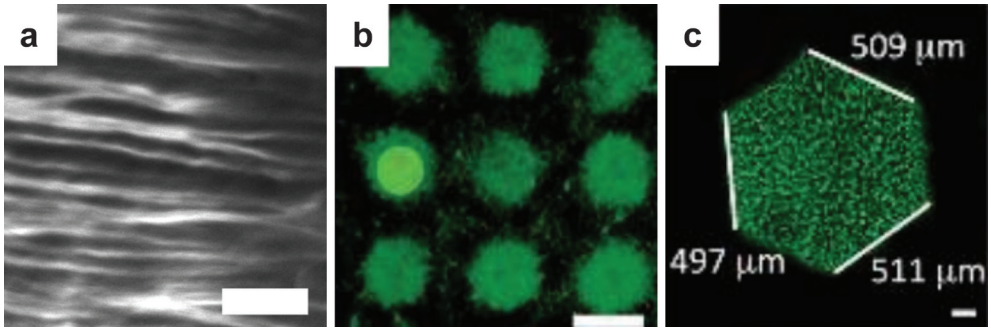

Figure 5. Fluorescence micrographs of low molecular weight hydrogel structures produced by combining molecular self-assembly with top-down fabrication techniques. (**a**) Self-assembled peptide hydrogel with fibrils aligned in an external magnetic field. Scale bar 200 μm. (**b**) LMWH objects formed via surface catalysis of a micro-patterned acidic catalyst. Scale bar 20 μm. (**c**) LMWH object produced by photo-induced self-assembly. Scale bar 100 μm. Images adapted from references 48, 49, 50.

macroscale spatial pH-gradient within the pre-gel solution.[47] Similarly, Wallace *et al.* have used an external magnetic field to align self-assemble peptide fibrils with their subsequent cross-linking with a gradient of Ca^{2+} ions (**Figure 5a**).[48] Furthermore, Olive *et al.* directed the formation and self-assembly of a low molecular weight hydrogelator by patterning the acidic catalyst on the glass surface using micro-contact printing technique (**Figure 5b**).[49] Maity *et al.* induced hydrogel assembly using photoacid generation by irradiating a solution containing gel precursors through a photomask, thus producing microscale objects formed by a supramolecular hydrogel (**Figure 5c**).[50] Unfortunately, while combining the best of the worlds of top-down microfabrication and bottom-up structuring has great potential for advancing applied hydrogel research, this field is incredibly broad and awaiting further exploration.

Outline of the thesis

This overview of hydrogel fabrication and structuring approaches summarizes general trends in the field, and shows that the current state of technology does not fully satisfy the increasing requirements for many, especially biomedical, applications. Moreover, the variety of hydrogel applications makes further development of fabrication and structuring techniques particularly challenging. Since traditional top-down approaches have nearly reached their practical limits, employing bottom-up self-assembly strategies may extend the degree of control over hydrogel micro-architectures. However, due to a limited amount of knowledge available in this field, there are very few reported examples of combining top-down and bottom-up strategies for hydrogel design. Therefore, a promising next step in this area of research could lie in complementing top-down microfabrication techniques with bottom-up microstructuring methods to engineer advanced functional hydrogel materials.

The aim of this doctoral dissertation is to investigate novel approaches to structuring and fabrication of polymeric and supramolecular hydrogels by employing modern microfabrication techniques and/or spontaneous structuring resulting from molecular incompatibility between certain hydrophilic polymers. The *second chapter* of this thesis describes a method for continuous production of hydrogel capsules with a hydrogel shell and a liquid core using all-aqueous double emulsion generated in a microfluidic device, thus potentially enabling future encapsulation of sensitive biomolecules and cells in mild, fully aqueous environment. In the *third chapter*, we present the first report of employing all-aqueous multiphase emulsions for micro-compartmentalizing a supramolecular hydrogel. This novel combination of molecular

self-assembly and microscopic phase separation of hydrophilic polymers opens a way to fabrication of previously unattainable architectures with the potential application in the area of tissue engineering. *Chapter 4* discusses a method exploiting selective dextran hydrogel photopatterning with confocal laser-scanning fluorescence microscope for single-cell isolation and release. Accessibility and flexibility of such image-assisted cell isolation approach may make it a valuable tool in cell analysis and disease diagnostics. In *chapter 5*, we present and detail a technique for microfluidic production of micron-sized polymeric hydrogel particles via controlled microfluidic dehydration of aqueous droplets. The developed approach allows concentrating aqueous solutes into sub-10-micrometer particles using easily attainable microfluidic devices, with a potential of extending the scope of the method to production of highly monodisperse sub-micron-sized microhydrogels. And finally, the dissertation is concluded with a summary of the obtained results.

References

(1) Sano, K.; Ishida, Y.; Aida, T. Synthesis of Anisotropic Hydrogels and Their Applications. *Angew. Chemie Int. Ed.* **2018**, *57* (10), 2532–2543.

(2) H. Gulrez, S. K.; Al-Assaf, S. Hydrogels: Methods of Preparation, Characterisation and Applications. In *Progress in Molecular and Environmental Bioengineering - From Analysis and Modeling to Technology Applications*; InTech, 2011.

(3) Caló, E.; Khutoryanskiy, V. V. Biomedical Applications of Hydrogels: A Review of Patents and Commercial Products. *Eur. Polym. J.* **2015**, *65*, 252–267.

(4) Kopeček, J.; Yang, J. Smart Self-Assembled Hybrid Hydrogel Biomaterials. *Angew. Chemie Int. Ed.* **2012**, *51* (30), 7396–7417.

(5) Gurkan, U. A.; Fan, Y.; Xu, F.; Erkmen, B.; Urkac, E. S.; Parlakgul, G.; Bernstein, J.; Xing, W.; Boyden, E. S.; Demirci, U. Simple Precision Creation of Digitally Specified, Spatially Heterogeneous, Engineered Tissue Architectures. *Adv. Mater.* **2013**, *25* (8), 1192–1198.

(6) Soman, P.; Chung, P. H.; Zhang, A. P.; Chen, S. Digital Microfabrication of User-Defined 3D Microstructures in Cell-Laden Hydrogels. *Biotechnol. Bioeng.* **2013**, *110* (11), 3038–3047.

(7) Malachowski, K.; Breger, J.; Kwag, H. R.; Wang, M. O.; Fisher, J. P.; Selaru, F. M.; Gracias, D. H. Stimuli-Responsive Theragrippers for Chemomechanical Controlled Release. *Angew. Chem. Int. Ed. Engl.* **2014**, *53* (31), 8045–8049.

(8) Ciuciu, A. I.; Cywiński, P. J. Two-Photon Polymerization of Hydrogels – Versatile Solutions to Fabricate Well-Defined 3D Structures. *RSC Adv.* **2014**, *4* (85), 45504–45516.

(9) Torgersen, J.; Qin, X.-H.; Li, Z.; Ovsianikov, A.; Liska, R.; Stampfl, J. Hydrogels for Two-Photon Polymerization: A Toolbox for Mimicking the Extracellular Matrix. *Adv. Funct. Mater.* **2013**, *23* (36), 4542–4554.

(10) Paretkar, D.; Xu, X.; Hui, C.-Y.; Jagota, A. Flattening of a Patterned Compliant Solid by Surface Stress. *Soft Matter* **2014**, *10* (23), 4084–4090.

(11) He, J.; Mao, M.; Liu, Y.; Shao, J.; Jin, Z.; Li, D. Fabrication of Nature-Inspired Microfluidic Network for Perfusable Tissue Constructs. *Adv. Healthc. Mater.* **2013**, *2* (8), 1108–1113.

(12) Murphy, S. V; Atala, A. 3D Bioprinting of Tissues and Organs. *Nat. Biotechnol.* **2014**, *32* (8), 773–785.

(13) Xu, T.; Zhao, W.; Zhu, J.-M.; Albanna, M. Z.; Yoo, J. J.; Atala, A. Complex Heterogeneous Tissue Constructs Containing Multiple Cell Types Prepared by Inkjet Printing Technology. *Biomaterials* **2013**, *34* (1), 130–139.

(14) Koch, L.; Deiwick, A.; Schlie, S.; Michael, S.; Gruene, M.; Coger, V.; Zychlinski, D.; Schambach, A.; Reimers, K.; Vogt, P. M.; et al. Skin Tissue Generation by Laser Cell Printing. *Biotechnol. Bioeng.* **2012**, *109* (7), 1855–1863.

(15) Cui, X.; Breitenkamp, K.; Finn, M. G.; Lotz, M.; D'Lima, D. D. Direct Human Cartilage Repair Using Three-Dimensional Bioprinting Technology. *Tissue Eng. Part A* **2012**, *18* (11–12), 1304–1312.

(16) Sydney Gladman, A.; Matsumoto, E. A.; Nuzzo, R. G.; Mahadevan, L.; Lewis, J. A. Biomimetic 4D Printing. *Nat. Mater.* **2016**, *15* (4), 413–418.

(17) Kim, T.; Park, S.; Lee, M.; Baek, S.; Lee, J. B.; Park, N. DNA Hydrogel Microspheres and Their Potential Applications for Protein Delivery and Live Cell Monitoring. *Biomicrofluidics* **2016**, *10* (3), 34112.

(18) Baah, D.; Floyd-Smith, T. Microfluidics for Particle Synthesis from Photocrosslinkable Materials. *Microfluid. Nanofluidics* **2014**, *17* (3), 431–455.

(19) Wang, W.; Zhang, M.-J.; Chu, L.-Y. Functional Polymeric Microparticles Engineered from Controllable Microfluidic Emulsions. *Acc. Chem. Res.* **2014**, *47* (2), 373–384.

(20) Shah, R. K.; Kim, J.-W.; Weitz, D. A. Monodisperse Stimuli-Responsive Colloidosomes by Self-Assembly of Microgels in Droplets. *Langmuir* **2010**, *26* (3), 1561–1565.

(21) Yang, S.; Guo, F.; Kiraly, B.; Mao, X.; Lu, M.; Leong, K. W.; Huang, T. J. Microfluidic Synthesis of Multifunctional Janus Particles for Biomedical Applications. *Lab Chip* **2012**, *12* (12), 2097.

(22) Hwang, D. K.; Oakey, J.; Toner, M.; Arthur, J. A.; Anseth, K. S.; Lee, S.; Zeiger, A.; Van Vliet, K. J.; Doyle, P. S. Stop-Flow Lithography for the Production of Shape-Evolving Degradable Microgel Particles. *J. Am. Chem. Soc.* **2009**, *131* (12), 4499–4504.

(23) Lee, H.; Kim, J.; Kim, H.; Kim, J.; Kwon, S. Colour-Barcoded Magnetic Microparticles for Multiplexed Bioassays. *Nat. Mater.* **2010**, *9* (9), 745–749.

(24) Pregibon, D. C.; Toner, M.; Doyle, P. S. Multifunctional Encoded Particles for High-Throughput Biomolecule Analysis. *Science* **2007**, *315* (5817), 1393–1396.

(25) Mora, S.; Pomeau, Y. Softening of Edges of Solids by Surface Tension. *J. Phys. Condens. Matter* **2015**, *27* (19), 194112.

(26) Mallick, S.; Sagiri, S. S.; Behera, B.; Pal, K.; Ray, S. S. Gelatin-Based Emulsion Hydrogels as a Matrix for Controlled Delivery System. *Mater. Manuf. Process.* **2012**, *27* (11), 1221–1228.

(27) Lin, T.; Zhao, X.; Zhang, Y.; Lian, H.; Zhuang, J.; Zhang, Q.; Chen, W.; Wang, W.; Liu, G.; Guo, S.; et al. Floating Hydrogel with Self-Generating Micro-Bubbles for Intravesical Instillation. *Materials (Basel).* **2016**, *9* (12).

(28) Appel, E. A.; Tibbitt, M. W.; Webber, M. J.; Mattix, B. A.; Veiseh, O.; Langer, R. Self-Assembled Hydrogels Utilizing Polymer–nanoparticle Interactions. *Nat. Commun.* **2015**, *6* (1), 6295.

(29) Wang, Q.; Mynar, J. L.; Yoshida, M.; Lee, E.; Lee, M.; Okuro, K.; Kinbara, K.; Aida, T. High-Water-Content Mouldable Hydrogels by Mixing Clay and a Dendritic Molecular Binder. *Nature* **2010**, *463* (7279), 339–343.

(30) Bodenberger, N.; Kubiczek, D.; Abrosimova, I.; Scharm, A.; Kipper, F.; Walther, P.; Rosenau, F. Evaluation of Methods for Pore Generation and Their Influence on Physio-Chemical Properties of a Protein Based Hydrogel. *Biotechnol. Reports* **2016**, *12*, 6–12.

(31) Hwangbo, K.-H.; Kim, M. R.; Lee, C.-S.; Cho, K. Y. Facile Fabrication of Uniform Golf-Ball-Shaped Microparticles from Various Polymers. *Soft Matter* **2011**, *7* (22), 10874.

(32) Costantini, M.; Colosi, C.; Jaroszewicz, J.; Tosato, A.; Święszkowski, W.; Dentini, M.; Garstecki, P.; Barbetta, A. Microfluidic Foaming: A Powerful Tool for Tailoring the Morphological and Permeability Properties of *Sponge-like* Biopolymeric Scaffolds. *ACS Appl. Mater. Interfaces* **2015**, *7* (42), 23660–23671.

(33) Choi, A.; Seo, K. D.; Kim, D. W.; Kim, B. C.; Kim, D. S.; Kwon, S.; Lee, C.-S.; Im, S. G.; Gu, Z.; Bratlie, K. M.; et al. Recent Advances in Engineering Microparticles and Their Nascent Utilization in Biomedical Delivery and Diagnostic Applications. *Lab Chip* **2017**, *17* (4), 591–613.

(34) Jeong, J.; Um, E.; Park, J.-K.; Kim, M. W.; Du, J.; O'Reilly, R. K.; Yang, S. M.; Guo, F.; Kiraly, B.; Mao, X.; et al. One-Step Preparation of Magnetic Janus Particles Using Controlled Phase Separation of Polymer Blends and Nanoparticles. *RSC Adv.* **2013**, *3* (29), 11801.

(35) Seiffert, S. Microgel Capsules Tailored by Droplet-Based Microfluidics. *Chemphyschem* **2013**, *14* (2), 295–304.

(36) Zhang, L.; Chen, K.; Zhang, H.; Pang, B.; Choi, C.-H.; Mao, A. S.; Liao, H.; Utech, S.; Mooney, D. J.; Wang, H.; et al. Microfluidic Templated Multicompartment Microgels for 3D Encapsulation and Pairing of Single Cells. *Small* **2018**, *14* (9), 1702955.

(37) Du, X.; Zhou, J.; Shi, J.; Xu, B. Supramolecular Hydrogelators and Hydrogels: From Soft Matter to Molecular Biomaterials. *Chem. Rev.* **2015**, *115* (24), 13165–13307.

(38) Jiang, L.; Xu, D.; Sellati, T. J.; Dong, H.; Yang, C.; Mariner, P. D.; Nahreini, J. N.; Anseth, K. S.; Tokuda, E. Y.; Leight, J. L.; et al. Self-Assembly of Cationic Multidomain Peptide Hydrogels: Supramolecular Nanostructure and Rheological Properties Dictate Antimicrobial Activity. *Nanoscale* **2015**, *7* (45), 19160–19169.

(39) Yang, Z.; Ho, P. L.; Liang, G.; Chow, K. H.; Wang, Q.; Cao, Y.; Guo, Z.; Xu, B. Using β-Lactamase to Trigger Supramolecular Hydrogelation. *J. Am. Chem. Soc.* **2007**, *129* (2), 266–267.

(40) Poolman, J. M.; Maity, C.; Boekhoven, J.; van der Mee, L.; le Sage, V. A. A.; Groenewold, G. J. M.; van Kasteren, S. I.; Versluis, F.; van Esch, J. H.; Eelkema, R.; et al. A Toolbox for Controlling the Properties and Functionalisation of Hydrazone-Based Supramolecular Hydrogels. *J. Mater. Chem. B*

2016, *4* (5), 852–858.

(41) Cardoso, A. Z.; Alvarez Alvarez, A. E.; Cattoz, B. N.; Griffiths, P. C.; King, S. M.; Frith, W. J.; Adams, D. J. The Influence of the Kinetics of Self-Assembly on the Properties of Dipeptide Hydrogels. *Faraday Discuss.* **2013**, *166* (0), 101.

(42) Qi, H.; Ghodousi, M.; Du, Y.; Grun, C.; Bae, H.; Yin, P.; Khademhosseini, A. DNA-Directed Self-Assembly of Shape-Controlled Hydrogels. *Nat. Commun.* **2013**, *4* (1), 2275.

(43) Du, Y.; Lo, E.; Ali, S.; Khademhosseini, A. Directed Assembly of Cell-Laden Microgels for Fabrication of 3D Tissue Constructs. *Proc. Natl. Acad. Sci. U. S. A.* **2008**, *105* (28), 9522–9527.

(44) Boekhoven, J.; van Rijn, P.; Brizard, A. M.; Stuart, M. C. A.; van Esch, J. H. Size Control and Compartmentalization in Self-Assembled Nano-Structures of a Multisegment Amphiphile. *Chem. Commun.* **2010**, *46* (20), 3490.

(45) Boekhoven, J.; Brizard, A. M.; Stuart, M. C. A.; Florusse, L.; Raffy, G.; Del Guerzo, A.; van Esch, J. H. Bio-Inspired Supramolecular Materials by Orthogonal Self-Assembly of Hydrogelators and Phospholipids. *Chem. Sci.* **2016**, *7* (9), 6021–6031.

(46) Yang, L.; Liu, A.; de Ruiter, M. V; Hommersom, C. A.; Katsonis, N.; Jonkheijm, P.; Cornelissen, J. J. L. M. Compartmentalized Supramolecular Hydrogels Based on Viral Nanocages towards Sophisticated Cargo Administration. *Nanoscale* **2018**, *10* (8), 4123–4129.

(47) Ziemecka, I.; Koper, G. J. M.; Olive, A. G. L.; van Esch, J. H. Chemical-Gradient Directed Self-Assembly of Hydrogel Fibers. *Soft Matter* **2013**, *9* (5), 1556–1561.

(48) Wallace, M.; Cardoso, A. Z.; Frith, W. J.; Iggo, J. A.; Adams, D. J. Magnetically Aligned Supramolecular Hydrogels. *Chem. - A Eur. J.* **2014**, *20* (50), 16484–16487.

(49) Olive, A. G. L.; Abdullah, N. H.; Ziemecka, I.; Mendes, E.; Eelkema, R.; Van Esch, J. H. Spatial and Directional Control over Self-Assembly Using Catalytic Micropatterned Surfaces. *Angew. Chemie - Int. Ed.* **2014**, *53* (16), 4132–4136.

(50) Maity, C.; Hendriksen, W. E.; Van Esch, J. H.; Eelkema, R. Spatial Structuring of a Supramolecular Hydrogel by Using a Visible-Light Triggered Catalyst. *Angew. Chemie - Int. Ed.* **2015**, *54* (3), 998–1001.

Chapter 2

Microcapsules with a permeable hydrogel shell and an aqueous core continuously produced in a 3D microdevice by all-aqueous microfluidics*

Abstract

We report the continuous production of microcapsules composed of an aqueous core and permeable hydrogel shell, rendered stable by controlled photo-cross-linking of the shell of an all-aqueous double emulsion. While most previous work on water-based emulsions focused on active droplet formation, here double emulsion droplets were spontaneously generated at a three-dimensional flow-focusing junction through the break-up of a double jet formed by immiscible aqueous solutions of polyethylene glycol and cross-linkable dextrans. The capsules obtained with this lipid-free, organic-solvent-free, and surfactant-free approach displayed excellent stability in a variety of harsh conditions ($3 < pH < 13$, high salinity). Drying and rehydration experiments demonstrate the permeability of the shell, which may enable molecular-weight-dependent release and uptake of polar solutes.

*This chapter has been published as S. Mytnyk *et al.*, *RSC Adv.* **2017**, *7*, 11331–11337.

Introduction

Microcapsules with an aqueous core and dispersed in an aqueous environment are omnipresent in nature, cells being perhaps the most well-known example. Aqueous microcapsules find use as vehicles for the delivery of pharmaceuticals and nutrients[1], storage and protection of incompatible components[2], as well as for catalyst control and recovery[3]. A common way to make aqueous microcapsules is to mimic nature by separating the aqueous inner and outer parts of the capsule using a lipid bilayer.[4–8] Another strategy, which omits the use of lipids, is to employ water-in-oil-in-water double emulsion droplets as templates, and cross-link the shell.[9–12] A major limitation of such capsules, however, is the decreased permeability of the shell to most polar solutes, including many biomolecules. Alternatively, a shell can be formed around an aqueous droplet dispersed in an immiscible aqueous environment based on an interfacial reaction, for example, that of alginate with Ca^{2+}, which often relies on the use of surfactants to be efficient in an all-aqueous environment.[13,14] Although these strategies enable the control of the release properties by tuning the properties of the shell, the use of an organic phase or interface stabilizers may degrade the material to be encapsulated in the core of the capsule. To overcome the aforementioned limitations, we developed a lipid-free, organic-solvent-free, and surfactant-free approach to produce all-aqueous microcapsules with a cross-linked permeable hydrogel shell.

Our approach is based on the use of aqueous two phase systems (ATPS), which constitute a bio-friendly class of fluids especially relevant for the partitioning and separation of polar constituents, biomolecules, and even living cells.[15–17] Particularly popular is the well-known and thoroughly characterized ATPS that forms upon mixing aqueous solutions of dextran (DEX) and polyethylene glycol (PEG). At sufficiently high polymer concentrations, phase separation occurs, resulting in two immiscible phases: a phase rich in one polymer exists in equilibrium with a phase low in that same polymer.[15–17] Recently, we and others explored the use of ATPS for the continuous generation of single and double emulsion microdroplets in a microfluidic device.[14,18–28] However, the lack of methods to stabilize the shell of all-aqueous double emulsion microdroplets under continuous flow, until now, precluded the ATPS approach from being applied for the production of microcapsules with an aqueous core and permeable hydrogel shell.

Here, we introduce and detail permeable microcapsules produced from all-aqueous double emulsion droplets, which are stabilized through thiol-yne-based photo-cross-linking of the shell. The capsules are stable under a wide range of conditions, presenting a novel alternative to currently existing bioencapsulation techniques, potentially allowing to better preserve the activity of loaded (bio)objects. Additionally, the permeability of the shell may enable the application of the capsules as micro-reactors with size-dependent uptake/release capabilities.

Results and discussion

The general concept for the continuous production of hydrogel microcapsules is illustrated in Fig. 1a: we focus a stream of an aqueous polyethylene glycol (PEG) solution by a stream of an aqueous dextran (DEX) solution at the junction on the left, and the resulting thread breaks up into droplets when focused by another stream of PEG at the second junction. Introducing both polymers at sufficiently high concentration leads to phase separation while the droplets flow through the channel, thus, forming an all-aqueous double emulsion. The resulting core-shell structure is then stabilized by on-chip photo-cross-linking of the dextran shell using the thiol-yne click-reaction (**Figure 1b**). Details on the synthesis and characterization of these

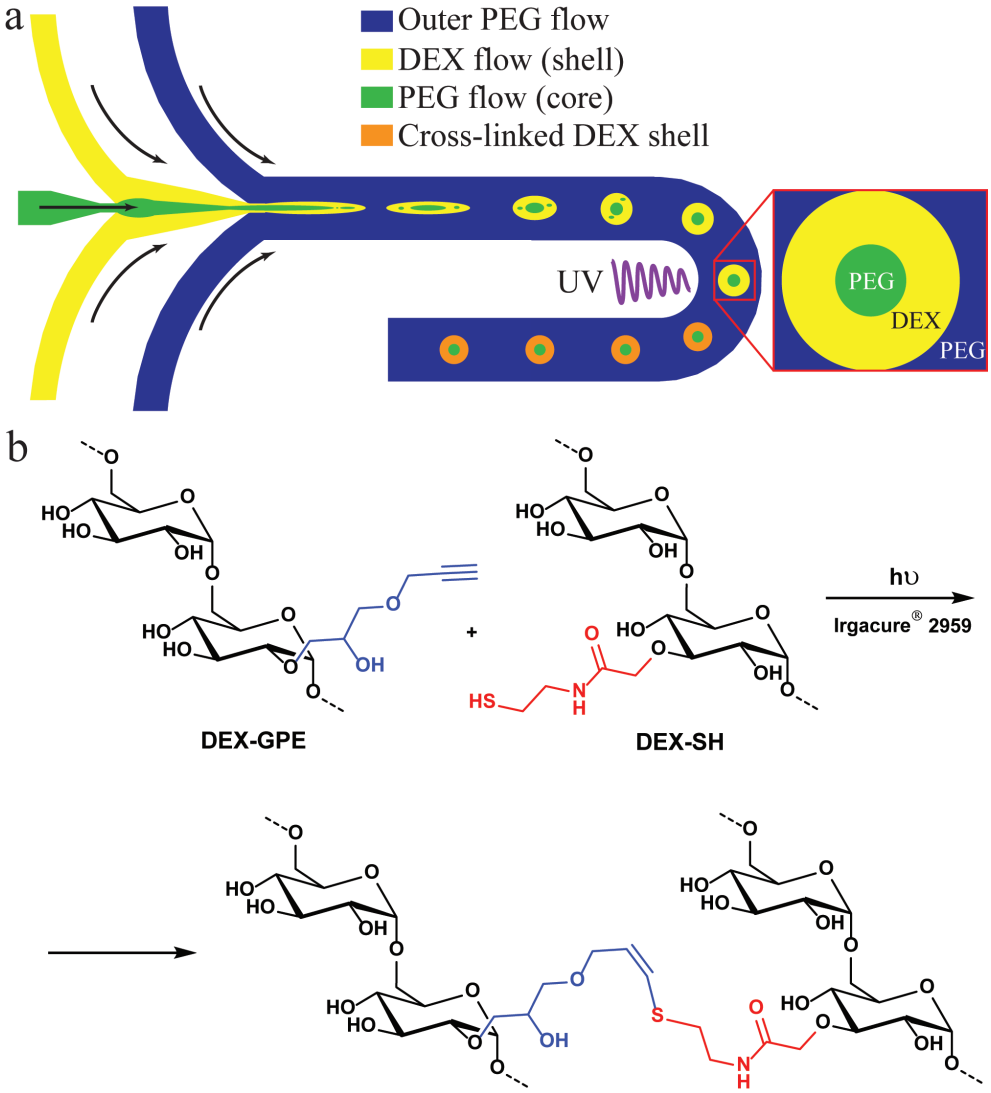

Figure 1. (**a**) Microfluidic production of particles with a permeable shell and a liquid core from aqueous solutions of PEG and DEX-SH & DEX-GPE; (**b**) Thiol-yne photo-cross-linking of the dextran phase.

polymers are provided in the Appendix (Fig.S1-S4).

The design of the three-dimensional (3D) PDMS device is shown in **Figure 2a-b**. The channels have a rectangular cross-section and are 300 μm deep, except for the two 40 μm deep and 80 μm wide nozzles illustrated in the close up. These nozzles are vertically centered with respect to the surrounding channels using the method described by Rotem *et al.*[29] The main channel after the flow focusing section is 550 μm wide.

Droplet generation

We introduced a 10% w/w PEG solution as the core-forming phase at the first flow-focusing junction at a flow rate of 0.1 μl/min into the shell-forming DEX-phase (solution

containing 5% w/w of both cross-linkable dextrans) flowing at 0.3 µl/min. The resulting PEG-in-DEX thread, shown in **Figure 2c-d**, spontaneously broke up into droplets downstream from the second flow-focusing junction, where a second solution of PEG (40% w/w) was introduced at 3.5 µl/min, see **Figure 2**. The mean velocity of all phases combined, downstream of the second junction, was 0.4 mm/s and the mean velocity of the droplets was 1.0 mm/s.

In sharp contrast to the highly stable ATPS threads reported previously,[19] we observed the spontaneous breakup of a PEG-in-DEX thread into droplets near the nozzle, presenting one of the first examples of non-forced formation of an all-aqueous double emulsion using microfluidics[30,31]. The spontaneous breakup is explained by the use of a 3D-device that reduces the stabilizing influence of the top and bottom walls on jet breakup.[32] Additionally, the concentration of PEG in the outer phase was chosen to be significantly higher than in previous work[19] to prevent the clogging of the channels (see below), with the added benefit of a larger interfacial tension facilitating droplet generation.[33] Hence, there was no need to mechanically force the formation of droplets as done previously,[14,18–21,26,27] which, besides requiring a simpler device, has the advantage that the encapsulated phases are not rigorously mixed upon encapsulation, resulting in a relatively fast phase separation.

Analysis of the core-shell droplets at the exposure location (**Figure 2e**) showed that they had a core diameter of 22 ± 6 µm and a total diameter of 82 ± 22 µm (Fig. S5). Operation of the microfluidic device in a jetting regime due to the low interfacial tension results in simultaneous growth of multiple jet instabilities, explaining the relatively broad droplet size distribution. As previously shown for double emulsion droplets,[26] the core diameter and shell thickness can be controlled by the relative flow rates of the core and the shell phases. Varying this ratio in the range between 0.33 and 3.0, the ratio of shell to core diameter varied from

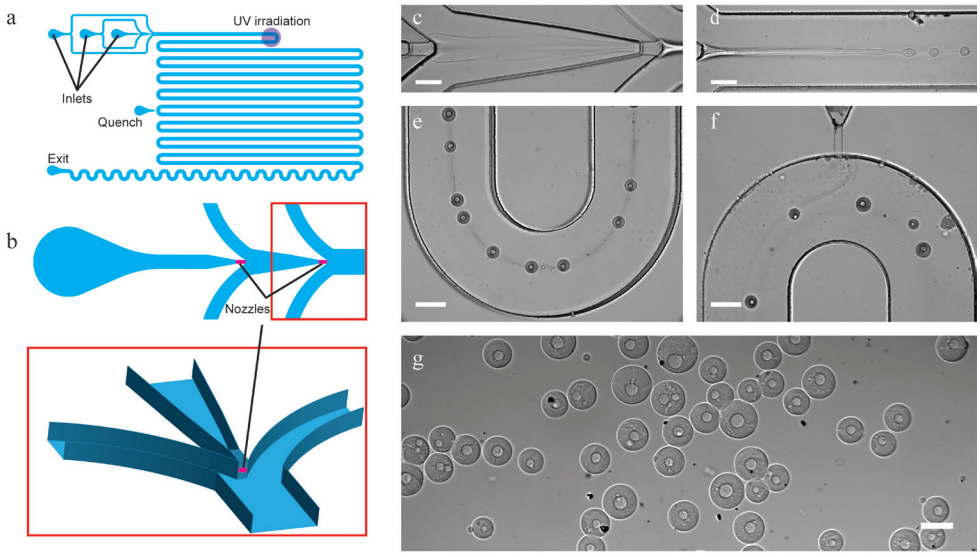

Figure 2. Scheme of microfluidic device used for producing capsules with a permeable shell and a liquid core (**a**) (unused inlets not depicted for clarity, detailed scheme can be found in Appendix), and a zoom-in on the 3D structure of its injection nozzles (**b**). In short, aqueous solutions of PEG and DEX-SH & DEX-GPE were injected at two consecutive flow-focusing junctions (**b, c**), resulting jet-in-jet spontaneously broke up into core-shell droplets (**d**), and their shells were then cross-linked by exposure to UV-light (**e**). Radicals were quenched further downstream (**f**), and stable core-shell particles were collected (**g**). (scale bars 200 µm) The trail observed between the droplets in (**e**) is caused by redistribution of water and phase-forming polymers leading to local differences in composition and hence refractive index of the carrying phase. These trails slowly disappear due to diffusion (**f**).

3.6 to 2.2, while the total droplet diameter decreased from 84 μm to 60 μm (Fig. S6-S8). Since a constant total droplet diameter was expected for a fixed outer PEG flow rate and a fixed combined flow rate of the inner PEG and DEX phases, the observed decrease in diameter suggests a partial escape of the core phase during droplet formation and its subsequent phase separation into a core-shell structure.

Finally, by increasing the flow rate of the outer phase up to 10.5 μl/min, the total droplet diameter could be reduced to 44 ± 16 μm, but the residence time in the UV beam was then too short to cross-link the droplets and form stable particles. We anticipate that the polydispersity reported here can be reduced by (mild) mechanical actuation of the forming droplets.[14,18–21,26,27]

Photo-cross-linking of the shells of the droplets

The core-shell droplets, obtained after phase separation, were stabilized by polymerizing the DEX shell using UV-light focused through the microscope objective lens. In order to maximize the exposure duration, droplets were irradiated in one of the channel bends (18 mm downstream from the nozzle, or approx. 15 s after the break-up), where they remained the longest in the field of irradiation (**Figure 2e**). On average droplets remained in the irradiated area for about 5 s. To prevent agglomeration of still reactive particles through cross-linking of their surfaces with one another downstream from the irradiation point, we introduced a third solution of PEG (40% w/w) containing a radical quenching agent (5% w/w sodium ascorbate) at 2.0 μl/min. The flow rate and PEG concentration (viscosity) were chosen to be sufficiently high to ensure proper contact between the injected stream and the particles as shown in **Figure 2f**. Quenched particles consisting of a liquid PEG core and a hydrogel DEX shell were then collected off-chip in a magnetically-stirred vial filled with demineralized water (**Figure 2g**). Before characterizing the particles, we had to address two challenges involved in stabilizing the microdroplets by photo-cross-linking in an all-aqueous environment. Initial cross-linking experiments were unsuccessful either due to incomplete polymerization of the particles or rapid clogging of the devices upon irradiation.

The issue on incomplete polymerization was caused by a generic feature of aqueous multi-phase systems, *i.e.* the largely nonspecific partitioning of especially low molecular weight components over *all* phases, compared to the much more specific partitioning in oil/water emulsions. Consequently, the photoinitiator can partition out of the cross-linkable phase. The resulting concentration of the photoinitiator in the cross-linkable dextran phase then can become insufficient for cross-linking of the dextran shell upon UV exposure. Initial polymerization tests, with the photoinitiator added solely to the DEX phase, indeed failed to produce stable particles, as noted from their immediate dissolution after exposure to pure water. Further tests, with the photoinitiator added in equal concentrations to all solutions to maintain a sufficient amount of the photoinitiator in the DEX phase, confirmed that the problem of insufficient cross-linking was resolved as demonstrated by the production of stable capsules.

The issue of clogging turned out to be more complicated. Although a full study on clogging mechanisms is beyond the scope of the present work, one mechanism observed in initial experiments is that still reactive particles sediment and stick to the bottom wall either immediately in the irradiation area, or several millimeters downstream, resulting in the rapid accumulation of partially cured particles and blocking of the main channel. This challenge was overcome by increasing the viscosity of the outer phase by increasing the outer phase PEG concentration from 15% to 40% w/w. This slowed down the sedimentation of the droplets, precluding them from contacting the bottom of the channel before their exposure to

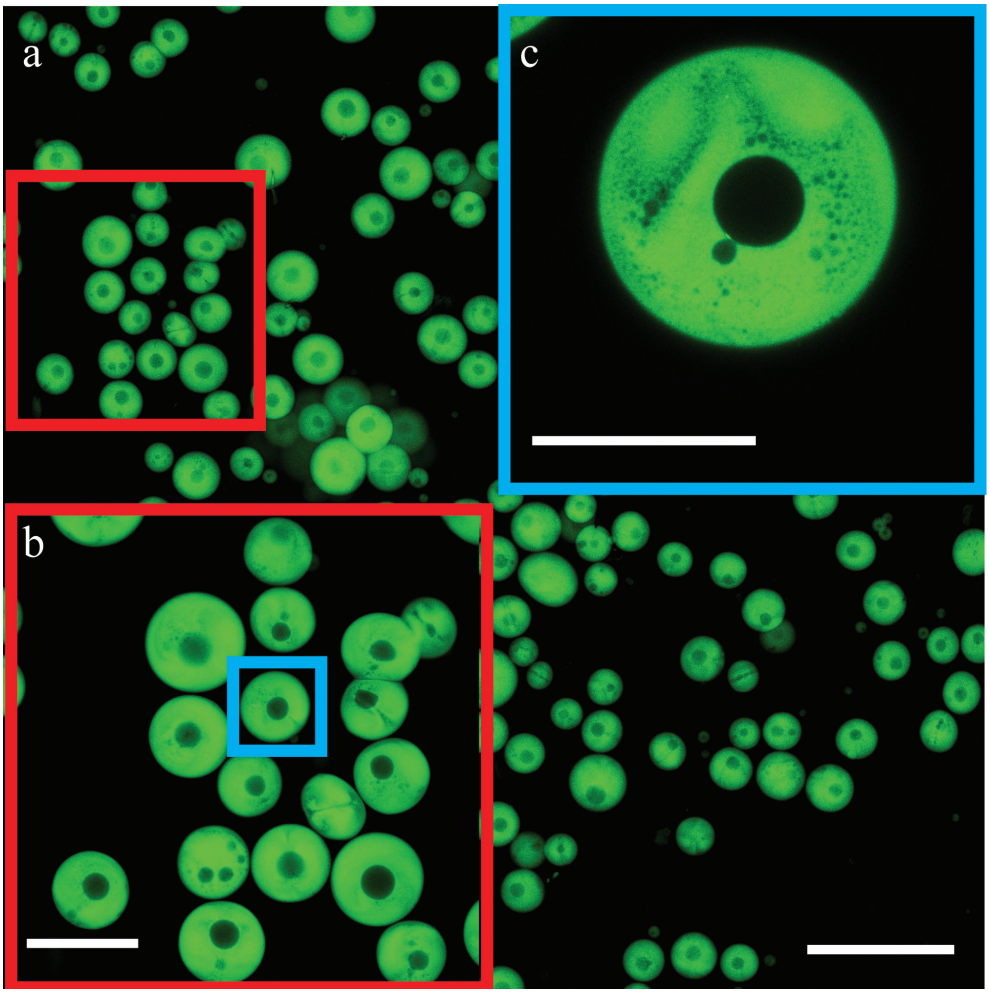

Figure 3. Confocal microscopy images of the collected core-shell particles. Scale bars: a) 400 μm b) 200 μm c) 100μm.

UV-light. Initial experiments in which we varied the concentration of PEG in the outer phase indeed showed that the distance needed for droplets to sediment to the bottom of the channel, increased with increasing PEG concentration. For a PEG concentration of 40%, we observed no droplets near the bottom wall over the length of the device. This observation agrees with the prediction that the sedimentation distance (estimated as $uH/2u_{\infty}$, with u the droplet velocity, H the height of the channel, and u_{∞} the terminal fall velocity) exceeds the length of the microchannel. We note that the increase in PEG concentration had an additional effect: it also reduced the amount of cross-linkable dextrans that partitioned in the outer phase, which further reduced the chance of clogging through the polymerization of the outer PEG flow.

The issues of incomplete cross-linking and clogging make stabilization of particles in an all-aqueous environment significantly more difficult compared to the stabilization of oil/water (double) emulsions. Above-mentioned considerations have allowed us to select polymer and photoinitiator concentrations that do allow complete cross-linking of the shell without clogging. Finally, we note that the time necessary for droplet formation, core-shell

phase separation, UV exposure, and cross-linking must all be considered in the stabilization of all-aqueous double (and higher order) emulsions.

Characterization of the capsules

Once collected in water, the particles swelled as is common to polymeric hydrogels.[34,35] Swollen particles were about twice the size they had at the irradiation point, while the core-shell structure remained intact. They had a core diameter of 44 ± 28 μm and a total diameter of 180 ± 50 μm (**Figure 2g**).

To study the structure of the particles in greater detail, we added Dextran-FITC to the DEX-phase and imaged the collected particles using confocal microscopy. As can be seen in **Figure 3a-c**, dextran indeed forms the shell and the particles have clearly defined cores. A small percentage of the particles have multiple cores, which we primarily attribute to merging of core-shell droplets prior to cross-linking. All particles displayed micro pores in their shell,

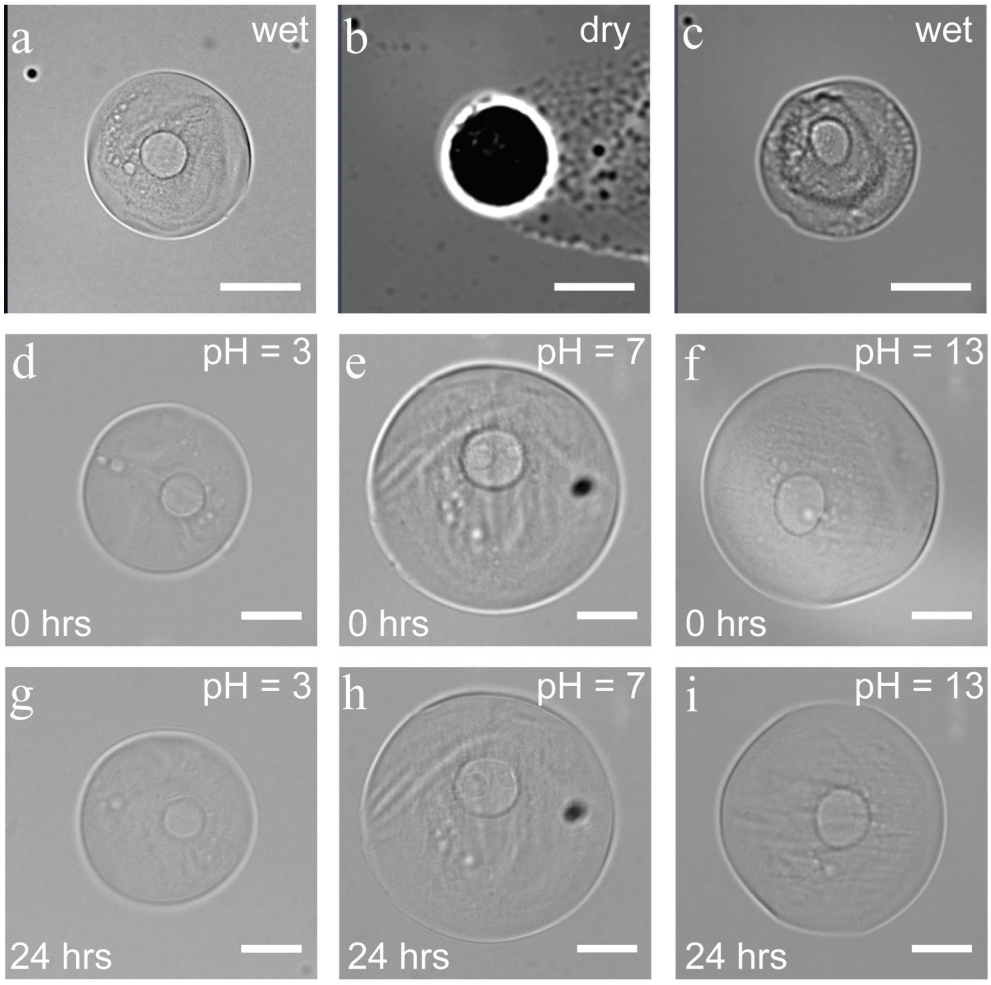

Figure 4. Core-shell capsule before drying (**a**), dried (**b**), and rehydrated (**c**). Particles immersed in solutions with pH = 3 (**d, g**), pH = 7 (**e, h**) and pH = 13 (**f, j**), imaged upon immersion (**d-f**) and 24 hours later (**g-j**) via bright field microscopy (scale bars 50 μm).

as shown in **Figure 3c**. Similar behavior has been observed previously for ATPS droplets[22,26] and has been explained as incomplete phase separation. We envision that arresting the intermediate stages of this process, for instance by changing the irradiation location, provides a way to tune the porosity of the shell.

Permeability and stability of the capsules

Core-shell particles displayed a great resistance to various external factors once the protective and stabilizing shell was formed. No changes in size and shape were observed during their storage in water for at least one month. The structure stayed intact in drying and rehydration experiments. After 12 hours in a dry state, they recovered their initial size and shape upon rehydration, without any visible disintegration (**Figure 4a-c**). These drying and rehydration experiments together with the observation of swelling, when the capsules were collected in water, clearly demonstrate the permeability of the shell, enabling their use in future release/uptake applications. Additionally, entrapment of non-cross-linkable Dextran-FITC in the shell, even after dilution, suggests a potential for molecular-weight/size-dependent control of permeability.

Capsules also showed good stability upon exposure to various harsh conditions. No changes were observed when the particles were submerged for 24 hours in solutions with a pH between 3 and 13 (see **Figure 4d-j**). In a more acidic environment (pH < 3), the 1,6-glycosidic bonds of dextran are expected to slowly hydrolyze, leading to chain fragmentation.[36] At pH = 1, capsules indeed remained intact for 30 minutes, while the shell visibly changed within 5 hours followed by complete dissolution within 24 hours. Besides the stability in basic and acidic environments (3 < pH < 13), the particles also showed excellent stability in high-salinity medium (1M KCl). Comparing these conditions to physiological ones, such as the salinity of blood (0.150 M of NaCl), gastric acid (pH ~ 1.5 to 3.5), and fluids in the small intestine (pH 7.0 to 9.0), demonstrates the potential use of the all-aqueous microcapsules for biomedical applications.

Conclusions

We have reported stable and permeable hydrogel microcapsules, obtained using a novel continuous approach comprising of the selectively cross-linking of the shell of a core-shell ATPS double emulsion produced in a microfluidic device. We do acknowledge the challenging nature of selecting the appropriate combination of ATPS and cross-linking chemistry which enables (1) a favorable partitioning of the material to be encapsulated, (2) the desired release properties of the shell, and, at the same time, (3) spontaneous formation of core-shell droplets. This process may require a great deal of optimization for a specific application. Fortunately, powerful tools to efficiently screen the huge parameter space (types of polymers and salts, their concentration, and partitioning coefficients) are already available. For example, several recently published reviews summarize known partitioning trends and outline the selection criteria of ATPS formulations for specific applications.[37,38] Additionally, Mace *et al.* have studied a large number of polymer combinations and successfully predicted the formation of more than 200 aqueous multiphase systems[39], and Lee *et al.* used droplet microfluidics to dynamically control the morphology of the phases.[22] Given the large number of known aqueous two-phase systems, we believe that the method demonstrated here for polyethylene glycol and dextran provides access to the continuous water-based production of a wide variety of compartmentalized water-permeable microcapsules. Our future work aims at controlling molecular-weight-dependent release from the PEG core to the outer environment

and application of the developed method for creating aqueous enzymatic micro reactors.

Materials and methods

Materials

All reagents were used as received. Polyethylene glycol (PEG, MW = 10 kDa), sodium hydroxide, sodium ascorbate, glycidyl propargyl ether, sodium chloroacetate, N-hydroxysuccinimde (NHS), cysteamine hydrochloride, 2-hydroxy-4'-(2-hydroxyethoxy)-2-methyl-propiophenone (Irgacure® 2959) and sodium azide were purchased from Sigma-Aldrich (Steinheim, Germany). Dextrans (MW = 500 and 20 kDa) and 1-ethyl-3-(3-dimethylaminopropyl)carbodiimide hydrochloride (EDC) were purchased from Alfa-Aesar (Karlsruhe, Germany).

Preparation of modified dextrans

The alkyne-functionalized dextran (DEX-GPE, MW = 500 kDa) was synthesized using the procedure of Nielsen *et al.*[40] The degree of substitution (DS) of DEX-GPE was determined by 1H NMR as 7%.

The thiol-functionalized dextran (DEX-SH, MW = 20 kDa) was prepared in two steps. First, commercial dextran (20 kDa) was carboxymethylated by sodium chloroacetate following the procedure of Brunsen *et al.*[41] Next, an aqueous solution of the resulting carboxymethyl dextran (CM-DEX, DS = 21%) was reacted with cysteamine hydrochloride using an EDC-NHS coupling to produce DEX-SH with DS = 10%. Detailed synthetic procedures and characterization data of the prepared polymers can be found in the SI[†].

Preparation of the fluids

Polymers were freshly dissolved in demineralized water to obtain solutions with the desired concentrations. Before use, photoinitiator (Irgacure 2959) was dissolved in all phases to obtain a concentration of 5 mg/mL for the outer PEG phase, and 3 mg/mL for both the core and shell phases. Solutions were then filtered through syringe filters (Sartorius, MicroSart, 0.45 μm) and injected in the microfluidic device using individual syringe pumps (Harvard Apparatus, 11 PicoPlus).

Microfabrication

The device was fabricated out of PDMS (Dow Corning, Sylgard 184 elastomer kit) using soft lithography. In short, a 4 inch silicon wafer was coated with a 40 μm thick layer of SU-8 photoresist. This layer was exposed to UV-light through a photomask, transferring the full two-dimensional design to the photoresist layer. After baking, the resulting wafer was coated with a second, 130 μm thick, layer of photoresist. It was exposed through a second photomask that only differs from the first one in having two non-transparent nozzle channels. The resulting photoresist structures on the wafer were 170 μm high except for the 40 μm high nozzles. Replica moulding in PDMS hence resulted in 170 μm deep channels and 40 μm deep nozzles. Bonding this piece of PDMS to another piece of PDMS in which all channels have a depth of 130 μm yields the desired three-dimensional devices with vertically centered nozzles. For further details, we refer to Rotem *et al.*[29]

Setup

All microfluidic experiments were performed on an Axio Observer A1 inverted microscope (Zeiss) and imaged using a Zyla 5.5 sCMOS camera (Andor) at 50 fps. The microscope was equipped with an EC-Plan Neofluar objective (10×, 0.3 NA) and Mercury-arc light source

(HXP 120V, 120 W), which was used with a band pass filter 300-400 nm (peak intensity at 365 nm, Zeiss, filter set 02) to initiate the thiol-yne cross-linking of the shells of the particles. In this way, the core-shell droplets were simultaneously irradiated and imaged. Total irradiance at the cross-linking spot was calculated to be 315 mW/cm^2.

Microfluidic experiments

Before connecting the tubes with the polymer solutions to the chip, the chip was flushed with filtered demineralized water to minimize the formation of air bubbles. Initially, all flows were set to a relatively high rate (5-20 μL/min) to ensure that the supply is stable and the formed jets are not in contact with the walls. After this was achieved, flow rates were lowered to the desired values.

Once the stable formation of core-shell droplets was observed, we cross linked the DEX shell via a thiol-yne "click"-reaction. Shortly before the start of irradiation, we put the tube (PEEK®, 1.6 mm outer and 0.5 mm inner diameter) connected to the exit of the device in a collection vial filled with 40 mL of demineralized water and stirred with a magnetic stirring bar (100-200 rpm). The reason to do this prior to the start of irradiation is that the mechanical disturbance induced by handling the tube affects the stability of jet break-up.

At the end of the experiment, the contents of the collection vial were well-stirred magnetically (700-800 rpm), transferred to a centrifugation tube, and repeatedly diluted and centrifuged (3000 rpm, ~800 g, 10 min x3) to ensure the removal of all dissolved polymers and additives. For prolonged storage of the capsules, sodium azide (0.01%) was added to prevent bacterial and algae growth.

Size distribution analysis

Bright-field microscopy was used to collect images of droplets and particles. For each set, the diameters of 250 – 400 droplets or particles were measured. The resulting data was plotted as histograms and fitted to a normal distribution, see SI† for further details. Values are reported as the mean plus/minus two times the standard deviation, $\mu \pm 2\sigma$, which captures over 95% of the droplets or particles.

Characterization of the capsules and their stability

Aqueous dispersions of collected particles were transferred into microwells (μ-Slide 8 Well Glass Bottom, Ibidi®), and analysed using bright-field and confocal laser-scanning microscopy (Zeiss LSM 710).

For the stability tests, excess of solutions with various pH and ionic strength was added, and particles were imaged using bright-field light microscopy.

For the drying and rehydration tests, the collected particles were drop-casted on a microscopy slide and allowed to dry at 20 °C while being imaged at 5 minute intervals for 12 hours. After complete drying, an excess of demineralized water was added and the rehydration process was imaged.

Acknowledgements

The authors gratefully acknowledge the financial support of the EC 7th Framework Programme Marie Curie Actions *via* the European ITN SMARTNET No. 316656 (S.M.), Netherlands Organization for Scientific Research (I.Z. and J.H.v.E. through NWO-VICI grant; V.v.S. through NWO-STW VENI grant; A.G.L.O. through the NWO-ECHO grant) and the NCTV (S.O.).

References

(1) Mitragotri, S.; Lahann, J. Materials for Drug Delivery: Innovative Solutions to Address Complex Biological Hurdles. *Adv. Mater.* **2012**, *24* (28), 3717–3723.

(2) Augustin, M. a.; Sanguansri, L. Encapsulation of Bioactives. *Food Mater. Sci. Princ. Pract.* **2008**, 577–601.

(3) Wei, Y.; Soh, S.; Apodaca, M. M.; Kim, J.; Grzybowski, B. a. Sequential Reactions Directed by Core/shell Catalytic Reactors. *Small* **2010**, *6* (7), 857–863.

(4) Stanley, C. E.; Elvira, K. S.; Niu, X. Z.; Gee, a D.; Ces, O.; Edel, J. B.; Demello, a J. A Microfluidic Approach for High-Throughput Droplet Interface Bilayer (DIB) Formation. *Chem. Commun. (Camb).* **2010**, *46* (10), 1620–1622.

(5) Long, M. S.; Jones, C. D.; Helfrich, M. R.; Mangeney-Slavin, L. K.; Keating, C. D. Dynamic Microcompartmentation in Synthetic Cells. *Proc. Natl. Acad. Sci. U. S. A.* **2005**, *102* (17), 5920–5925.

(6) Dewey, D. C.; Strulson, C. A.; Cacace, D. N.; Bevilacqua, P. C.; Keating, C. D.; Ichikawa, S.; Walde, P.; Johnston, A. P. R.; Cortez, C.; Angelatos, A. S.; et al. Bioreactor Droplets from Liposome-Stabilized All-Aqueous Emulsions. *Nat. Commun.* **2014**, *5*, 4670.

(7) Yanagisawa, M.; Nigorikawa, S.; Sakaue, T.; Fujiwara, K.; Tokita, M. Multiple Patterns of Polymer Gels in Microspheres due to the Interplay among Phase Separation, Wetting, and Gelation. *Proc. Natl. Acad. Sci. U. S. A.* **2014**, *111* (45), 15894–15899.

(8) Deshpande, S.; Caspi, Y.; Meijering, A. E. C.; Dekker, C. Octanol-Assisted Liposome Assembly on Chip. *Nat. Commun.* **2016**, *7*, 10447.

(9) Kim, B.; Jeon, T. Y.; Oh, Y.-K.; Kim, S.-H. Microfluidic Production of Semipermeable Microcapsules by Polymerization-Induced Phase Separation. *Langmuir* **2015**, *31* (22), 6027–6034.

(10) Choi, C.-H.; Wang, H.; Lee, H.; Kim, J. H.; Zhang, L.; Mao, A.; Mooney, D. J.; Weitz, D. A. One-Step Generation of Cell-Laden Microgels Using Double Emulsion Drops with a Sacrificial Ultra-Thin Oil Shell. *Lab Chip* **2016**, *16* (9), 1549–1555.

(11) Kim, S.-H.; Kim, J. W.; Cho, J.-C.; Weitz, D. A. Double-Emulsion Drops with Ultra-Thin Shells for Capsule Templates. *Lab Chip* **2011**, *11* (18), 3162–3166.

(12) Lee, S. S.; Abbaspourrad, A.; Kim, S.-H. Nonspherical Double Emulsions with Multiple Distinct Cores Enveloped by Ultrathin Shells. *ACS Appl. Mater. Interfaces* **2014**, *6* (2), 1294–1300.

(13) Bremond, N.; Santanach-Carreras, E.; Chu, L.-Y.; Bibette, J. Formation of Liquid-Core Capsules Having a Thin Hydrogel Membrane: Liquid Pearls. *Soft Matter* **2010**, *6* (11), 2484.

(14) Cheung Shum, H.; Varnell, J.; Weitz, D. A. Microfluidic Fabrication of Water-in-Water (W/w) Jets and Emulsions. *Biomicrofluidics* **2012**, *6* (1), 12808–128089.

(15) Beijerinck, M. W. Ueber Emulsionsbildung Bei Der Vermischung Wässeriger Lösungen Gewisser Gelatinierender Kolloide. *Zeitschrift für Chemie und Ind. der Kolloide* **1910**, *7* (1), 16–20.

(16) Walter, H.; Johansson, G. Partitioning in Aqueous Two-Phase Systems: An Overview. *Anal.*

Biochem. **1986**, *155* (2), 215–242.

(17) ALBERTSSON, P.-Å. Partition of Proteins in Liquid Polymer–Polymer Two-Phase Systems. *Nature* **1958**, *182* (4637), 709–711.

(18) Geschiere, S. D.; Ziemecka, I.; van Steijn, V.; Koper, G. J. M.; Esch, J. H. Van; Kreutzer, M. T. Slow Growth of the Rayleigh-Plateau Instability in Aqueous Two Phase Systems. *Biomicrofluidics* **2012**, *6* (2), 22007.

(19) Ziemecka, I.; van Steijn, V.; Koper, G. J. M.; Rosso, M.; Brizard, A. M.; van Esch, J. H.; Kreutzer, M. T. Monodisperse Hydrogel Microspheres by Forced Droplet Formation in Aqueous Two-Phase Systems. *Lab Chip* **2011**, *11* (4), 620–624.

(20) Hardt, S.; Hahn, T. Microfluidics with Aqueous Two-Phase Systems. *Lab Chip* **2012**, *12* (3), 434–442.

(21) Lai, D.; Frampton, J. P.; Sriram, H.; Takayama, S. Rounded Multi-Level Microchannels with Orifices Made in One Exposure Enable Aqueous Two-Phase System Droplet Microfluidics. *Lab Chip* **2011**, *11* (C), 3551.

(22) Hui Sophia Lee, S.; Wang, P.; Kun Yap, S.; Alan Hatton, T.; Khan, S. A. Tunable Spatial Heterogeneity in Structure and Composition within Aqueous Microfluidic Droplets. *Biomicrofluidics* **2012**, *6* (2), 22005–220058.

(23) Ma, S.; Thiele, J.; Liu, X.; Bai, Y.; Abell, C.; Huck, W. T. S. Fabrication of Microgel Particles with Complex Shape via Selective Polymerization of Aqueous Two-Phase Systems. *Small* **2012**, *8* (15), 2356–2360.

(24) Vijayakumar, K.; Gulati, S.; deMello, A. J.; Edel, J. B. Rapid Cell Extraction in Aqueous Two-Phase Microdroplet Systems. *Chem. Sci.* **2010**, *1* (4), 447.

(25) Yasukawa, M.; Kamio, E.; Ono, T. Monodisperse Water-in-Water-in-Oil Emulsion Droplets. *ChemPhysChem* **2011**, *12* (2), 263–266.

(26) Ziemecka, I.; van Steijn, V.; Koper, G. J. M.; Kreutzer, M. T.; van Esch, J. H. All-Aqueous Core-Shell Droplets Produced in a Microfluidic Device. *Soft Matter* **2011**, *7* (21), 9878.

(27) Song, Y.; Shum, H. C. Monodisperse W/w/w Double Emulsion Induced by Phase Separation. *Langmuir* **2012**, *28* (33), 12054–12059.

(28) Song, Y.; Chan, Y. K.; Ma, Q.; Liu, Z.; Shum, H. C. All-Aqueous Electrosprayed Emulsion for Templated Fabrication of Cytocompatible Microcapsules. *ACS Appl. Mater. Interfaces* **2015**, *7* (25), 13925–13933.

(29) Rotem, A.; Abate, A. R.; Utada, A. S.; Van Steijn, V.; Weitz, D. A. Drop Formation in Non-Planar Microfluidic Devices. *Lab Chip* **2012**, *12* (21), 4263–4268.

(30) Moon, B.-U.; Abbasi, N.; Jones, S. G.; Hwang, D. K.; Tsai, S. S. H. Water-in-Water Droplets by Passive Microfluidic Flow Focusing. *Anal. Chem.* **2016**, *88* (7), 3982–3989.

(31) Zhang, L.; Cai, L.-H.; Lienemann, P. S.; Rossow, T.; Polenz, I.; Vallmajo-Martin, Q.; Ehrbar, M.; Na, H.; Mooney, D. J.; Weitz, D. A. One-Step Microfluidic Fabrication of Polyelectrolyte Microcapsules

in Aqueous Conditions for Protein Release. *Angew. Chemie Int. Ed.* **2016**, *55* (43), 13470–13474.

(32) Guillot, P.; Colin, A.; Ajdari, A. Stability of a Jet in Confined Pressure-Driven Biphasic Flows at Low Reynolds Number in Various Geometries. *Phys. Rev. E* **2008**, *78* (1), 16307.

(33) Forciniti, D.; Hall, C. K.; Kula, M. R. Interfacial Tension of Polyethyleneglycol-Dextran-Water Systems: Influence of Temperature and Polymer Molecular Weight. *J. Biotechnol.* **1990**, *16* (3–4), 279–296.

(34) Ganji, F.; Vashenghani-Farahani, S.; Vashenghani-Farahani, E. Theoretical Description of Hydrogel Swelling: A Review. *Iran. Polym. J.* **2010**, *19* (5), 375–398.

(35) Hoffman, A. S. Hydrogels for Biomedical Applications. *Adv. Drug Deliv. Rev.* **2012**, *64*, 18–23.

(36) Swanson, M. A.; Cori, C. F. Studies on the Structure of Polysaccharides I. Acid Hydrolysis of Starch-like Polysaccharides. *J. Biol. Chem.* **1948**, *172*, 797–804.

(37) Soares, R. R. G.; Azevedo, A. M.; Van Alstine, J. M.; Aires-Barros, M. R. Partitioning in Aqueous Two-Phase Systems: Analysis of Strengths, Weaknesses, Opportunities and Threats. *Biotechnol. J.* **2015**, *10* (8), 1158–1169.

(38) Iqbal, M.; Tao, Y.; Xie, S.; Zhu, Y.; Chen, D.; Wang, X.; Huang, L.; Peng, D.; Sattar, A.; Shabbir, M. A. B.; et al. Aqueous Two-Phase System (ATPS): An Overview and Advances in Its Applications. *Biol. Proced. Online* **2016**, *18*, 18.

(39) Mace, C. R.; Akbulut, O.; Kumar, A. A.; Shapiro, N. D.; Derda, R.; Patton, M. R.; Whitesides, G. M. Aqueous Multiphase Systems of Polymers and Surfactants Provide Self-Assembling Step-Gradients in Density. *J. Am. Chem. Soc.* **2012**, *134* (22), 9094–9097.

(40) Nielsen, T. T.; Wintgens, V.; Amiel, C.; Wimmer, R.; Larsen, K. L. Facile Synthesis of Beta-Cyclodextrin-Dextran Polymers By "click" chemistry. *Biomacromolecules* **2010**, *11* (7), 1710–1715.

(41) Brunsen, A.; Ritz, U.; Mateescu, A.; Höfer, I.; Frank, P.; Menges, B.; Hofmann, A.; Plastira, N. Photocrosslinkable Dextran Hydrogel Films as Substrates for Osteoblast and Endothelial Cell Growth. *J. Mater. Chem.* **2012**, *22*, 19590-19604.

Appendix

Synthesis of modified dextrans

Dextran-GPE

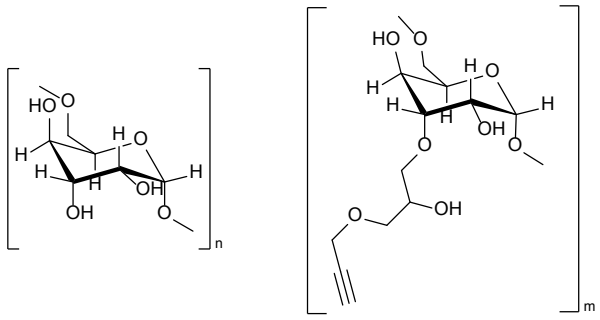

Scheme S1. Structure of Dextran-GPE.

The glycidyl propargyl ether derivatized dextran (DEX-GPE, MW = 500 kDa, Scheme S1) was prepared using the procedure of Nielsen *et al.*[1] The degree of substitution of DEX-GPE was determined by ^{1}H NMR as 0.075 (Fig. S1).

^{1}H NMR (400 MHz, D_2O), δ ppm: 5.34, 5.19, 5.00 (anomeric CH, 1H); 4.28 (O-CH_2-C, 2H, s); 4.15-3.45 (6H, m).

^{13}C NMR (100 MHz, D_2O), δ ppm: 100.56 (C1), 76.25 (C3), 74.26 (C2), 73.57 (C5), 73.04 (C4), 68.39 (C6), 61.15.

CM-dextran (CM-DEX)

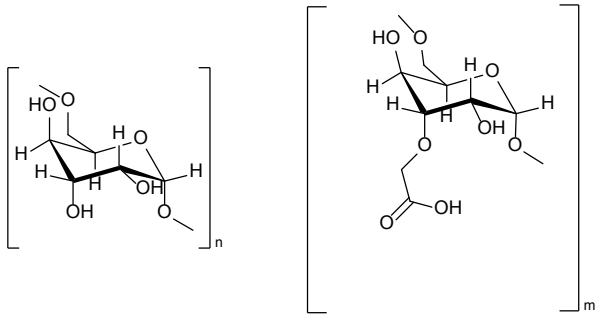

Scheme S2. Structure of CM-dextran.

Carboxymethylation of dextran (MW = 20 kDa, scheme S2) with sodium chloroacetate was performed following the procedure of Brunsen *et al.*[2] The degree of substitution was determined by ^{1}H NMR as 0.21 (Fig. S2).

^{1}H NMR (400 MHz, D_2O), δ ppm: 5.34, 5.19, 4.99 (anomeric CH, 1H); 4.24, 4.21 (-O-CH_2-COO, 2H); 4.15-3.45 (6H, m).

^{13}C NMR (100 MHz, D_2O), δ ppm: 180.63 (COOH), 100.61 (C1), 82.68, 76.29 (C3), 74.30 (C2), 73.08 (C5), 72.41 (C4), 68.41 (C6).

Dextran-SH

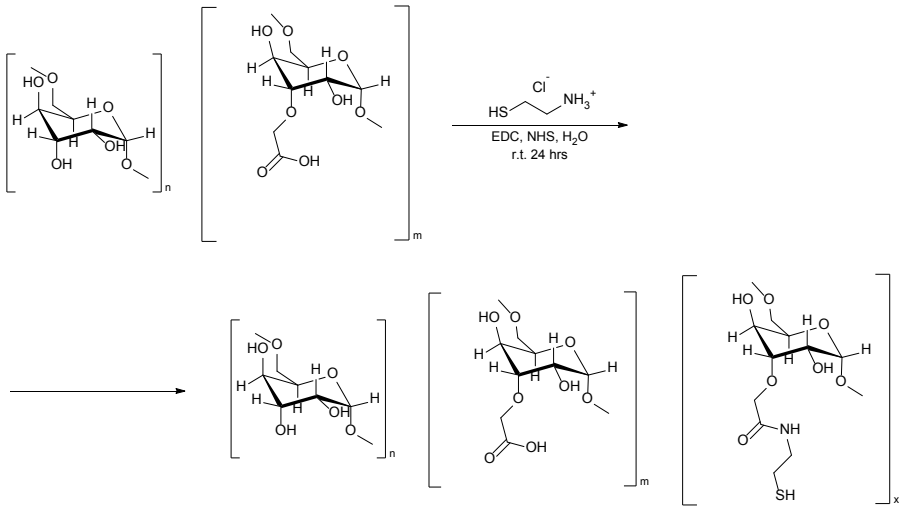

Scheme S3. Preparation of thiol-modified dextran.

The thiol derivatized dextran (DEX-SH, MW = 20 kDa) was synthesized as shown in Scheme S3. First, Cysteamine hydrochloride was coupled to carboxymethyl dextran (CM-DEX) in water using EDC-NHS coupling. Typically, 5 g of CM-DEX was dissolved in 50 mL of demineralized water and cysteamine hydrochloride (1.0 g, 8.8 mmol), EDC (1.5 g, 7.8 mmol) and NHS (0.92 g, 8 mmol) were added and stirred overnight at 25°C. The reaction mixture was then transferred to a dialysis bag (MWCO = 6500 Da), dialyzed first against 0.1 M KCl for 48 hrs (3x2L), then demineralized water for 48 hrs (3x2 L) and freeze-dried. The degree of substitution with SH was 0.10 as determined by ^{1}H NMR (Fig. S3). Yield 4-4.5 g.

^{1}H NMR (400 MHz, D_2O), δ ppm: 5.34, 5.19, 5.00 (1H, anomeric CH), 4.23, 4.19 (2H, O-$\underline{CH_2}$-CO-), 4.15-3.45 (6H, m), 3.26, 3.21 (2H, -$\underline{CH_2}$-SH).

^{13}C NMR (100 MHz, D_2O), δ ppm: 181.67, 180.53 (COOH), 100.60 (C1), 82.70, 76.3 (C3), 74.31 (C2), 73.08 (C5), 72.43 (C4), 68.41 (C6), 45.70 (-C-NH-).

NMR spectra of modified dextrans

All spectra were recorded using an Agilent-400 MR DD2 spectrometer operating at 400 MHz for ^{1}H NMR and 100 MHz for ^{13}C NMR, in D_2O.

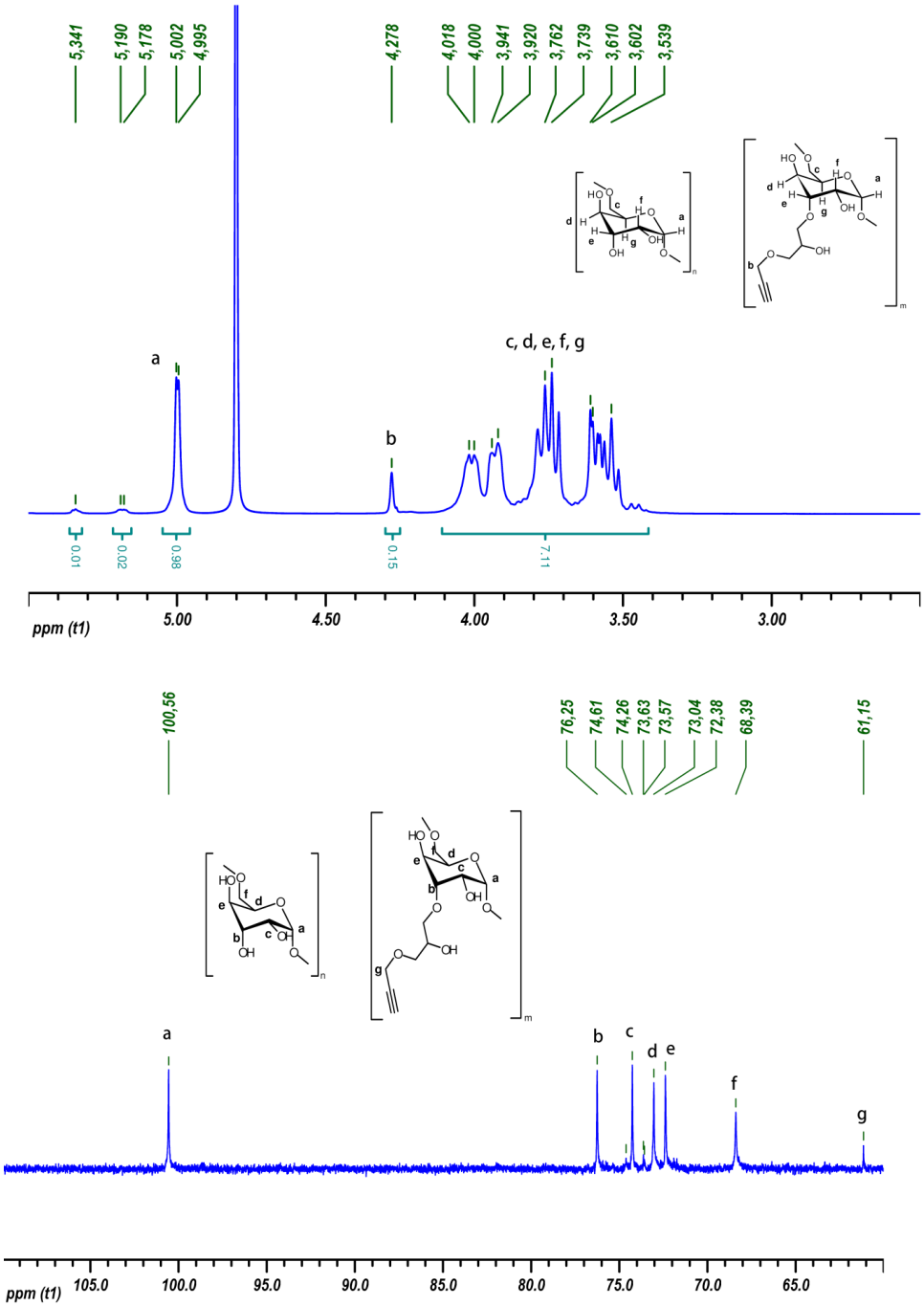

Fig. S1. ^{1}H and ^{13}C NMR spectra of Dextran-GPE in D_2O.

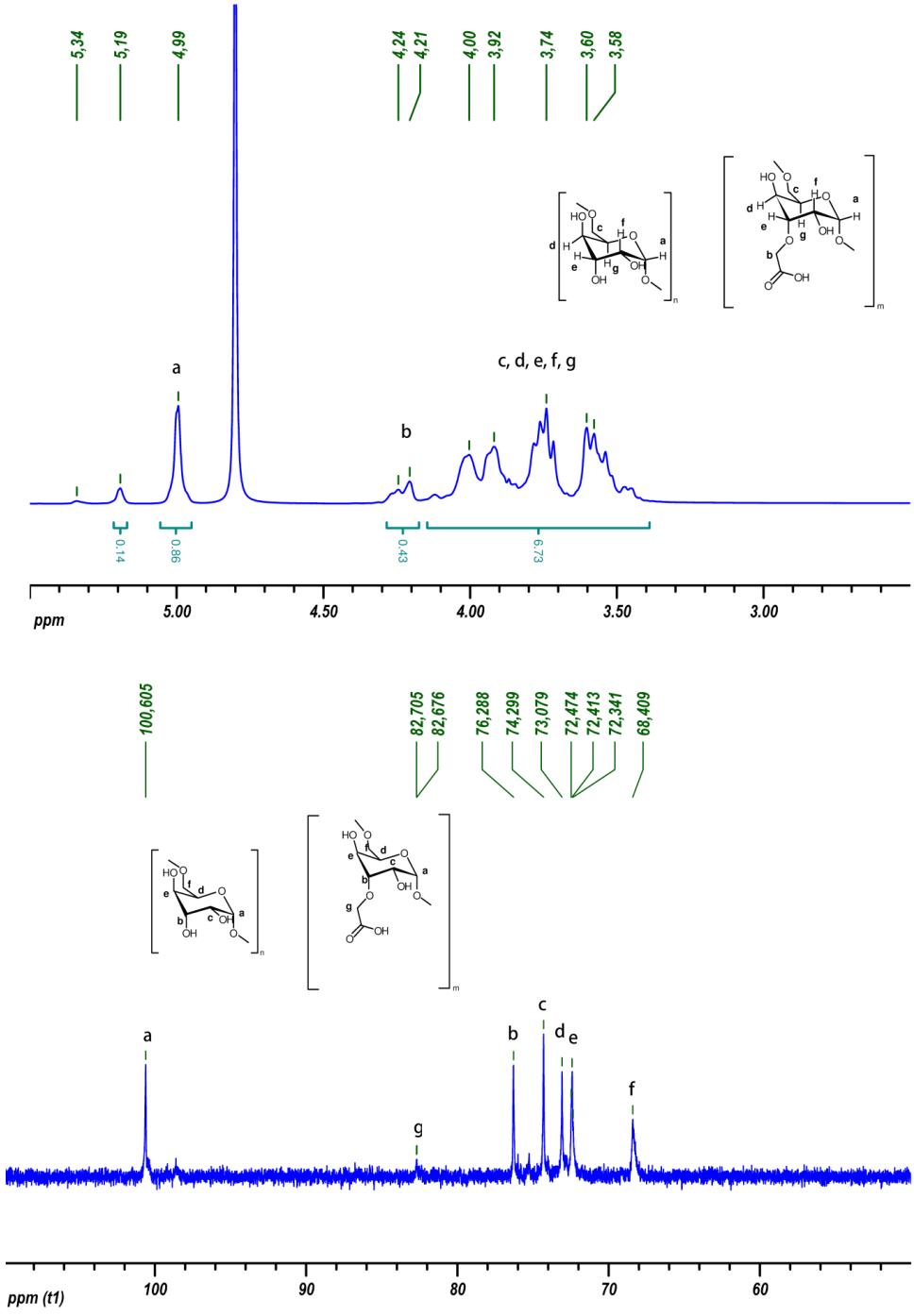

Fig. S2. ^{1}H and ^{13}C NMR spectra of CM-Dextran in D_2O.

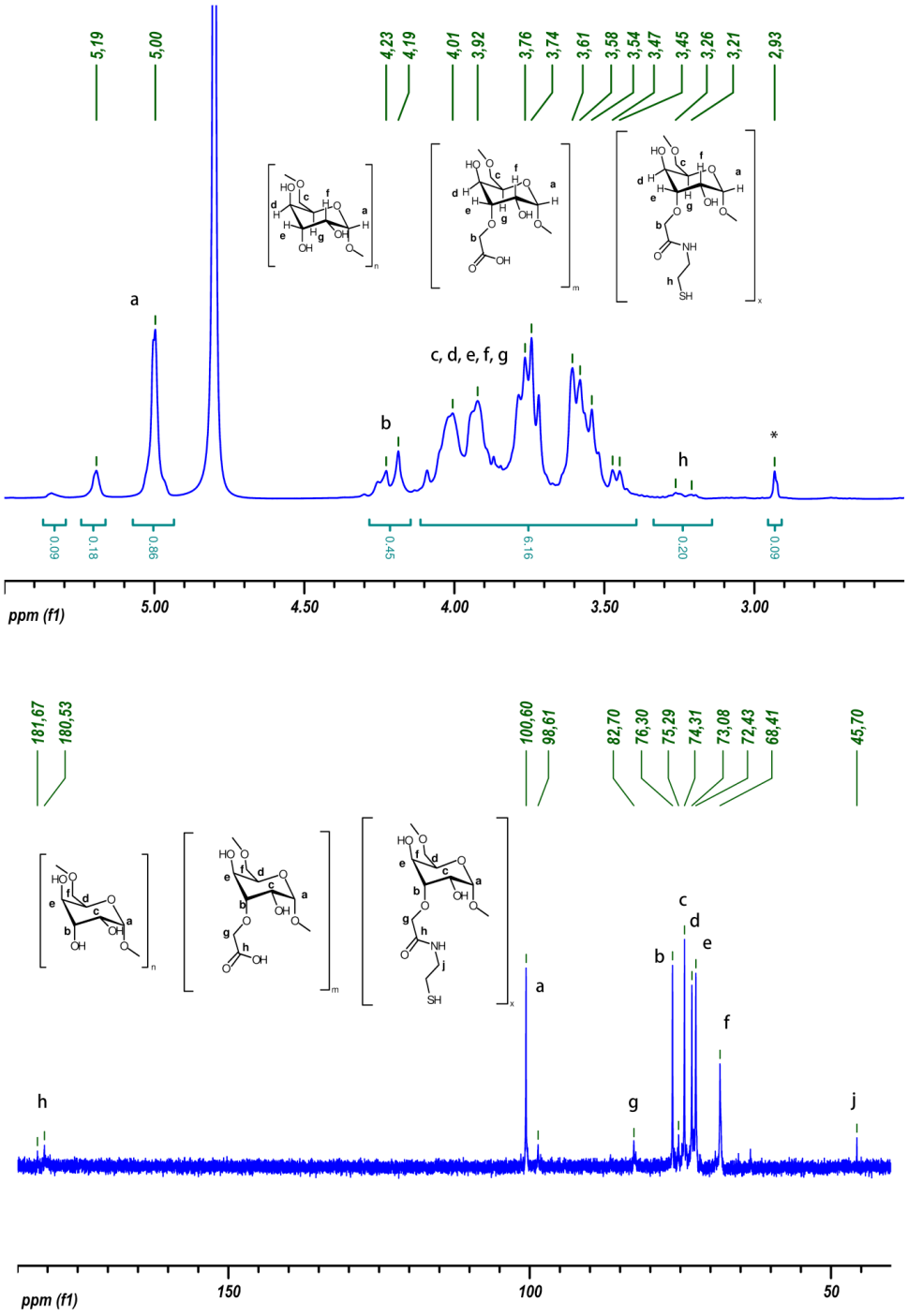

Fig. S3. ^{1}H NMR spectrum of Dextran-SH (* - residual coupling agent (EDC), less than1.5 mol %) and ^{13}C NMR spectrum of Dextran-SH in D_2O.

Molecular weight estimation of modified dextrans

Molecular weight of modified dextrans used in this study was estimated via gel permeation chromatography (GPC) using Shimadzu Prominence GPC system equipped with with 2x PL aquagel-OH MIXED H columns (Agilent, 8 µm, 300x7.5 mm) and refractive index detector (RID). 10 µL of 5 mg/ml polymers solutions were injected and eluted with a buffer system (0.01 M phosphate buffer, pH =7 + 0.0027 M KCl + 0.13 M NaCl) at 1ml/min and 40°C for 30 minutes. This particular eluent composition was reported suitable for the analysis of CM-dextrans by Brunsen *et al* [2], and is adjusted to screen the charges of carboxylate, which otherwise leads to significant swelling of the polymers coils and subsequent increase of their apparent molecular weight.

As can be seen from Fig. S4 modification of dextrans did not lead to significant changes in their molecular weights or polydispersity, which suggests that no chain fragmentation has occurred. In case of modification of dextran 20 kDa, the molecular weight increases slightly, as could be expected. In case of dextran-GPE (MW = 500 kDa), the peak is more symmetrical compared to commercial starting material, potentially due to removal of lower molecular weight fraction during purification by precipitation.

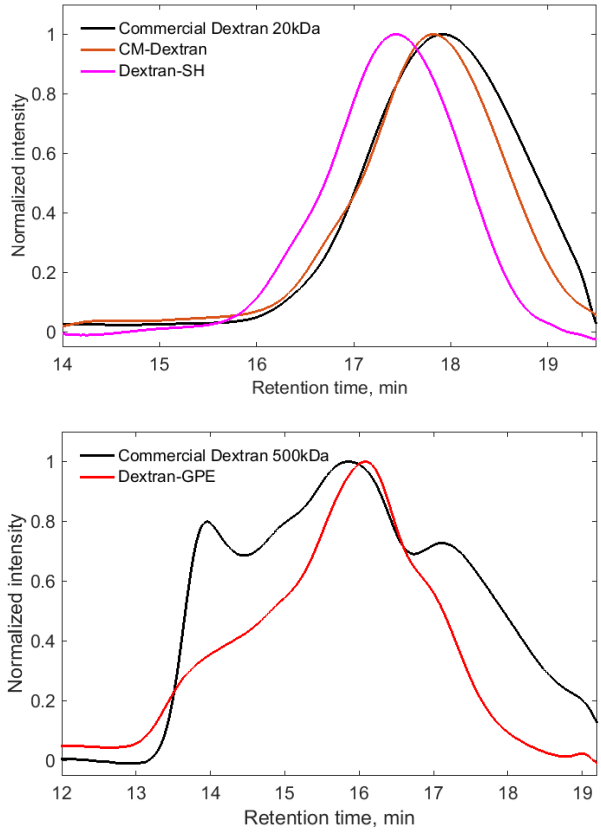

Fig. S4. Molecular weight comparison of modified dextrans with starting polymers.

Characterization of the diameter of droplets and particles

Droplets and particles were imaged using optical transmission microscopy. Due to the low contrast of the hydrogel particles on resulting images, particle diameters were determined manually. For each set, the diameter of 250-400 droplets or particles was measured. The resulting data was plotted as histograms and fitted to a normal distribution function. A typical example of the distribution of core and shell diameters of the droplets at optimal particle production conditions is shown in Fig. S5. Values are reported in the main paper as the mean plus/minus two times the standard deviation, $\mu \pm 2\sigma$, which captures over 95% of the droplets or particles.

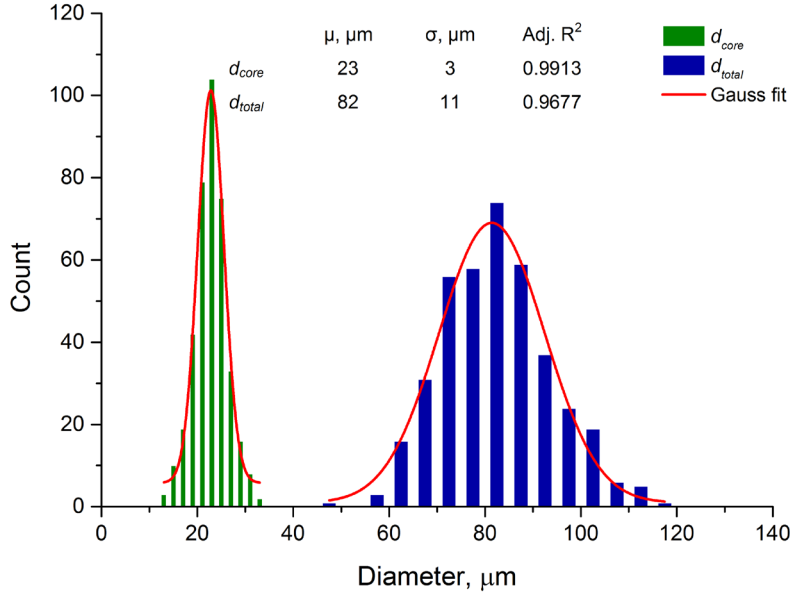

Fig. S5. Histograms of the core diameter and total diameter of the droplets at irradiation point.

Variation of shell to core ratio

We investigated the relationship between volumetric flowrates of shell and core phases (Q_{shell} and Q_{core} respectively) and the size of shells and cores of resulting droplets. Outer phase flowrate (Q_{out}) was fixed at 3.5 µl/min and Q_{shell} + Q_{core} at 0.40 µl/min, while their ratio was varied in range between 3/1 and 1/3. Collected data is represented below.

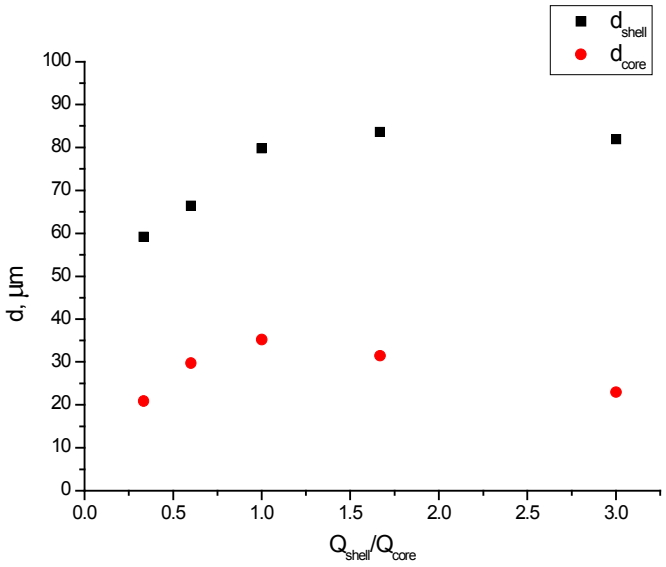

Fig. S6. Dependence of droplets' shell and core mean diameters on the ratio of shell to core flowrates.

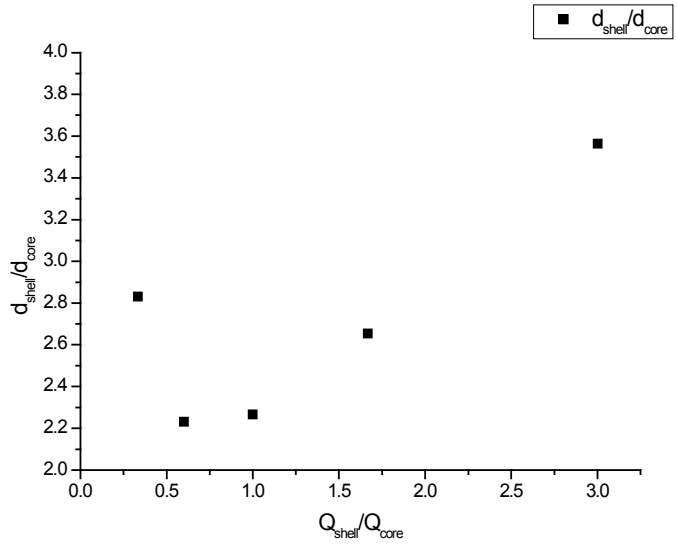

Fig. S7. Dependence of the ratio of droplets' shell to core mean diameters on the ratio of shell to core flowrates.

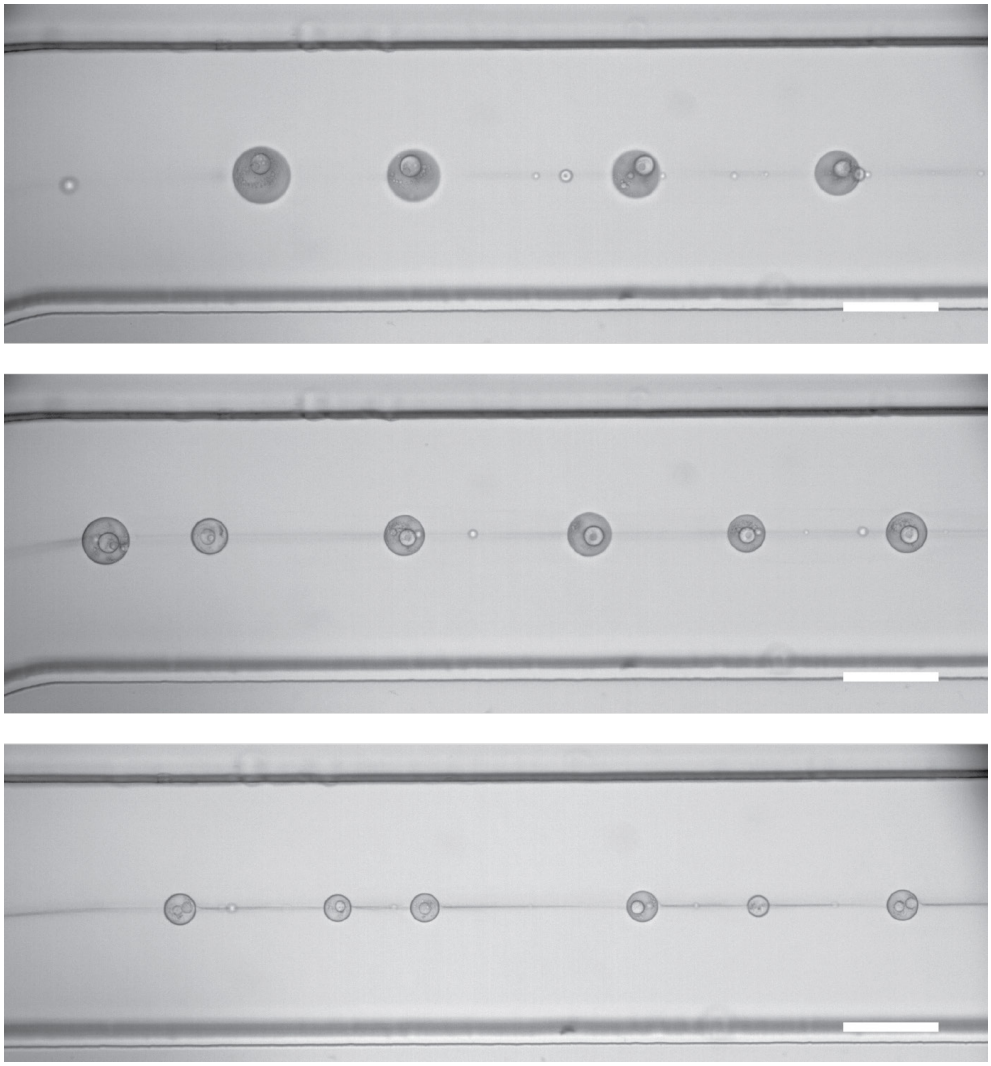

Fig. S8. Representative images of the droplets generated at different ratios of shell to core flowrates. Top to bottom: Q_{shell}/Q_{core} = 3/1, 1/1 , 1/3.

References

(1) Nielsen, T. T., Wintgens, V., Amiel, C., Wimmer, R. & Larsen, K. L. Facile synthesis of beta-cyclodextrin-dextran polymers by 'click' chemistry. *Biomacromolecules* **11,** 1710–5 (2010).

(2) Brunsen, A. Ritz, U., Mateescu, A., Höfer, I., Frank, P., Menges, B., Hofmann, A., Rommens, P. M., Knoll, W. & Jonas, U. Photocrosslinkable dextran hydrogel films as substrates for osteoblast and endothelial cell growth. *J. Mater. Chem.* **22,** 19590 (2012).

Chapter 3

Compartmentalizing supramolecular hydrogels using aqueous multi-phase systems*

Abstract

We present a generic method for compartmentalization of supramolecular hydrogels by using water-in-water emulsions based on aqueous multi-phase systems (AMPS). By forming the low-molecular-weight hydrogel throughout all phases of all-aqueous emulsions, we created distinct, micro-compartmentalized materials. This structuring approach offers control over the composition of each type of the compartments by directing the partitioning of objects to be encapsulated. Moreover, our method allows for barrier-less, dynamic exchange of even large hydrophilic solutes (MW ~ 60 kDa) between separate aqueous compartments. We expect these features to find use in the fields of, for instance, micro-structured catalysts, templating, and tissue engineering.

*This chapter has been published as S. Mytnyk *et al.*, *Angew. Chemie Int. Ed.* **2017**, *56*, 14923–14927.

Introduction

Compartmentalization plays a central role in a variety of biological and industrial processes. For instance, it allows incompatible metabolic reactions to run simultaneously inside eukaryotic cells by prohibiting mutual interference.[1] Additionally, compartmentalization is crucial for encapsulation, delivery and release of active ingredients (drugs, flavors), as well as for structuring various materials through templating and scaffolding.[2,3] In synthetic systems compartmentalization is generally achieved either by emulsification of immiscible phases, or through encapsulation of solutes inside various vesicles.[4–6]

However, most common approaches have limitations. For example, emulsification techniques are widely used for creating hydrophobic domains in aqueous phases, but are inherently limited in terms of the possible number of accessible types of compartments. On the other hand, vesicles-based approaches can effectively encapsulate various aqueous phases within their membranes and can be used to create numerous different coexisting micro-compartments with excellent control over their composition. However, while hydrophobic membranes grant vesicles their outstanding properties, they also seriously limit the transport of many polar solutes.[7] Furthermore, in contrast to emulsions, which can be generated and stabilized relatively easily even on a large scale, preparation of loaded vesicles can be a long, not easily scalable process. Therefore, there is a need for a simple and elegant approach, which allows creating micro-compartments containing polar molecules without introducing any hydrophobic barriers.

One of the most promising directions for membrane-less structuring of aqueous media is to employ aqueous multi-phase systems (AMPS). AMPS are multi-component water-based mixtures generally containing several incompatible polymers and/or salts that can form distinct macroscopic aqueous phases.[8] Aqueous two- and three-phase systems are widely used in biotechnology for extraction and separation of biomolecules, organelles and even living cells, since they offer a large number of mild, fully aqueous environments.[9] In recent years, the group of Keating has exploited aqueous phase-separation as a tool for compartmentalizing biomolecules by encapsulating aqueous two- and three-phase systems within lipid vesicles to create prototype artificial cells.[10–13] Several other examples of stabilization of water-in-water emulsions using various nano-particles have also been reported,[14–16] however these methods are system-specific and cannot be universally applied to form stable arbitrary AMPS emulsions. An alternative surfactant-free route to stabilize emulsions has been recently demonstrated by the group of Ulijn, who have generated stable oil-in-water emulsions by creating an interfacial supramolecular gel network around the dispersed droplets.[17,18] Therefore, formation of a supramolecular hydrogel network within AMPS emulsions should allow capturing their fine structure, resulting in micro-compartmentalized, fully aqueous hydrogel materials.

In this article, we present a generic method for compartmentalizing aqueous media using aqueous phase separation of incompatible polymers and formation of supramolecular hydrogel. Additionally, by localizing streptavidin in a hydrogel, we suggest a route to biomimetic micro-structuring of soft materials. Since the method presented here has the potential for creating multiple levels of specific compartments without any diffusion-limiting hydrophobic membranes, we expect it to have an impact in the fields of, for instance, micro-structured catalysts, templating, and tissue engineering.

Results and discussion

AMPS-based all-aqueous emulsions with micron-sized droplets can be easily prepared

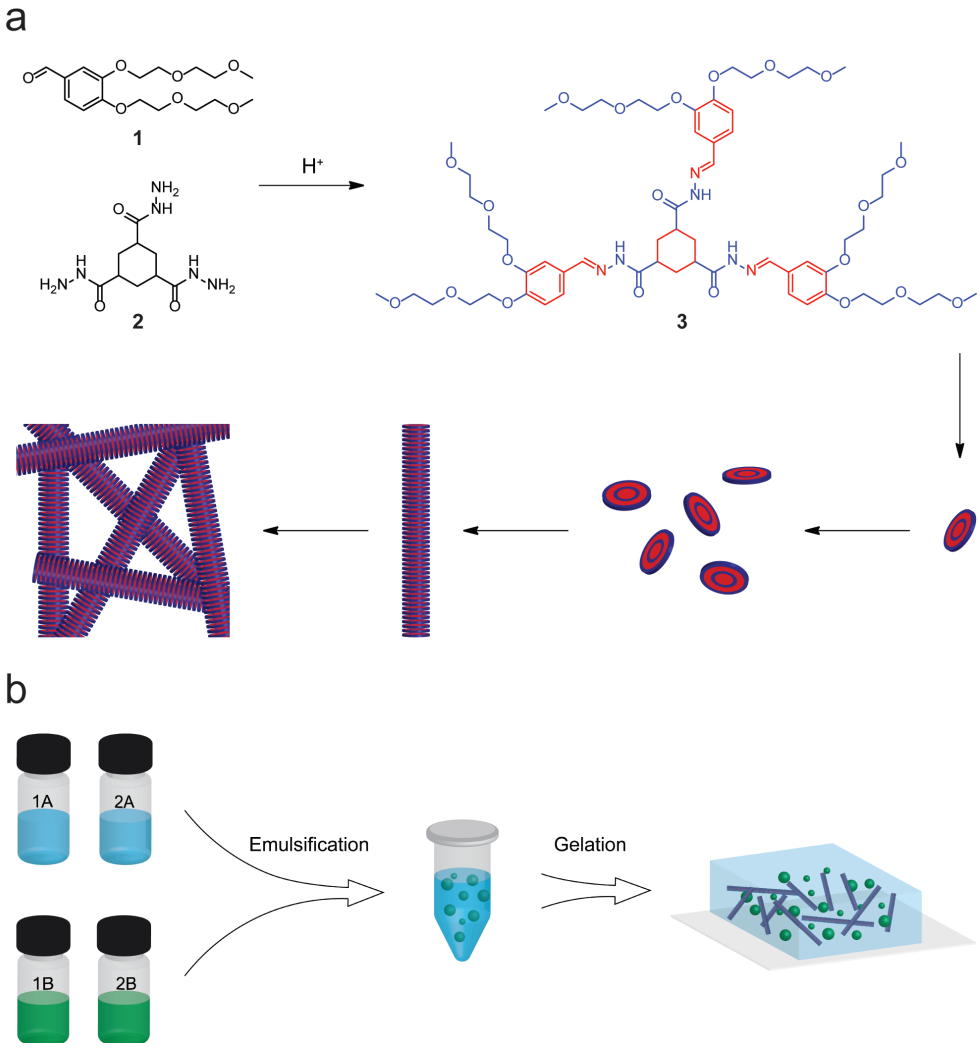

Figure 1. (**a**) Reaction of the gelator precursors **1** and **2** to form *tris*-hydrazone hydrogelator **3**, followed by its self-assembly into fiber network forming a gel; (**b**) preparation of compartmentalized hydrogels: solutions of compounds **1** and **2** in immiscible polymeric phases A and B are combined to form an emulsion with its consequent gelation.

even by manual shaking, due to the extremely low interfacial tension between coexisting aqueous phases. Properties of the individual phases, such as interfacial tension, density, and viscosity, determine the speed at which macroscopic phase separation of any given water-in-water (W/W) emulsion occurs. Therefore, to control the size of the compartments by capturing different stages of phase-separation *via* gelation, the timescales of two key processes have to be considered: first, the timescale of phase-separation of a given all-aqueous emulsion (t_{sep}), and second, the timescale of formation of a hydrogel that is meant to trap the structure of such an emulsion (t_{gel}).

These two timescales define the distribution and the size of the compartments in the final material. When $t_{gel} << t_{sep}$, the gel network forms sufficiently fast to capture the fine structure of corresponding water-in-water emulsion by mechanically fixing the microdroplets in place

and preventing them from coalescing. In the opposite case ($t_{gel} >> t_{sep}$), phase separation would be complete before the gel network has formed, thus resulting in a macro-phase-separated material, likely with nearly no micro-compartments. In this article we focus on the first scenario to achieve homogeneous micro-structuring of hydrogels.

As a prototype system, we used a supramolecular hydrogel that has been previously developed in our group.[19] In short, gelator precursors **1** (aldehyde) and **2** (hydrazide) react in aqueous solution at 3:1 ratio to form hydrogelator **3** (hydrazone), it self-assembles into fibers and forms a supramolecular gel network (**Figure 1a**). In this work, we chose the concentration of gelator precursors **1** and **2,** and the pH of the medium such as to ensure rapid gelation (<15 minutes) after emulsification.

In a typical experiment, compounds **1** and **2** were introduced into both phases of an aqueous two-phase system formed by poly(2-ethyl-2-oxazoline) (PEtOx) and dextran at pH 5. After combining the polymer solutions in appropriate ratios, they were vigorously stirred to obtain a W/W emulsion, left to form a compartmentalized gel overnight (**Figure 1b**). Detailed description of the preparation of polymer solutions, corresponding aqueous two-phase systems (ATPS), compartmentalized hydrogels and their characterization can be found in the online Supplementary Information (SI).

The obtained PEtOx – dextran emulsions appeared as soft, opaque hydrogels, without any signs of macroscopic phase-separation. This observation was confirmed by detailed investigations into the microscopic structure of the materials using confocal laser-scanning microscopy (CLSM). We found that microscopic spherical domains of one of the phases were homogeneously dispersed and immobilized in a second, continuous phase (**Figure 2a-c**). Upon increasing the volume fraction of dextran-rich phase (red), we observed the reversal of the phases from dextran-in-PEtOx (**Figure 2a**) to PEtOx-in-dextran emulsions (**Figure 2b-c**). Structure of prepared hydrogels remained unchanged within 1 week of observation (Fig. S1-S2). Importantly, the size of the micro-compartments depended on the volume fraction of corresponding polymer phases: while small well-dispersed droplets were formed at the volume fraction of the dispersed phase of 25% v/v, much larger domains were present at 50% v/v. This phenomenon can be explained by an increase in droplet coalescence rate at high volume fraction of the dispersed phase, which is generally observed for emulsions.[20] This means that t_{sep} increases, while t_{gel} remains constant, thus resulting in materials with larger compartments.

Having established the dependence of material structure on the ratio of the phases, we investigated the scope of the method by extending it to other ATPS, namely poly(N-vinyl pyrrolidone) (PVP) – dextran and Ficoll – dextran. We found that hydrogels, compartmentalized using W/W emulsions formed by these ATPS, behaved similarly to those prepared with the PEtOx – dextran system, although we observed a clear difference in their micro-structure. Compartments in PVP – dextran gels appeared to be larger than in case of PEtOx – dextran, and often possessed a core-shell structure (**Figure 2d-f**). In Ficoll – dextran system, however, large interconnected pores filled with a dense gel network were observed (**Figure 2g-i**). Interestingly, both the size and the distribution of micro-compartments varied depending on the combination of the polymers used for compartmentalization. We attribute these differences to the influence of individual polymers on the speed of phase-separation and the speed of gelation of the corresponding emulsions. Thus, by carefully choosing ATPS used for hydrogel compartmentalization one can tune the properties of prepared materials: their structure and the nature of micro-compartments.

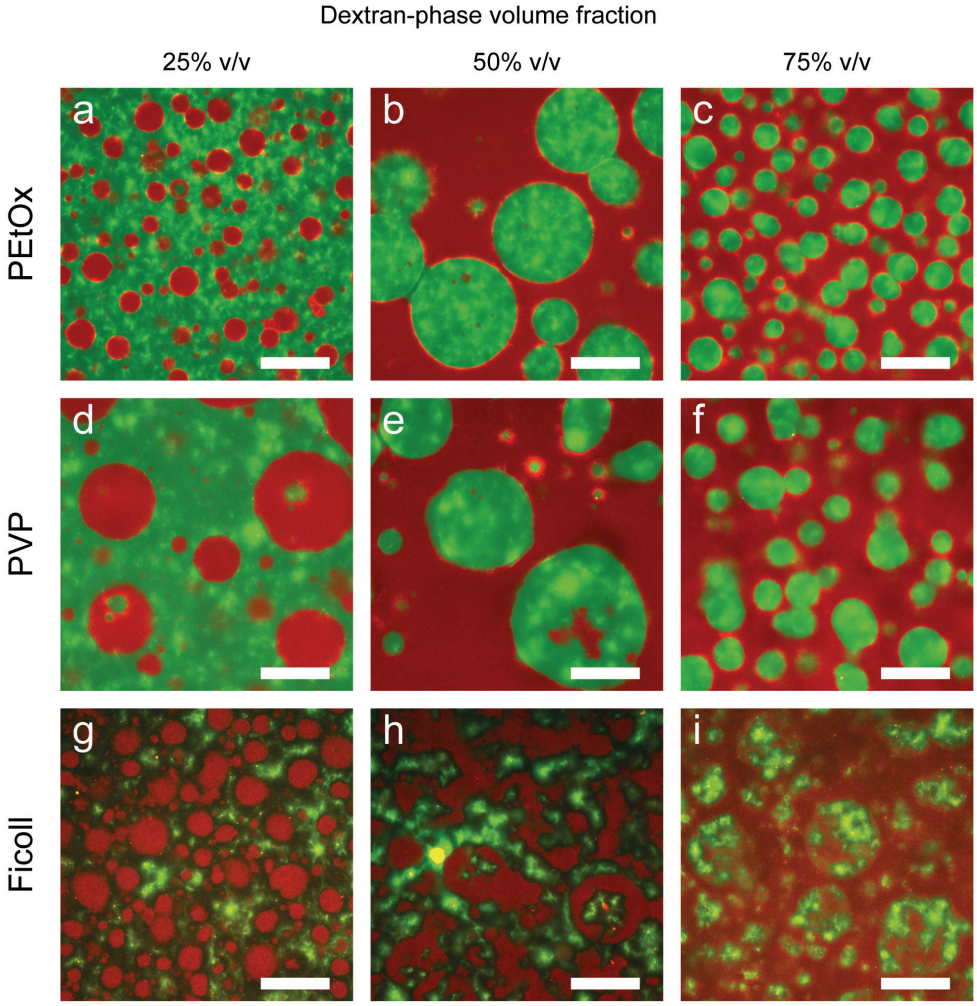

Figure 2. CLSM micrographs of hydrogels structured with PEtOx – dextran (**a-c**), PVP – dextran (**d-f**), and Ficoll – dextran ATPS (**g-i**), using different volume ratios of the polymer phases (left to right) – 75:25, 50:50, and 25:75. Dextran phases were labelled with TRITC-dextran (red) and gel network was labelled with fluorescein-modified aldehyde **1** (green)[21]. Scale bars 50 μm

Importantly, the method presented here not only allows creating aqueous compartments in a hydrogel, but also offers control over the composition of individual types of compartments. Such control can be achieved either by exploiting the selective partitioning of (bio)molecules in aqueous multi-phase systems, or by making use of specific interactions to drive the partitioning in the desired direction. Here we illustrate this feature by localizing fluorescently-labelled streptavidin (SA) in a PEtOx – dextran hydrogel. While normally SA displays a homogeneous distribution between PEtOx and dextran phases, addition of a dextran-biotin conjugate during preparation of the gels drove SA partitioning almost entirely to the dextran-rich phase (Figure S3). This experiment highlights the potential of our approach to be used for creating biomimetic materials, which enable the simultaneous performance of several catalytic/enzymatic reactions localized to specific droplet-microreactors. Since

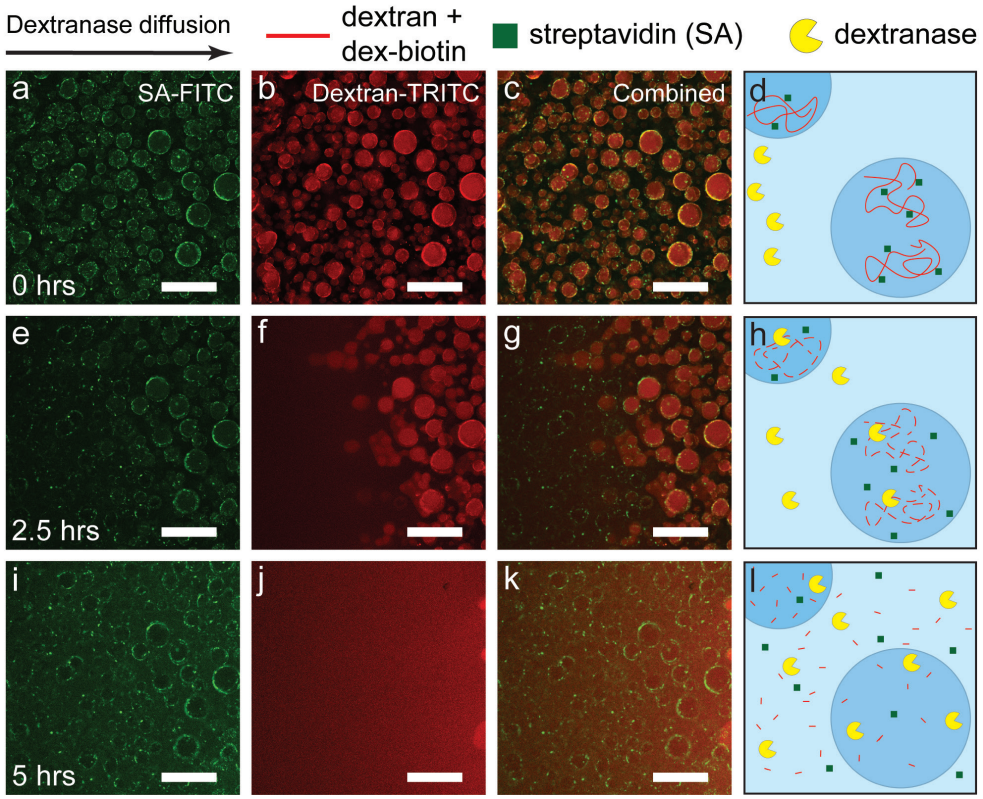

Figure 3. CLSM micrographs of the dextranase diffusion through hydrogel structured with PEtOx – dextran ATPS and containing SA-FITC with dextran-biotin: (**a-c**) at the start of the experiment, dextranase enters from the left, (**e-g**) after 2.5 hours, (**i-k**) after 5 hours. SA-FITC channel is displayed in green, dextran-TRITC channel in red. Images (**d**), (**h**) and (**l**) are schematic representations of corresponding stages of dextran degradation using dextranase. Scale bars 200 μm.

such an application would require a dynamic exchange of the contents of the compartments among the continuous phase and the other compartment types, we further investigated the permeability of the prepared materials.

The permeability of the micro-compartments was estimated by studying the diffusion of several polar molecules through PEtOx – dextran hydrogels. Fast diffusion of charged dyes (Pyranine and Rhodamine B) through the hydrogel's compartments confirmed the absence of hydrophobic barriers at the interface of the micro-domains (Fig. S4-S5). Furthermore, compartmentalized hydrogels were even permeable to large polar biomolecules.

To illustrate this property, we brought a streptavidin-containing PEtOx – dextran hydrogel in contact with the solution of dextranase — a bacterial enzyme that selectively hydrolyses 1,6-glycosidic linkages of dextran, thus degrading the polymer to glucose monomers. We followed this process by monitoring the dextran-phase fluorescence, which over the course of experiment has changed from highly localized to uniformly distributed (**Figure 3**). This observation suggests that after the diffusion of dextranase through the material no dextran chains remained, and so the fluorescent label was able to distribute homogeneously throughout the resulting dextran-free hydrogel. Therefore, dextranase, with a molecular

weight of approximately 60 kDa, diffused through *ca.* 1 mm of the gel within 5 hours, while simultaneously hydrolyzing the dextran present in the material. Similarly, streptavidin fluorescence became more evenly distributed, due to its unhindered diffusion after degradation of dextran-biotin. Importantly, the initial structure of the compartmentalized hydrogel remained intact and the material retained its solidity. These results confirm that our method allows for barrier-less, dynamic exchange of even large hydrophilic solutes between the separate aqueous compartments.

In sharp contrast to conventional emulsification approaches used for the structuring of soft materials, the AMPS-based method is not limited to only two immiscible phases — as many as 16 immiscible *aqueous* phases in equilibrium have been reported, and systems with 3 to 6 immiscible phases are being continuously discovered.[9,22] To demonstrate the versatility and potential of this technique, we prepared a set of compartmentalized hydrogels using a polyethylene glycol (PEG) – Ficoll – dextran aqueous three phase system (A3PS). By simply using one of the polymer solutions as a continuous phase and dispersing the other two in it, we were able to access an extremely wide range of structures (**Figure 4**). Distribution of the gel network and polymer-rich phases appears to be far more complex than in examples discussed above. We observed structures ranging from homogeneously distributed two types of spherical compartments (**Figure 4a**) to core-shell-like domains displayed in **Figure 4b**. These results demonstrate the potential of using higher order AMPS to create complex, artificially compartmentalized hydrogel materials reminiscent of biological tissues. And while the actual

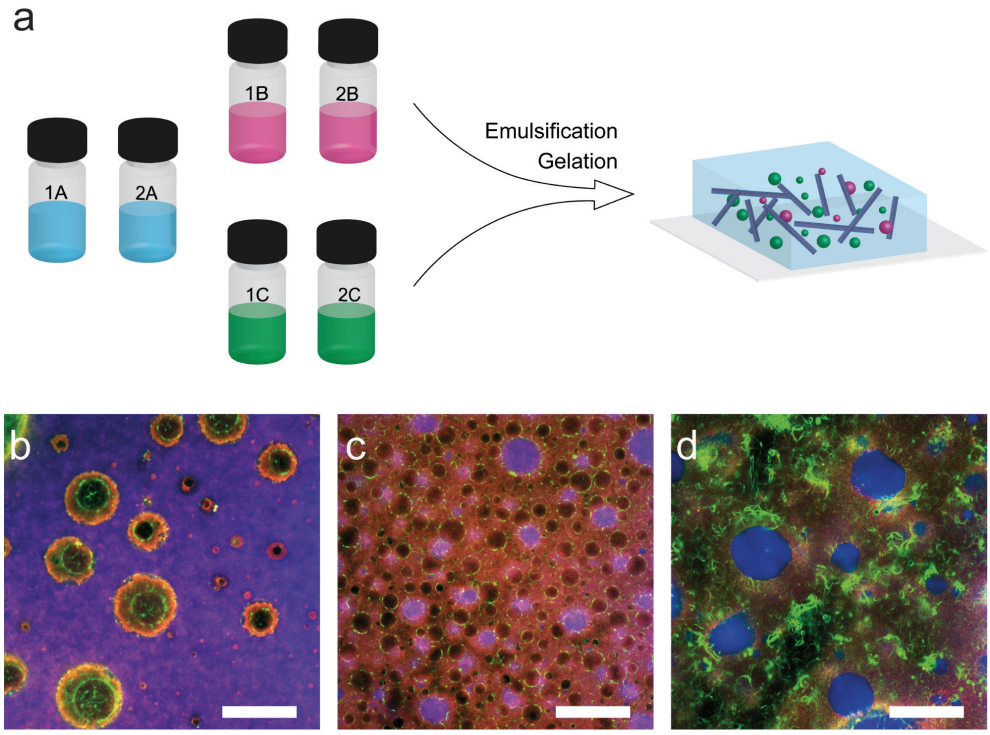

Figure 4. (**a**) Compartmentalizing hydrogels with aqueous three-phase system (A3PS) formed by polymers A, B and C; (**b-d**) CLSM micrographs of hydrogels structured with PEG – Ficoll – Dextran A3PS with phase-volume ratios of PEG/Ficoll/dextran equal to: (**b**) 4/1/1, (**c**) 1/4/1, and (**d**) 1/1/4. Dextran phase labelled green, Ficoll – red, and gel network – blue. Scale bars 50 μm.

laws governing the formation of these complex composites are yet to be fully investigated and understood, we expect that the main design considerations ($t_{gel} << t_{sep}$) will also apply to other aqueous multi-phase systems.

Conclusions

In conclusion, we have reported a versatile, generic approach for creating compartmentalized water-based materials by forming a supramolecular hydrogel within mixtures of aqueous phase-separating polymers. We have successfully applied our method to several all-aqueous emulsions and we expect it to be easily extended to the majority of aqueous multi-phase systems, thus opening access to a large number of tunable aqueous micro-environments. In addition to the potential of such hydrogel materials to mimic biological compartmentalization of biomolecules, we have demonstrated their permeability to even large polar solutes. We envision that these features may find use in, for instance, the design of novel biomimetic hydrogel catalysts, for templating of porous soft materials or in fabrication of supramolecular hydrogel scaffolds for tissue engineering.

Acknowledgements

The authors gratefully acknowledge the financial support of the EC 7th Framework Programme Marie Curie Actions *via* the European ITN SMARTNET No. 316656 (S.M.), and the Netherlands Organization for Scientific Research (R.E. and F.V. through NWO-Vidi grant; A.O. and J.P. through NWO-ECHO grants).

References

(1) Alberts, B.; Johnson, A.; Lewis, J.; Raff, M.; Roberts, K.; Walter, P. *Molecular Biology of the Cell*, 4th ed.; Garland Science: New York, 2002.

(2) Schoonen, L.; van Hest, J. C. M. Compartmentalization Approaches in Soft Matter Science: From Nanoreactor Development to Organelle Mimics. *Adv. Mater.* **2016**, *28* (6), 1109–1128.

(3) Chen, A. H.; Silver, P. A. Designing Biological Compartmentalization. *Trends Cell Biol.* **2012**, *22* (12), 662–670.

(4) Kelly, B. T.; Baret, J.-C.; Taly, V.; Griffiths, A. D. Miniaturizing Chemistry and Biology in Microdroplets. *Chem. Commun.* **2007**, *3* (18), 1773.

(5) Li, M.; Huang, X.; Tang, T.-Y. D.; Mann, S. Synthetic Cellularity Based on Non-Lipid Micro-Compartments and Protocell Models. *Curr. Opin. Chem. Biol.* **2014**, *22C*, 1–11.

(6) Massignani, M.; Lomas, H.; Battaglia, G. Polymersomes: A Synthetic Biological Approach to Encapsulation and Delivery; Springer Berlin Heidelberg, 2010; pp 115–154.

(7) Mansy, S. S.; Schrum, J. P.; Krishnamurthy, M.; Tobé, S.; Treco, D. A.; Szostak, J. W. Template-Directed Synthesis of a Genetic Polymer in a Model Protocell. *Nature* **2008**, *454* (7200), 122–125.

(8) Grilo, A. L.; Raquel Aires-Barros, M.; Azevedo, A. M.; Zhu, Y.; Chen, D.; Wang, X.; Huang, L.; Peng, D.; Sattar, A.; Shabbir, M. A. B.; et al. Partitioning in Aqueous Two-Phase Systems: Fundamentals, Applications and Trends. *Sep. Purif. Rev.* **2016**, *45* (1), 68–80.

(9) Albertsson, P.-A. *Partition of Cell Particles and Macromolecules, 3rd Ed.*; WIley: New York, 1986.

(10) Keating, C. D. Aqueous Phase Separation as a Possible Route to Compartmentalization of Biological Molecules. *Acc. Chem. Res.* **2012**, *45* (12), 2114–2124.

(11) Torre, P.; Keating, C. D.; Mansy, S. S. Multiphase Water-in-Oil Emulsion Droplets for Cell-Free Transcription–Translation. *Langmuir* **2014**, *30* (20), 5695–5699.

(12) Aumiller, W. M.; Davis, B. W.; Hashemian, N.; Maranas, C.; Armaou, A.; Keating, C. D. Coupled Enzyme Reactions Performed in Heterogeneous Reaction Media: Experiments and Modeling for Glucose Oxidase and Horseradish Peroxidase in a PEG/citrate Aqueous Two-Phase System. *J. Phys. Chem. B* **2014**, *118* (9), 2506–2517.

(13) Aumiller, W. M.; Keating, C. D. Experimental Models for Dynamic Compartmentalization of Biomolecules in Liquid Organelles: Reversible Formation and Partitioning in Aqueous Biphasic Systems. *Adv. Colloid Interface Sci.* **2017**, *239*, 75–87.

(14) Nguyen, B. T.; Nicolai, T.; Benyahia, L. Stabilization of Water-in-Water Emulsions by Addition of Protein Particles. *Langmuir* **2013**, *29* (34), 10658–10664.

(15) Gonzalez-Jordan, A.; Nicolai, T.; Benyahia, L. Influence of the Protein Particle Morphology and Partitioning on the Behavior of Particle-Stabilized Water-in-Water Emulsions. *Langmuir* **2016**, *32* (28), 7189–7197.

(16) Vis, M.; Opdam, J.; van 't Oor, I. S. J.; Soligno, G.; van Roij, R.; Tromp, R. H.; Erné, B. H. Water-in-Water Emulsions Stabilized by Nanoplates. *ACS Macro Lett.* **2015**, *4* (9), 965–968.

(17) Bai, S.; Pappas, C.; Debnath, S.; Frederix, P. W. J. M.; Leckie, J.; Fleming, S.; Ulijn, R. V. Stable Emulsions Formed by Self-Assembly of Interfacial Networks of Dipeptide Derivatives. *ACS Nano* **2014**, *8* (7), 7005–7013.

(18) Moreira, I. P.; Sasselli, I. R.; Cannon, D. A.; Hughes, M.; Lamprou, D. A.; Tuttle, T.; Ulijn, R. V. Enzymatically Activated Emulsions Stabilised by Interfacial Nanofibre Networks. *Soft Matter* **2016**, *12* (9), 2623–2631.

(19) Boekhoven, J.; Poolman, J. M.; Maity, C.; Li, F.; van der Mee, L.; Minkenberg, C. B.; Mendes, E.; van Esch, J. H.; Eelkema, R. Catalytic Control over Supramolecular Gel Formation. *Nat. Chem.* **2013**, *5* (5), 433–437.

(20) McClements, D. J. Emulsion Stability. In *Food Emulsions*; Contemporary Food Science; CRC Press, 2004.

(21) Poolman, J. M.; Maity, C.; Boekhoven, J.; van der Mee, L.; le Sage, V. A. A.; Groenewold, G. J. M.; van Kasteren, S. I.; Versluis, F.; van Esch, J. H.; Eelkema, R. A Toolbox for Controlling the Properties and Functionalisation of Hydrazone-Based Supramolecular Hydrogels. *J. Mater. Chem. B* **2016**, *4* (5), 852–858.

(22) Mace, C. R.; Akbulut, O.; Kumar, A. A.; Shapiro, N. D.; Derda, R.; Patton, M. R.; Whitesides, G. M. Aqueous Multiphase Systems of Polymers and Surfactants Provide Self-Assembling Step-Gradients in Density. *J. Am. Chem. Soc.* **2012**, *134* (22), 9094–9097.

Appendix

Experimental Procedures

Materials

Dextran (MW = 500 kDa) and poly(2-ethyl oxazoline) (MW = 200 kDa) were purchased from Alfa Aesar (Karlsruhe, Germany). Poly(vinyl pyrrolidone) (MW = 360 kDa), poly(ethylene glycol), (20 kDa), Ficoll PM 400, dextran-TRITC (MW = 500 kDa), Ficoll PM 400-TRITC, dextran-biotin (MW = 20 kDa), streptavidin-FITC and dextranase solution were purchased from Sigma Aldrich (Steinheim, Germany). All chemicals were used as received. Compounds **1**, **2** and FITC-labelled aldehyde have been prepared and purified according to the procedures reported by Poolman *et al.*[1,2] All AMPS were prepared by dissolving corresponding polymers in 0.1M citric acid – sodium citrate buffer at pH 5, prepared using demineralized water (conductivity of 1.3 μS/cm).

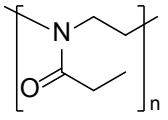

poly(2-ethyl-2-oxazoline)
(PEtOx)

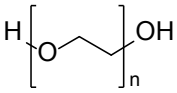

polyethylene glycol
(PEG)

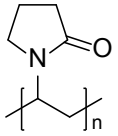

poly(*N*-vinyl pyrrolidone)
(PVP)

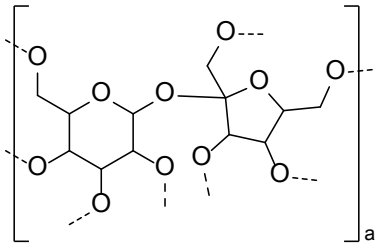

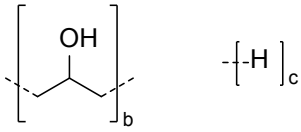

Ficoll® PM

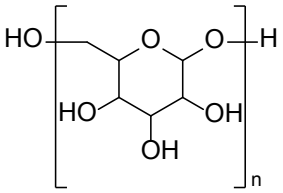

dextran

Scheme S1. Structures of the polymers used.

Preparation of AMPS

Table below summarizes the composition of aqueous multi-phase systems that have been used in this work. Names of AMPS are presented in a format Polymer A – Polymer B – Polymer C.

Table S1. Composition of the AMPS used for compartmentalization of a suparamolecular hydrogel

AMPS	Polymer A, % w/w	Polymer B, % w/w	Polymer C, % w/w	0.1 M citrate buffer, % w/w
PEtOx – dextran	10	10	-	80
PVP – dextran	7	7	-	85
Ficoll – dextran	10	7	-	83
PEG – Ficoll – dextran	3	10	6	81

To prepare the AMPS, corresponding polymers and buffer amounts were weighed into centrifugation tubes, vigorously mixed to ensure full dissolution of the polymers and allowed to equilibrate overnight. To ensure complete phase-separation prepared AMPS samples were centrifuged at 7500 g for 30 minutes. Top and bottom phases were then collected separately using Pasteur pipettes and used for preparing the stock solutions of compounds **1** and **2**.

Preparation of compartmentalized hydrogels

180 mM solutions of aldehyde **1** in polymer A and polymer B phases (stocks **1A** and **1B**), and 30 mM solutions of hydrazide **2** in polymer A and polymer B phases (stocks **2A** and **2B**) were prepared shortly before the experiments. Final concentration of the hydrogelator was 15 mM. The volumes of corresponding stock solutions were calculated as follows. To prepare 1 ml of an emulsion containing x ml of phase A and (1-x) ml of phase B, x/2 ml of stock **1A** was first combined with (1-x)/2 ml of stock **1B** and rigorously mixed for 20 seconds. Then, x/2 ml of stock **2A** and (1-x)/2 ml of stock **2B** were added, resulting mixture vigorously stirred for 30 seconds and transferred *via* pipette to a microscopy well (µ-Slide 8 Well Glass Bottom, Ibidi®). Then, emulsion was covered, isolated with Parafilm® to prevent evaporation and allowed to gel overnight before imaging.

Preparation of PEtOx-DEX hydrogels containing streptavidin

187 µl of solution of aldehyde (180 mM) in PEtOx-phase were combined with 63 µl of solution of aldehyde (180 mM) in dextran-phase, 10 µl of dextran-TRITC solution (1 mg/ml), 10 µl of streptavidin-FITC (1 mg/ml) and 10 µl of dextran-biotin solution (1 mg/ml). Obtained mixture was vigorously stirred for 20 seconds and then 187 µl of hydrazide solution (30 mM) in PEtOx-phase and 63 µl of hydrazide solution (30 mM) in dextran-phase were added. Mixture was vigorously stirred for 30 seconds, transferred to microscopy well and allowed to gel overnight prior to imaging.

Confocal laser-scanning microscopy (CLSM)

Confocal laser scanning micrographs were obtained in the fluorescence mode on a Zeiss LSM 710. In order to visualize the polymeric phases and the hydrogel network, we added 10 µl of 1 mg/ml aqueous solutions of dextran-TRITC or Ficoll-TRITC, and 10 µl of 1 mM aqueous solution of FITC-aldehyde during the preparation of the samples.

Results and Discussion

Stability of compartmentalized hydrogels

To demonstrate the influence of the gelator on phase-separation of PEtOx – dextran w/w emulsion, we have prepared 2 samples using identical procedure with and without hydrogelator, and followed their structure in time using CLSM. As can be seen in Fig. S1, both emulsions initially show the increase in the droplet size through coalescence. However, structure of the emulsion containing gelator reached its final state within 20 minutes and further remained unchanged, while in the emulsion without the gelator demulsification continued even after 40 min.

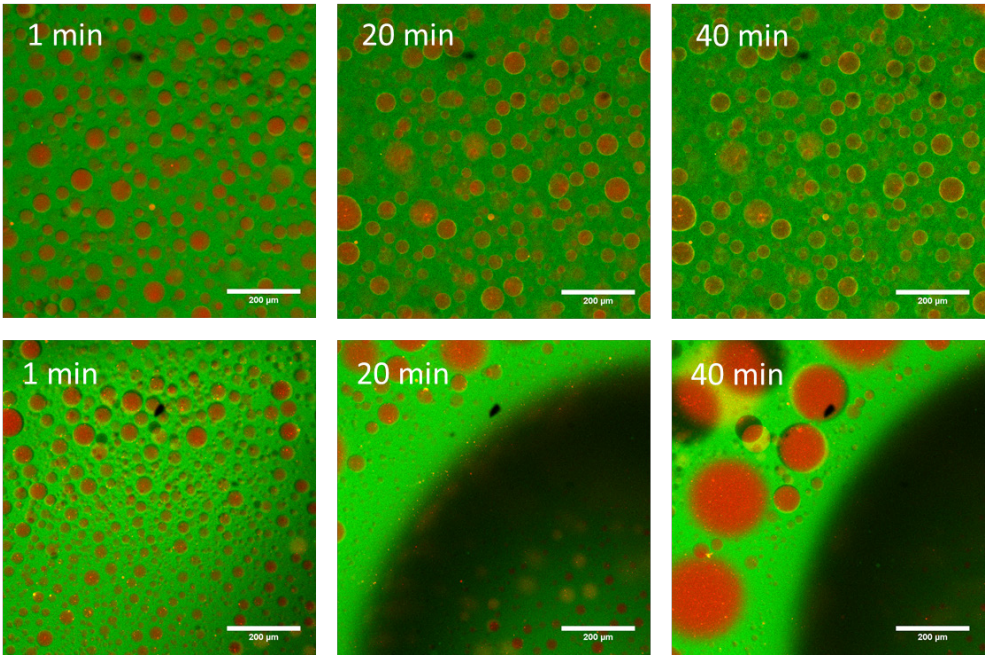

Figure S1. CLSM micrographs of PEtOx-Dextran emulsions with (top row) and without (bottom row) adding a hydrogelator. Scale bars 200 µm

Furthermore, we have also studied the structural stability of prepared materials over long time (Figure S2). Freshly prepared compartmentalized hydrogels were imaged with CLSM and then stored for 7 days in microscopy wells sealed with Parafilm tape to minimize the drying. Upon imaging the aged samples we could not observe any significant structural changes in fabricated materials.

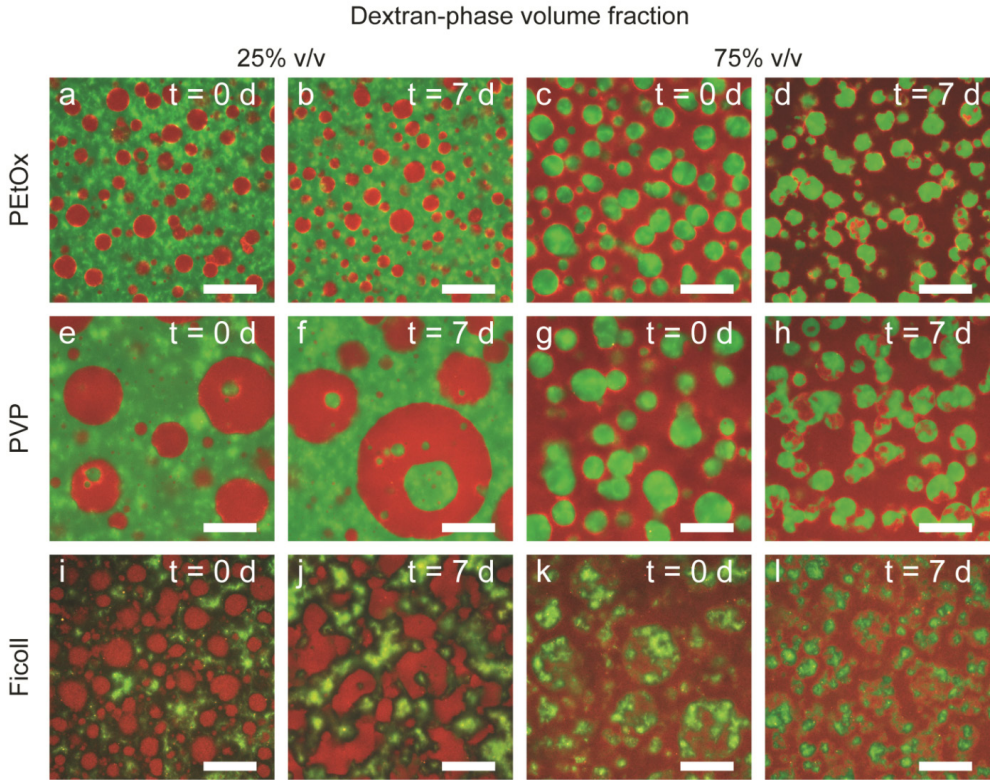

Figure S2. CLSM micrographs of hydrogels compartmentalized with PEtOx-Dextran, PVP-Dextran and Ficoll-Dextran ATPS imaged freshly prepared and after 1 week of storage. Dextran phases were labelled with TRITC-dextran (red) and gel network was labelled with fluorescein-modified aldehyde 1 (green). Scale bars 50 μm.

Compartmentalization of streptavidin in PEtOx – dextran hydrogels

In order to localize streptavidin to dextran-phase droplets, we exploited the affinity of streptavidin to biotin. By introducing dextran-biotin conjugate we managed to change the distribution of streptavidin from nearly homogeneous to strongly favoring dextran-phase, as can be seen in Figure S3.

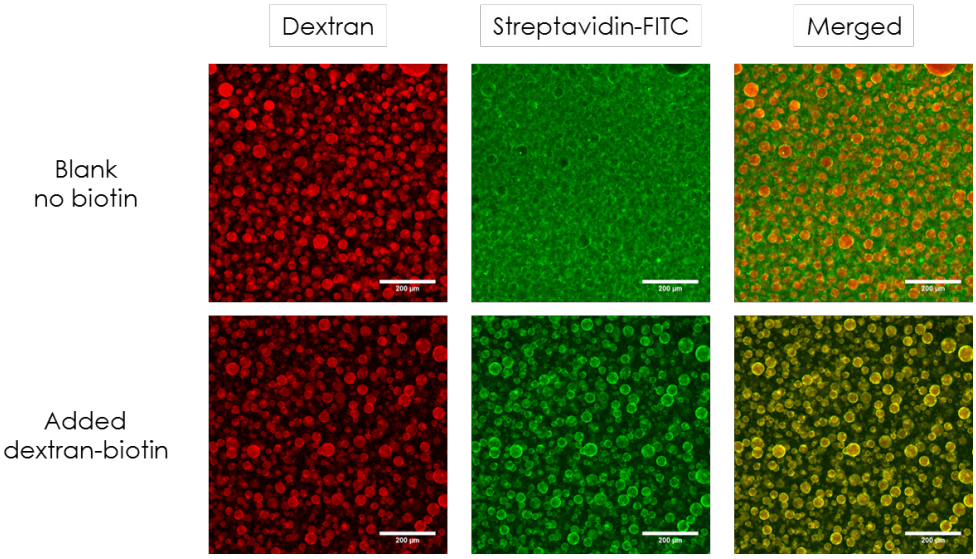

Figure S3. CLSM micrographs of PEtOx-Dextran gels containing SA-FITC with (top row) and without (bottom row) dextran-biotin addition. Left to right: dextran-TRITC channel, SA-FITC channel, merged image. Scale bars 200 μm.

Gel permeability experiments

To study the diffusion of polar solutes through the PEtOx-dextran compartmentalized gels, samples having PEtOx as a continuous phase and dextran compartments were prepared using the above-mentioned procedure. After overnight gelation in the microscopy wells, ~ 1 mm of the gel samples was cut off and removed. We introduced the solutions of Rhodamine B (100 μM) and Pyranine (100 μM) the corresponding cuts, and followed the change in fluorescence intensity of the dyes in time using CLSM. In the experiment with dextranase diffusion, dextranase solution (1 mg/ml) was introduced and changes in fluorescence of dextran-TRITC and streptavidin-FITC were followed. Figure S4 displays the micrographs of the samples after 1 and 40 min since the beginning of experiment. As can be seen from the images and fluorescence intensity profiles (Fig. S4-S5), dyes freely diffused through the gel.

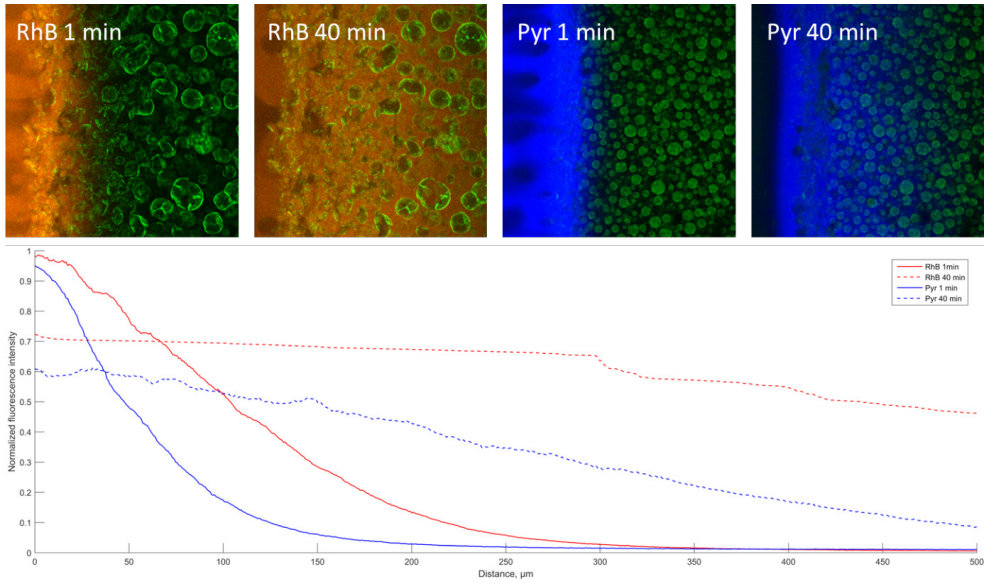

Figure S4. Diffusion of RhB (a-b) and Pyranine (c-d) dyes through PEtOx-Dextran-structured hydrogel. (e) Average fluorescence intensity profiles of the samples after 1 min (solid) and 40 min (dashed).

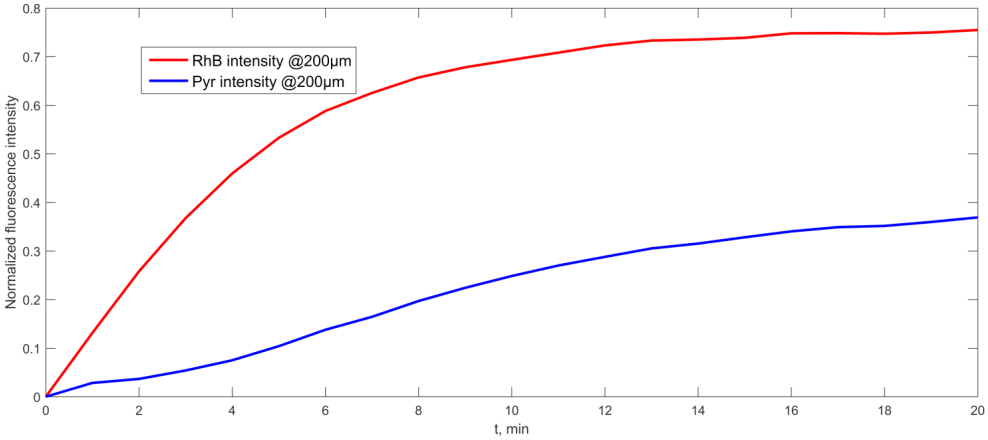

Figure S5. Diffusion of RhB (red) and Pyranine (blue) dyes through PEtOx – dextran hydrogel: increase in average fluorescence intensity over time at a distance of 200μm from solution/gel interface.

References

(1) J. M. Poolman, J. Boekhoven, A. Besselink, A. G. L. Olive, J. H. van Esch, R. Eelkema, *Nat. Protoc.* **2014**, *9*, 977–988.

(2) J. M. Poolman, C. Maity, J. Boekhoven, L. van der Mee, V. A. A. le Sage, G. J. M. Groenewold, S. I. van Kasteren, F. Versluis, J. H. van Esch, R. Eelkema, *J. Mater. Chem. B* **2016**, *4*, 852–858.

Chapter 4

Imaging-assisted hydrogel formation for single cell isolation*,+

Abstract

We report a flexible single-cell isolation method by imaging-assisted hydrogel formation. Our approach consists of imaging-aided selective capture of cells of interest by encasing them into a polymeric hydrogel, followed by removal of unwanted cells and subsequent release of isolated cells using enzymatic hydrogel degradation, thus offering an opportunity for further analysis or cultivation of selected cells. We achieved high sorting efficiency and observed excellent viability rates (>98%) for NIH/3T3 fibroblasts and A549 carcinoma cells isolated using this procedure. The method presented here offers a mask-free, cost-efficient and easy-to-use alternative to many currently existing surface-based cell-sorting techniques, and has the potential to impact the field of cell culturing/isolation.

* Patent application published as WO2018097715 "Hydrogel Micro-Patterning For Embedding Purposes"

+ Manuscript in preparation

Introduction

The ability to perform isolation of single cells from a heterogeneous population is highly valuable in biomedical research, because it allows carrying out selective follow-up studies, such as molecular profiling or cell line development.[1–4] Currently, most cell isolation methods are based on flow manipulation (flow cytometry) of fluorescently stained cell suspensions, e.g. fluorescence activated cell sorting (FACS).[3,5–9] However, such approaches cannot be employed when desired cells are attached to a substrate. Therefore, techniques for isolating adherent cells have been developed, including laser capture microdissection (LCM), IsoRaft™ Array, and CellCelector™. They generally require complex equipment, challenging mechanical manipulations and/or culturing of cells on specific supports.[10–17]

Recently, methods involving photo-induced degradation or generation of hydrogels have also been employed to isolate adherent cells.[18–22] For example, cultivation of the cells on or inside of a photo-degradable hydrogel support, followed by its selective light-mediated disintegration, has been used to release only the cell(s) of interest.[19,21,22] Unfortunately, this approach relies on the use of not readily accessible photodegradable hydrogels and requires specialized equipment or a photomask to generate the illumination profiles necessary for selective hydrogel degradation. Alternatively, light-induced hydrogel generation can be used to trap the unwanted cells in a hydrogel *via* selective illumination of the areas containing such cells through a photomask.[18,20] Such approach requires designing, fabricating and aligning a specific photomask for every isolation experiment, which limits the obtained resolution and isolation success rate, therefore impeding its routine application. An alternative approach was recently presented that covalently attaches selected cells to a pre-treated surface by a photochemical reaction.[23] Although this method was shown to be appropriate for single-cell isolation, it requires using a custom-made digital micromirror device (DMD) and was found to be prone to false positives. Therefore, the development of a technology that enables online selection, isolation, and release of adherent cells directly from cell cultures using common microscopy techniques would be a major breakthrough.

Here we present a method for direct, imaging-based selection, capture, and subsequent release of living single cells *via* light-induced hydrogel formation. Crucially, we are able to fabricate arbitrary hydrogel patterns by visible light illumination of selected areas using a confocal laser-scanning microscope (CLSM). With our method, hydrogel objects can be produced without the need for using a photomask, allowing to separate even adjacent cells quickly and effectively. Moreover, prepared hydrogels are biocompatible and can be rapidly enzymatically degraded, enabling the release of the isolated cells in an easy and mild manner.

Results and discussion

Our method represents imaging-assisted selective capture of cells by encasing them into a polymeric hydrogel, removal of unwanted cells and subsequent release of isolated cells by enzymatic hydrogel degradation, thus offering an opportunity for their further analysis or cultivation. Our approach involves four steps: (1) selection, (2) capture, (3) purification and (4) release (**Figure 1**). First, a population of adherent cells in a corresponding medium containing photo-cross-linkable polymer is imaged using CLSM and cells of interest are identified and selected in regions of interest (ROI). Next, regions containing the selected cells are illuminated with visible violet light (405 nm) to initiate the formation of a polymeric hydrogel and to capture the selected cells. After the removal of unwanted cells by dispersing them *via* trypsinization followed by the replacement of the medium (step 3), only hydrogel-encased cells remain behind. These cells are then easily released by enzymatically degrading

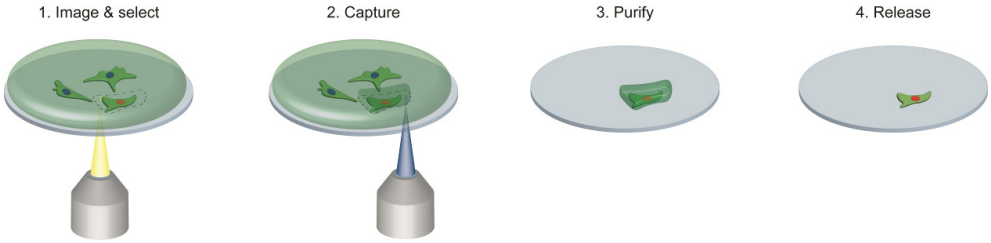

Figure 1. Schematic representation of four-step single-cell isolation procedure.

the hydrogel and isolated for analysis or further cultivation. We have confirmed high sorting efficiency of the technique using micro-particles as model objects, and successfully applied our approach to separation of co-cultures of living mammalian cells. We have observed excellent viability rates (>98%) for NIH/3T3 fibroblasts and A549 carcinoma cells isolated using our procedure thus illustrating its future application in cell-based studies. Since our method relies on illumination controlled by commercial confocal laser-scanning microscopes, no additional specialized equipment is required, therefore our cell-isolation technique can be directly applied in most biomedical labs.

In order to achieve efficient, cell-friendly isolation, we had to ensure fast, spatially controlled hydrogel formation and combine it with mild, bio-orthogonal hydrogel degradation. These two design criteria had to be met to maximize the precision of cell capture while minimizing the cell-damage. With this in mind, for hydrogel formation we have selected methacrylate-modified dextran (Dex-MA) – a polysaccharide that was shown to be non-toxic to mammalian cells (**Figure 2**).[24–26] Dex-MA hydrogels can be rapidly generated *via* photo-initiated cross-linking, and the polymer itself is well-characterized and easily accessible.[27–29]

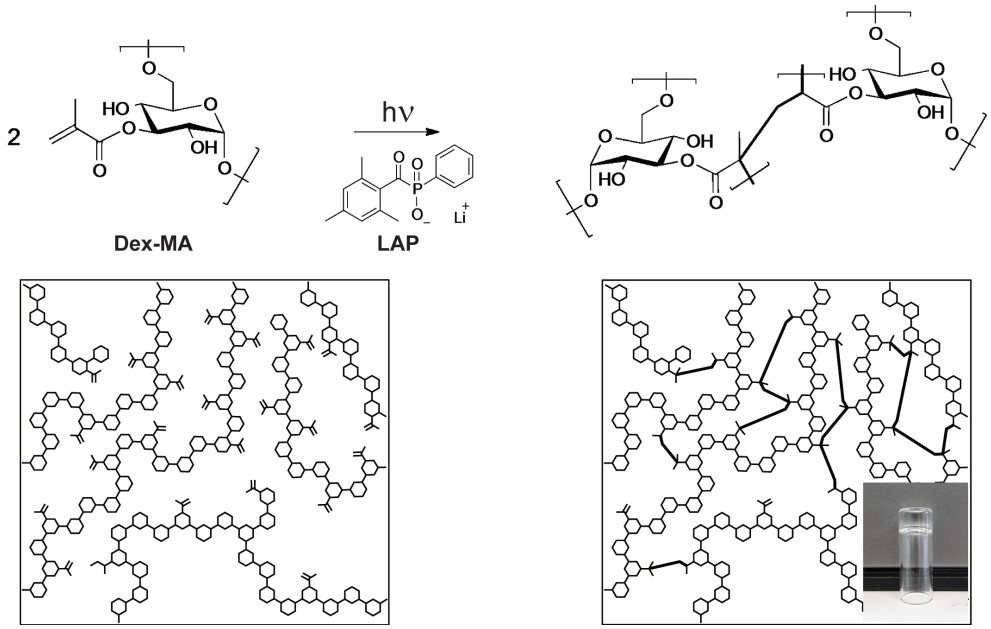

Figure 2. Molecular structure and schematic representation of Dex-MA before and after cross-linking via photoinitiated polymerization with LAP, with a photograph of a resulting hydrogel generated by cross-linking Dex-MA10 (5 wt%) displayed in the inset.

Importantly, Dex-MA hydrogels can also be degraded under biological conditions using dextran-specific enzyme – dextranase.[30–41] Additionally, to ensure the adhesion of fabricated hydrogels to glass surface during rinsing steps, we employed methacrylate-modified glass coverslips, thus leading to covalent bonding of hydrogel objects to the surface. To further decrease potential cell damage, we employed a water-soluble photo-initiator, LAP (lithium-phenyl-2,4,6-trimethylbenzoyl-phosphinate), that absorbs light up to a wavelength of 420 nm, thus also allowing to use light with longer wavelengths for cell-imaging without inducing hydrogel polymerization.

To select optimal conditions for fast photo-gelation, we have polymerized 5 wt% solutions of Dex-MA with degrees of substitutions (DS) ranging from 2.5 to 30% while using 0.5 wt% of photo-initiator. Upon exposure to unfiltered light of a 130W mercury lamp, 500 µl samples turned into transparent, slightly yellowish gels within one second, except for the Dex-MA with the lowest DS (DS = 2.5%), which required around 6 seconds. Out of the tested polymers, Dex-MA with DS = 10% proved to be the most suitable for our application since it provided the best compromise between speed of gelation, strength of the formed gel and viscosity of the pre-gel solution (data not shown).

By exploiting the LAP's absorbance of visible violet light, we successfully performed Dex-MA gelation using 405 nm laser light controlled by a commercial CLSM system. In order to do so, we deposited 29 µl of above-mentioned solution of Dex-MA (5 wt%) and LAP (0.5 wt%), additionally containing Dex-FITC (0.02 wt%), on a 24×24 mm glass slide, with the surface modified with methacrylate groups to ensure adhesion of the gel after polymerization. Once the sample was covered with a transparent flexible cover slip (24×24 mm, cut out of a transparency sheet compatible with laser printing), an approximately 50 µm thick layer of pre-gel solution was formed. Obtained sample was then imaged using 488 nm laser for excitation (standard fluorescein imaging conditions), thus allowing us to focus the optics approximately in the middle of the pre-gel solution layer without initiating the polymerization. Next, the full area of view was illuminated using 405 nm laser diode, and once polymerization was complete, the plastic coverslip was carefully removed and hydrogels were rinsed with water and observed using bright-field and fluorescence microscopy using FITC channel. This procedure was repeated several times for different laser intensities and exposure times using 10× magnification. We determined the optimal settings for hydrogel formation as the minimal time required to form stable well-defined hydrogel objects, which was 3.71 µs/µm^2 for 10× magnification using full power of a 30 mW 405 nm diode laser. Additional details on preparation of the components (Dex-MA, LAP), microscope details and optimization of hydrogel patterning conditions can be found in Appendix.

Furthermore, CLSM has an inherent advantage of irradiating a sample in a point-by-point fashion, thus allowing for selective imaging, analysis and bleaching of user-defined regions. We exploited this feature to spatially control the photo-induced hydrogel formation, i.e. to produce well-defined hydrogel objects of arbitrary shape and size (**Figure 3**). CLSM allows designing illumination profiles online, while imaging the sample, instead of requiring to design and fabricate new photomasks or to use sophisticated and expensive DMDs. Using this mask-less gel fabrication approach we were able to prepare hydrogels with features down to 50 µm and 15 µm, with minimal separation of 35 µm and 15 µm, using 10× and 40× objectives respectively (Figures S5-S8). Furthermore, combining the customizable illumination profiles with tile-scanning feature of CLSM, offers a way to produce large numbers of identical hydrogel objects in a matter of minutes (Figure 3c and S9-10). Such flexibility of this approach

makes it attractive for fast and simple fabrication of microscopic hydrogel objects.

Moreover, sequential application of our approach using different cross-linkable polymers and, potentially, different patterns presents the means to fabricate multi-layer composite hydrogel objects. To illustrate this feature, we first fabricated an array of Dex-MA hydrogel squares loaded with dextran-FITC (250×250 μm, green), followed by patterning smaller Dex-MA hydrogel squares loaded with dextran-TRITC (100×100 μm, red) on top of the hydrogels prepared during the first step (**Figure 4**). The simplicity of our approach allows applying it to fabrication of complex hydrogel 3D structures in a very flexible manner in a matter of minutes.

Most importantly, by coupling our hydrogel fabrication technique with biodegradability of dextran we were able to develop a method for selective capture and release of microscopic objects. To demonstrate its performance, we applied our approach to separation of a mixture

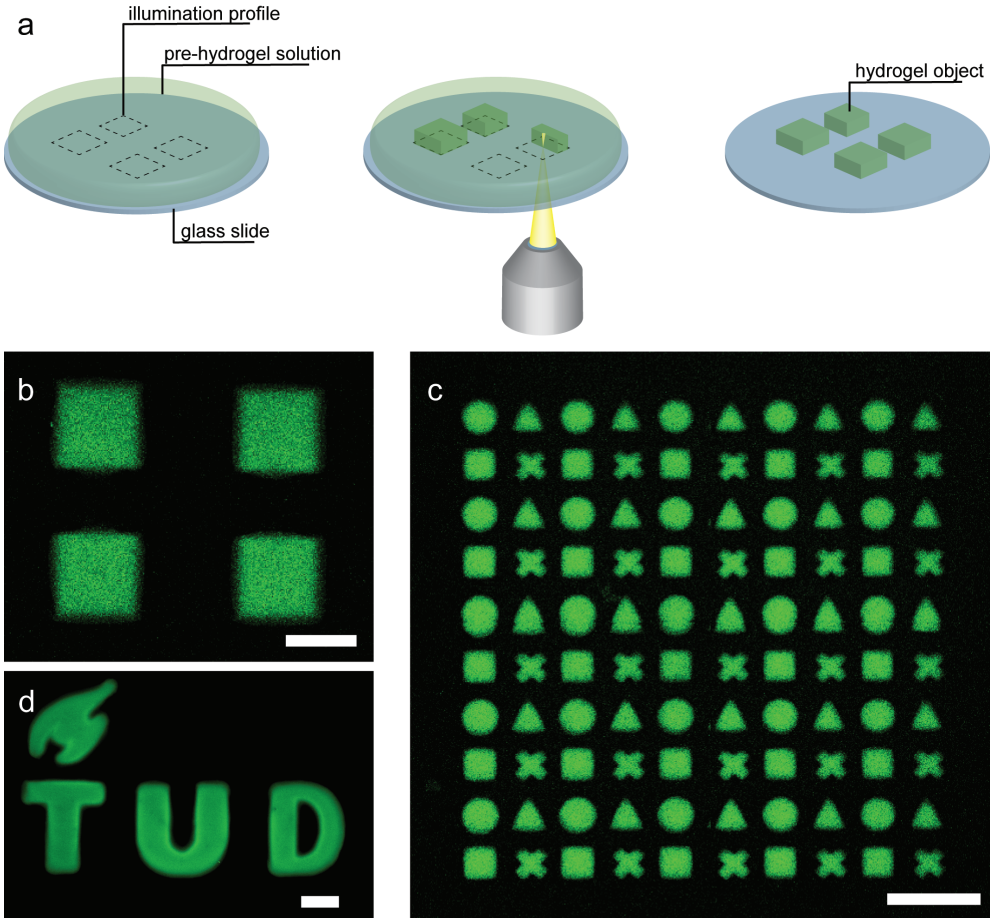

Figure 3. (**a**) Schematic representation of direct hydrogel writing experiment. First, an illumination profile is designed (dashed lines), the selected areas are illuminated and hydrogels are produced, followed by rinsing and isolation of obtained hydrogel objects. CLSM micrographs of fabricated hydrogels: (**b**) four square Dex-MA hydrogels fabricated using 10× objective and exposure time of 3.71 μs/μm^2 at 100% laser power (**c**) 5 × 5 tile-scan pattern containing four individual hydrogel objects in each tile (circle, triangle, square, and cross); (**d**) TU Delft logo hydrogel object. Scale bars: (b,c) 200 μm; (d) 100 μm.

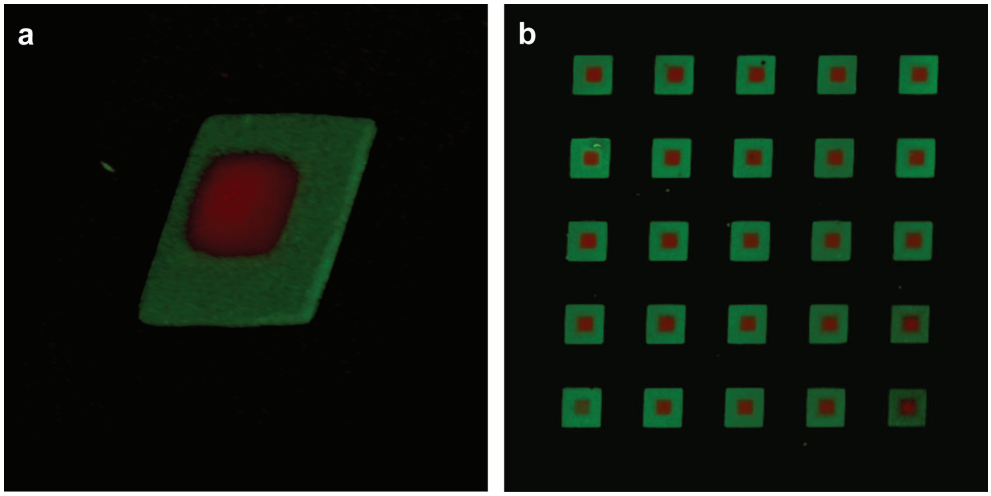

Figure 4. 3D-projections of CLSM micrographs of two-layer composite Dex-MA hydrogels fabricated using sequential imaging-assisted hydrogel patterning approach. Dex-MA-FITC hydrogel is colored green and is 250×250 μm, Dex-MA-TRITC hydrogel is colored red and is 100×100 μm.

of micro-particles having the same size, shape, made of the same material and differing only in color (25 μm, red and green). By selectively illuminating the area of the sample containing five micro-particles within a pre-gel solution (three red and two green), we have encased only the red ones in Dex-MA hydrogel (**Figure 5a**). After removing the non-embedded micro-spheres by simply rinsing the sample with water, we successfully isolated only the selected red micro-particles (**Figure 5b**). In object isolation, the minimal distance between objects that allows successful separation is an important parameter, and while we have not specifically determined it for our method, successful separation of particles 3 and 4 in **Figure 5a-b** demonstrates the efficiency of our method for separation of objects further apart than at least ~20 μm. Subsequently, isolated particles were released by using enzymatic degradation of the hydrogels surrounding them as monitored by CLSM (**Figure 4e-h**). Addition of a Dextranase solution (0.02 KDU-A/G) to the trapped particles, led to almost immediate fading of the fluorescence from the hydrogels surrounding the particles, indicating hydrogel degradation and dissolution.

One of the key characteristics of object isolation methods is efficacy of capture. To determine the capture efficacy for our technique, we performed several isolation experiments of green fluorescent 25 μm particles sedimented on the surface of a glass slide. For example, we selected 15 micro-particles from an area containing 53 individual green fluorescent micro-particles, and instructed the CLSM software to automatically apply a circular illumination profile (d = 200 μm) to the coordinates of the selected beads. Subsequent rinsing with water resulted in successful isolation of all 15 micro-spheres as was confirmed by CLSM (**Figure 5c-d**). By repeating this isolation procedure several times in different areas of the sample, we successfully isolated all 113 selected particles (100% success rate). Importantly, we observed no false positives, i.e. particles outside or in the periphery of the illuminated areas. Such high performance highlights the potential of our method for automated detection and embedding of objects based on their fluorescent signal.

Flexibility of this image-based selection and capture method is of particular interest for (single-) cell selection and isolation in a minimally invasive manner. For instance, it enables

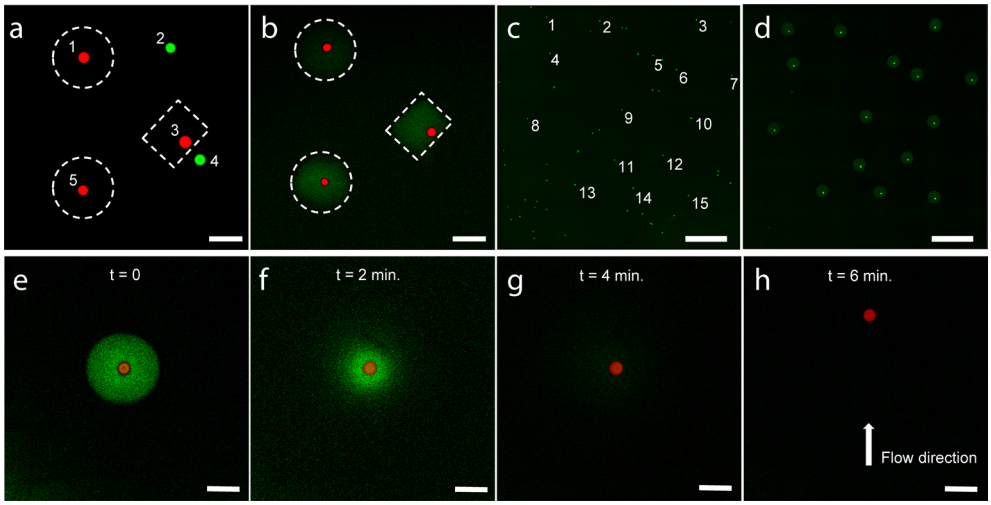

Figure 5. (**a-b**) CLSM micrographs illustrating selective capture and isolation of micro-particles from a mixture of green and red micro-particles. (**a**) First, illumination profiles are drawn to surround only the objects of interest (dashed lines). By illuminating the designated areas, hydrogels are formed selectively embedding the red particles. (**b**) After washing, the embedded objects are isolated while others are removed. (**c-d**) Micrographs of semi-automatic isolation of several selected particles from a group. The coordinates of 15 out of 53 particles were marked on the overview image (**c**). By applying circular illumination profiles of 100 µm to selected positions followed by rinsing with water, resulted in capture of selected particles (**d**). (**e-h**) Release of a captured micro-particle by enzymatic hydrogel degradation (Dextranase 0.02 KDU-A/G). Hydrogel (green) is quickly hydrolyzed upon exposure to Dextranase solution (**e-g**) and the particle is completely released within 6 min, as can be seen from its mobility when the flow is induced (**h**). Scale bars: a, b, e-h 100 µm; c, d 500 µm.

the isolation of cells with certain characteristics from a heterogeneous population, which can then be used for further analysis and/or propagation in diagnostics, cell-line development, and single-cell genomics studies. In order to be useful in these applications, our method has to guarantee high survival rate of captured cells. Even though Dex-MA has been reported to display excellent biocompatibility both *in vitro* and *in vivo*[24,42,43], to evaluate the impact of the developed technique on viability of isolated cells, we have performed live/dead assay on two types of adherent mammalian cells.

For this assay, NIH/3T3 or A549 cells were seeded in several glass-bottom petri dishes pre-functionalized with methacrylate groups and allowed to attach overnight. First, we determined the influence of embedding of these cells into Dex-MA hydrogels for several periods of time up to three hours. In short, culture medium was replaced with a 5% solution of Dex-MA containing 5 mg/ml LAP in PBS, cells were imaged by bright-field microscopy and a fraction of the populations was embedded into an array of hydrogel objects of ~250 µm by irradiating these areas with 405 nm light. Upon removal of the remaining Dex-MA solution by washing twice with PBS, we have obtained an array of cell-containing hydrogel objects surrounded by non-embedded cells, which served as an internal standard for comparing the impact of general toxicity of chemicals employed in this procedure and the effect of actual irradiation and encasing within a hydrogel matrix. After ~30 minutes after gel formation, cells were incubated for 30 minutes at room temperature with a live/dead labeling solution composed of 2 µM Calcein AM and 4 µM Ethidium homodimer-1 in PBS buffer. After a total time of one and three hours since the beginning of experiment, cells were imaged with CLSM allowing us to estimate the fraction of alive (green) and dead cells (red) (**Figure 6**). NIH/3T3

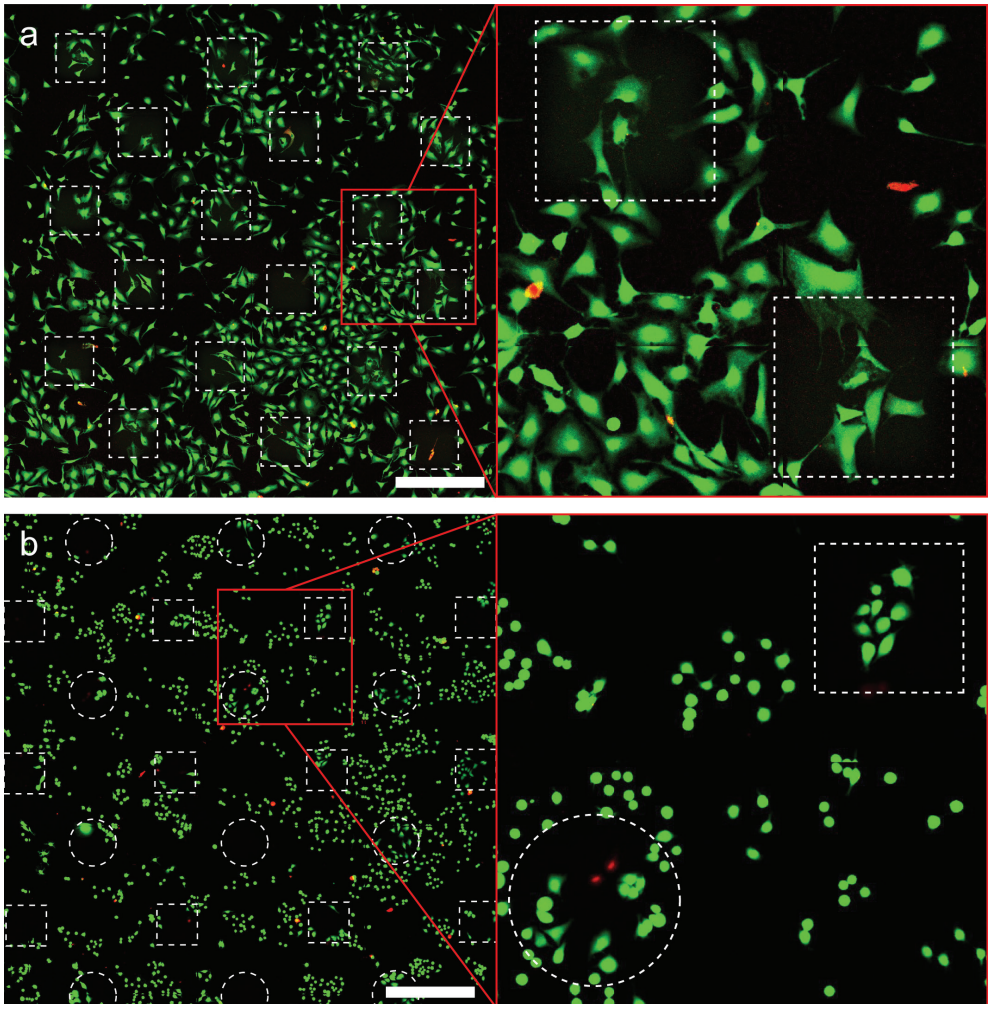

Figure 6. Fluorescence confocal micrographs of NIH/3T3 (**a**) and A549 (**b**) cells after three hours of being embedded in hydrogel stained using live/dead assay (green cells are alive, red cells are dead). In both cases the viability of cells within and outside of hydrogel was nearly identical. Scale bars 500 μm.

cells that were embedded into hydrogel blocks displayed viability of 99.2% (1 hour) and 98.1% (3 hours), which corresponded well to the viability of the cells surrounding the hydrogels, 98.6% and 97.3% respectively (**Table 1**). A549 cells incubated within the hydrogel displayed somewhat lower survival rate (95.7% after 1 hour, 92.0% after 3 hours), than the cells that remained outside, 97.8% and 97.7% respectively. Overall, average viability of the NIH/3T3 and A549 cells in the area of patterned gel objects after one hour was determined as 98.7% and 98.5%, which is nearly identical to the values observed for untreated control samples (99.2% and 99.6%).

Another group of cell samples was treated according to our developed cell-isolation protocol excluding the trypsinization step, to evaluate the effect of the cell-embedding and release using Dextranase. We repeated the embedding of the cells into hydrogel according to the above described procedure. However, instead of prolonged incubation of the cells

Cell type	Type of treatment	Live cells, % after 1 hr
NIH/3T3	***No treatment***	99.2
	Only gel formation:	
	Embedded in hydrogel	99.2
	Outside of hydrogel	98.6
	Average	98.7
	Gel formation + degradation	98.8
A549	***No treatment***	99.6
	Only gel formation:	
	Embedded in hydrogel	95.7
	Outside of hydrogel	97.8
	Average	98.5
	Gel formation + degradation	99.0

Table 1. Results of the viability assays performed on untreated, treated and hydrogel-embedded NIH/3T3 and A549 cells

inside of the hydrogel, after being embedded for 15 minutes, the samples were washed twice with PBS, after which Dextranase solution was introduced to degrade hydrogel and release the cells (15 minutes). Next, samples were rinsed twice with PBS and incubated for 30 minutes at room temperature with labeling solution composed of 2 μM Calcein AM and 4 μM Ethidium homodimer-1 in PBS buffer. After the incubation period, the cells were again washed twice with PBS and imaged by CLSM to determine the numbers of dead and alive cells. Since the gel objects were fully degraded, we could not measure separate viability rates for cells that were inside and outside of the hydrogel, instead we determined average cell viability in the areas where the patterning was performed. Both cell lines that were subjected to our separation procedure displayed excellent average viability of 98.8% and 99.0% for NIH/3T3 and A549 respectively. These results clearly demonstrate that such factors as irradiation with 405 nm light, potential toxicity of photo-initiator, generated radicals and Dextranase treatment, as well as encasing the cells into a Dex-MA hydrogel matrix, have nearly no effect on survival rate of the cells studied here. However, even though these observations indicate suitability of our method for live cell isolation, live/dead cell viability assay does not allow estimating any potential non-lethal damage incurred by the cells as a result of the treatment. Therefore, in order to assess full breadth of impact of this method on genetic and/or proteomic makeup of isolated cells, additional evaluations would need to be performed for cell types of interest.

To illustrate the potential of our cell-isolation technique, we performed a separation of a heterogeneous population of adherent cells. As a model of such cell population, we prepared a co-culture of NIH/3T3 mouse fibroblasts and A549 carcinoma cells, which were labeled

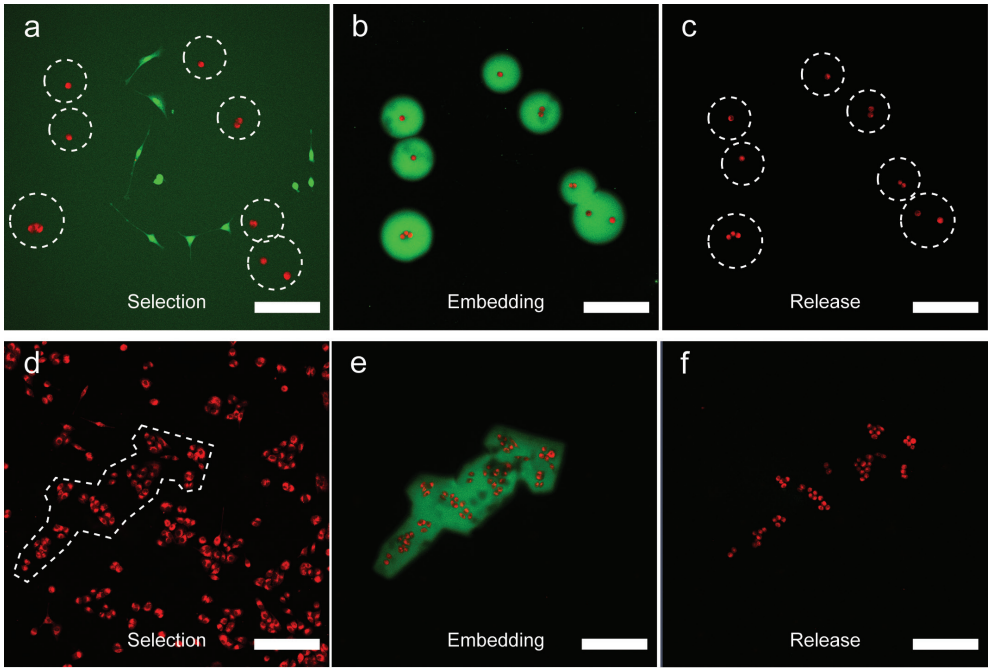

Figure 7. CLSM micrographs showing the selection, isolation, and release of A549 cells: (**a-c**) from a co-culture of green NIH/3T3 fibroblasts and red A549 carcinoma cells; (**d-f**) a large arbitrary population of red A549 cells. Scale bars 200 μm.

with green and red fluorescent dyes respectively, see Appendix for detailed experimental conditions. By directly applying developed four-step procedure to a co-culture of 3T3 and A549 cells, we have successfully isolated several selected A549 cells (**Figure 7**). In short, once the selected cells were embedded in a gel, the sample was washed twice with PBS. Next, trypsin-EDTA solution was applied to detach non-embedded cells, followed by their removal via washing sample twice with fresh PBS buffer, and thus leaving only cells trapped in the gel left behind. All embedded cells were then released by degrading the hydrogels with Dextranase solution, rinsed twice with PBS and re-introduced in their original cell-growth medium. As can be seen from **Figure 7b**, all initially selected A549 cells (red) out of the mixed population were isolated, while 3T3 fibroblasts (green) were removed, thus demonstrating the applicability of our technique for cell isolation based on their phenotypic properties, such as size and shape. Furthermore, due to the flexibility of hydrogel fabrication with our approach, it is also possible to isolate larger, arbitrarily shaped clusters of cells, as illustrated in **Figure 7d-f** by capture and release of a group of A549 cells (for more similar experiments see Figures S1-13). Finally, in view of high cell viability after such treatment, we expect all isolated cells to survive, since the entire procedure required less than 30 minutes to complete.

Conclusions

We have developed a convenient and flexible method for imaging-assisted cell isolation. It combines visualization, spatially controlled hydrogel formation and mild, enzymatic hydrogel degradation to identify, capture and separate specific cells or groups of cells from the rest of the population. We demonstrated the efficacy of the method by successfully isolating NIH/3T3 and A549 cells with high accuracy and nearly no cell damage as confirmed by

appropriate viability assays (>98%), thus illustrating a potential of this method for use in cell line development. While lower spatial resolution of our approach compared to existing cell-capture techniques may limit its application to medium density cell cultures, this potential drawback is overcome by our methods' speed, simplicity and no need for specialized expensive equipment. We believe that versatility and accessibility of the method presented here make it a useful tool in the field of cell culturing/isolation.

References

(1) Method of the Year 2013. *Nat. Publ. Gr.* **2014**, *11* (1).

(2) de Souza, N. Single-Cell Methods. *Nat. Methods* **2012**, *9* (1).

(3) Gross, A.; Schoendube, J.; Zimmermann, S.; Steeb, M.; Zengerle, R.; Koltay, P. Technologies for Single-Cell Isolation. *Int. J. Mol. Sci.* **2015**, *16* (8), 16897–16919.

(4) Nawy, T. Single-Cell Sequencing. *Nat. Methods* **2013**, *11* (1), 18–18.

(5) Anderson, M. T.; Tjioe, I. M.; Lorincz, M. C.; Parks, D. R.; Herzenberg, L. A.; Nolan, G. P. Simultaneous Fluorescence-Activated Cell Sorter Analysis of Two Distinct Transcriptional Elements within a Single Cell Using Engineered Green Fluorescent Proteins. *Proc. Natl. Acad. Sci.* **1996**, *93* (16), 8508–8511.

(6) Aubry, G.; Zhan, M.; Lu, H. Hydrogel-Droplet Microfluidic Platform for High-Resolution Imaging and Sorting of Early Larval Caenorhabditis Elegans. *Lab Chip* **2015**, *15* (6), 1424–1431.

(7) Kovac, J. R.; Taff, B. M.; Voldman, J. Enabling Technologies for Image-Based Cell Sorting. In *Microdevices in Biology and Medicine*; 2009; pp 129–148.

(8) Lau, A. K. S.; Shum, H. C.; Wong, K. K. Y.; Tsia, K. K.; Fritzsch, F.; Dusny, C.; Frick, O.; Schmid, A.; Zare, R.; Kim, S.; et al. Optofluidic Time-Stretch Imaging – an Emerging Tool for High-Throughput Imaging Flow Cytometry. *Lab Chip* **2016**, *16* (10), 1743–1756.

(9) Ozaki, Y.; Uda, S.; Saito, T. H.; Chung, J.; Kubota, H.; Kuroda, S. A Quantitative Image Cytometry Technique for Time Series or Population Analyses of Signaling Networks. *PLoS One* **2010**, *5* (4), e9955.

(10) Espina, V.; Wulfkuhle, J. D.; Calvert, V. S.; VanMeter, A.; Zhou, W.; Coukos, G.; Geho, D. H.; Petricoin, E. F.; Liotta, L. A. Laser-Capture Microdissection. *Nat. Protoc.* **2006**, *1* (2), 586–603.

(11) Emmert-Buck, M. R.; Bonner, R. F.; Smith, P. D.; Chuaqui, R. F.; Zhuang, Z.; Goldstein, S. R.; Weiss, R. A.; Liotta, L. A. Laser Capture Microdissection. *Science* **1996**, *274* (5289), 998–1001.

(12) Nancy Allbritton, Christopher Sims, Yuli Wang, P. K. S. Array of Micromolded Structures for Sorting Adherent Cells. US20130065795, **2010**.

(13) Koller, M. R.; Hanania, E. G.; Stevens, J.; Eisfeld, T. M.; Sasaki, G. C.; Fieck, A.; Palsson, B.

High-Throughput Laser-Mediated in Situ Cell Purification with High Purity and Yield. *Cytom. Part A* **2004**, *61* (2), 153–161.

(14) Hosokawa, M.; Arakaki, A.; Takahashi, M.; Mori, T.; Takeyama, H.; Matsunaga, T. High-Density Microcavity Array for Cell Detection: Single-Cell Analysis of Hematopoietic Stem Cells in Peripheral Blood Mononuclear Cells. *Anal. Chem.* **2009**, *81* (13), 5308-5313.

(15) Környei, Z.; Beke, S.; Mihálffy, T.; Jelitai, M.; Kovács, K. J.; Szabó, Z.; Szabó, B.; Herzenberg, L. A.; Sweet, R. G.; Herzenberg, L.; et al. Cell Sorting in a Petri Dish Controlled by Computer Vision. *Sci. Rep.* **2013**, *3*, 108–117.

(16) Yoshimoto, N.; Kida, A.; Jie, X.; Kurokawa, M.; Iijima, M.; Niimi, T.; Maturana, A. D.; Nikaido, I.; Ueda, H. R.; Tatematsu, K.; et al. An Automated System for High-Throughput Single Cell-Based Breeding. *Sci. Rep.* **2013**, *3*, 42.

(17) Ungai-Salánki, R.; Gerecsei, T.; Fürjes, P.; Orgovan, N.; Sándor, N.; Holczer, E.; Horvath, R.; Szabó, B.; Shendure, J.; Ji, H.; et al. Automated Single Cell Isolation from Suspension with Computer Vision. *Sci. Rep.* **2016**, *6*, 20375.

(18) Kovac, J.; Gerardin, Y.; Voldman, J. Image-Predicated Sorting of Adherent Cells Using Photopatterned Hydrogels. *Adv. Healthc. Mater.* **2013**, *2* (4), 552–556.

(19) Shin, D.-S.; You, J.; Rahimian, A.; Vu, T.; Siltanen, C.; Ehsanipour, A.; Stybayeva, G.; Sutcliffe, J.; Revzin, A. Photodegradable Hydrogels for Capture, Detection, and Release of Live Cells. *Angew. Chem. Int. Ed. Engl.* **2014**, *53* (31), 8221–8224.

(20) Sun, T.; Kovac, J.; Voldman, J. Image-Based Single-Cell Sorting via Dual-Photopolymerized Microwell Arrays. *Anal. Chem.* **2014**, *86* (2), 977–981.

(21) Tamura, M.; Yanagawa, F.; Sugiura, S.; Takagi, T.; Sumaru, K.; Matsui, H.; Kanamori, T. Optical Cell Separation from Three-Dimensional Environment in Photodegradable Hydrogels for Pure Culture Techniques. *Sci. Rep.* **2014**, *4*, 4793.

(22) Truong, V. X.; Tsang, K. M.; Simon, G. P.; Boyd, R. L.; Evans, R. A.; Thissen, H.; Forsythe, J. S. Photodegradable Gelatin-Based Hydrogels Prepared by Bioorthogonal Click Chemistry for Cell Encapsulation and Release. *Biomacromolecules* **2015**, *16* (7), 2246–2253.

(23) Chien, M.-P.; Werley, C. A.; Farhi, S. L.; Cohen, A. E. Photostick: A Method for Selective Isolation of Target Cells from Culture. *Chem. Sci.* **2015**, *6* (3), 1701–1705.

(24) Cadée, J. A.; van Luyn, M. J.; Brouwer, L. A.; Plantinga, J. A.; van Wachem, P. B.; de Groot, C. J.; den Otter, W.; Hennink, W. E. In Vivo Biocompatibility of Dextran-Based Hydrogels. *J. Biomed. Mater. Res.* **2000**, *50* (3), 397–404.

(25) De Groot, C. In Vitro Biocompatibility of Biodegradable Dextran-Based Hydrogels Tested with Human Fibroblasts. *Biomaterials* **2001**, *22* (11), 1197–1203.

(26) *Polysaccharides II*; Klemm, D., Ed.; Advances in Polymer Science; Springer Berlin Heidelberg: Berlin, Heidelberg, **2006**; Vol. 205.

(27) van Dijk-Wolthuis, W. N. E.; Franssen, O.; Talsma, H.; van Steenbergen, M. J.; Kettenes-van

den Bosch, J. J.; Hennink, W. E. Synthesis, Characterization, and Polymerization of Glycidyl Methacrylate Derivatized Dextran. *Macromolecules* **1995**, *28* (18), 6317–6322.

(28) van Dijk-Wolthuis, W. N. E.; Kettenes-van den Bosch, J. J.; van der Kerk-van Hoof, A.; Hennink, W. E. Reaction of Dextran with Glycidyl Methacrylate: An Unexpected Transesterification. *Macromolecules* **1997**, *30* (11), 3411–3413.

(29) Kim, S. H.; Chu, C. C. Synthesis and Characterization of Dextran-Methacrylate Hydrogels and Structural Study by SEM. *J. Biomed. Mater. Res.* **2000**, *49* (4), 517–527.

(30) Bertz, A.; Wöhl-Bruhn, S.; Miethe, S.; Tiersch, B.; Koetz, J.; Hust, M.; Bunjes, H.; Menzel, H. Encapsulation of Proteins in Hydrogel Carrier Systems for Controlled Drug Delivery: Influence of Network Structure and Drug Size on Release Rate. *J. Biotechnol.* **2013**, *163* (2), 243–249.

(31) Das, D.; Pal, S. Modified Biopolymer-Dextrin Based Crosslinked Hydrogels: Application in Controlled Drug Delivery. *RSC Adv.* **2015**, *5* (32), 25014–25050.

(32) Gao, Y.; Kieltyka, R. E.; Jesse, W.; Norder, B.; Korobko, A. V; Kros, A. Thiolated Human Serum Albumin Cross-Linked Dextran Hydrogels as a Macroscale Delivery System. *Soft Matter* **2014**, *10* (27), 4869–4874.

(33) Ghugare, S. V.; Chiessi, E.; Cerroni, B.; Telling, M. T. F.; Sakai, V. G.; Paradossi, G. Biodegradable Dextran Based Microgels: A Study on Network Associated Water Diffusion and Enzymatic Degradation. *Soft Matter* **2012**, *8* (8), 2494.

(34) Hennink, W. E.; Talsma, H.; Borchert, J. C. H.; De Smedt, S. C.; Demeester, J. Controlled Release of Proteins from Dextran Hydrogels. *J. Control. Release* **1996**, *39* (1), 47–55.

(35) Kim, S. H.; Won, C. Y.; Chu, C. C. Synthesis and Characterization of Dextran-Based Hydrogel Prepared by Photocrosslinking. *Carbohydr. Polym.* **1999**, *40* (3), 183–190.

(36) Li, D.; Kordalivand, N.; Fransen, M. F.; Ossendorp, F.; Raemdonck, K.; Vermonden, T.; Hennink, W. E.; van Nostrum, C. F. Reduction-Sensitive Dextran Nanogels Aimed for Intracellular Delivery of Antigens. *Adv. Funct. Mater.* **2015**, *25* (20), 2993–3003.

(37) Liu, Z. Q.; Wei, Z.; Zhu, X. L.; Huang, G. Y.; Xu, F.; Yang, J. H.; Osada, Y.; Zrínyi, M.; Li, J. H.; Chen, Y. M. Dextran-Based Hydrogel Formed by Thiol-Michael Addition Reaction for 3D Cell Encapsulation. *Colloids Surf. B. Biointerfaces* **2015**, *128*, 140–148.

(38) Lo, C.-W.; Jiang, H. Photopatterning and Degradation Study of Dextran-Glycidyl Methacrylate Hydrogels. *Polym. Eng. Sci.* **2010**, *50* (2), 232–239.

(39) Vermonden, T.; Censi, R.; Hennink, W. E. Hydrogels for Protein Delivery. *Chem. Rev.* **2012**, *112* (5), 2853–2888.

(40) W. N. E. van Dijk-Wolthuis; J. A. M. Hoogeboom; M. J. van Steenbergen; S. K. Y. Tsang, A.; Hennink*, W. E. Degradation and Release Behavior of Dextran-Based Hydrogels. **1997**.

(41) Xu, D.; Wu, F.; Chen, Y.; Wei, L.; Yuan, W. pH-Sensitive Degradable Nanoparticles for Highly Efficient Intracellular Delivery of Exogenous Protein. *Int. J. Nanomedicine* **2013**, *8* (1), 3405–3414.

(42) De Groot, C. J.; Van Luyn, M. J. .; Van Dijk-Wolthuis, W. N. .; Cadée, J. A.; Plantinga, J. A.;

Otter, W. Den; Hennink, W. E. In Vitro Biocompatibility of Biodegradable Dextran-Based Hydrogels Tested with Human Fibroblasts. *Biomaterials* **2001**, *22* (11), 1197–1203.

(43) Wang, H.; Zhou, L.; Liao, J.; Tan, Y.; Ouyang, K.; Ning, C.; Ni, G.; Tan, G. Cell-Laden Photocrosslinked GelMA–DexMA Copolymer Hydrogels with Tunable Mechanical Properties for Tissue Engineering. *J. Mater. Sci. Mater. Med.* **2014**, *25* (9), 2173–2183.

(44) Majima, T.; Schnabel, W.; Weber, W. Phenyl-2,4,6-trimethylbenzoylphosphinates as Water-soluble Photoinitiators. Generation and Reactivity of $O{=}P^{\cdot}(C_6H_5)(O^{-})$ Radical Anions. *Die Makromol. Chemie* **1991**, *192* (10), 2307–2315.

(45) Fairbanks, B. D.; Schwartz, M. P.; Bowman, C. N.; Anseth, K. S. Photoinitiated Polymerization of PEG-Diacrylate with Lithium Phenyl-2,4,6-Trimethylbenzoylphosphinate: Polymerization Rate and Cytocompatibility. *Biomaterials* **2009**, *30* (35), 6702–6707.

Appendix

General procedure of Dextran functionalization (Dex-MA)

The preparation of Dex-MA was performed according to previously described procedure.[27] In short, 10 g of dextran (500kDa) and 2 g DMAP were dissolved in 100 mL DMSO by vigorous stirring. To this solution the required amount of glycidylmethacrylate was added and the reaction mixture was stirred at 30°C for 24 hours. The pH of the reaction mixture was adjusted to 7 by the addition of a 1M HCl solution and subsequently diluted with 100 mL water. Subsequently, the reaction mixture was extensively dialyzed at 5°C over a period of 10 days after which it was freeze dried and Dex-MA was obtained as a white fluffy powder. Degree of substitution (DS; the amount of methacrylate groups per 100 dextran glucopyranose residues) was determined by ^{1}H-NMR.

Preparation of Lithium-phenyl-2,4,6-trimethylbenzoyl-phosphinate (LAP)

The photoinitiator (LAP, see Figure S1c) was prepared according to procedure previously described.44,45 In short, under a nitrogen atmosphere 2,4,6-trimethylbenzoyl-chloride (4.8 g) was added drop-wise to an equimolar amount of dimethyl phenylphosphonite (4.5 g). The reaction mixture was stirred for 18 hours at room temperature after which a solution of lithium bromide (9.2 g) in 2-butanone (150 mL) was added. The reaction mixture was subsequently heated to 50°C for one hour leading to the formation of a suspension which was allowed to cool down to room temperature and left to rest for four hours. The suspension was filtered and the residue was washed with 2-butanone and subsequently dried under vacuum and a white powder was obtained in near quantitative yields. Product was characterized by ^{1}H-, ^{13}C-, and ^{31}P-NMR and matched previous literature.

Glass surface modification

Glass surfaces were cleaned with ethanol, dried with air, and subsequently plasma treated for 2:20 minutes. Silanization was performed by vapour deposition of 3-(Trichlorosilyl) propyl methacrylate. The activated glass slides were placed in a desiccator containing 75 µL of 3-(Trichlorosilyl)propyl methacrylate placed in an open petri dish. The chamber was evacuated a left under static vacuum for two hour followed by a dynamic vacuum for an additional two hour. The modified surfaces showed a contact angle 70-80° with water

Macroscopic hydrogel preparation

A 500 µL aqueous solution containing Dex-MA (5 wt%), LAP (0.5 wt%) was stirred in the dark at room temperature until a homogenous solution was obtained. The clear solution was illuminated for one second (except for Dex-MA2.5 which needed six second of illumination) using a Nikon Intensilight C-HGFI equipped with a 1.5-meter optical fiber, instantly leading to the formation of a stable transparent hydrogel.

Macroscopic hydrogel degradation by dextranase

A 250 µL aqueous solution containing Dex-MA (5 wt%), LAP (0.5 wt%) was stirred in the dark at room temperature until a homogenous solution is obtained. The clear solution was illuminated for one second using a Nikon intensilight C-HGFI equipped with a 1.5-meter optical fiber and a hydrogel was obtained, Figure S1a. To the hydrogel 250 µL of dextranase solution (activity: ≥ 100 KDU-A/G) was added (Figure S1b) and the vial was heated to 35°C. Within 10 minutes the hydrogel was completely degraded and a non-viscous solution was obtained as could be visually observed, see Figure S1c.

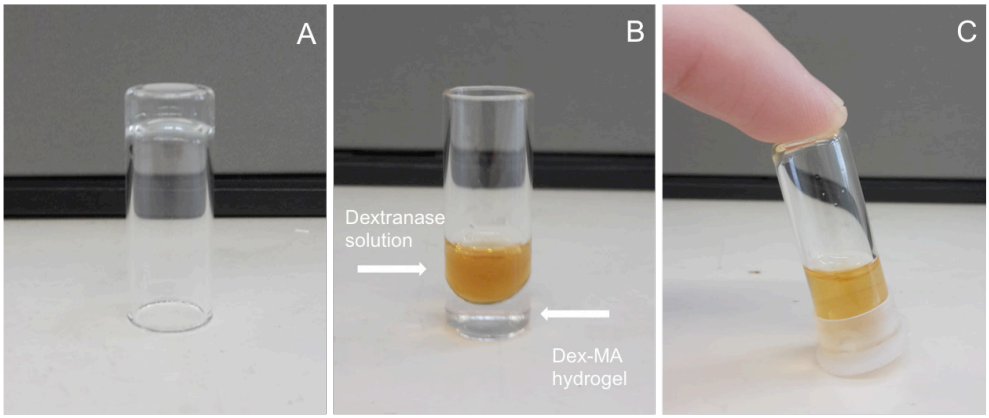

Figure S1. a) A 0.25 mL Dex-MA10 hydrogel, b) Dex-MA10 hydrogel covered with 0.25 mL dextranase solution at t = 0, c) solution of completely degraded Dex-MA10 hydrogel by dextranase after 10 minutes at 35°C.

CLSM direct hydrogel writing procedure

A solution (29 µL) of Dex-MA10 (5 wt%), LAP (0.5 wt%) and dextran labeled with fluorescein (Dex-FITC, 0.02 wt%) was placed upon a methacrylate tethered glass slide. The sample was covered with a plastic cover slide (24 × 24 mm) to form a 50 µm layer. The sample was imaged using laser wavelength of 488 nm, and collection from 495 – 700 nm (standard fluorescein imaging conditions) and focus point was placed in the middle of the sample. The desired illumination profile is drawn, see Figure S2a, and illuminated unidirectionally with 405 nm. For specified illumination settings using 10× and 40× objectives see description below. Subsequently, imaging the sample using standard fluorescein conditions, showed bleaching of the illuminated area where the hydrogels are formed, see Figure S2b. The transparency sheet is carefully removed and the hydrogel objects are rinsed with water. The fabricated objects are subsequently visualized, see Figure S2c.

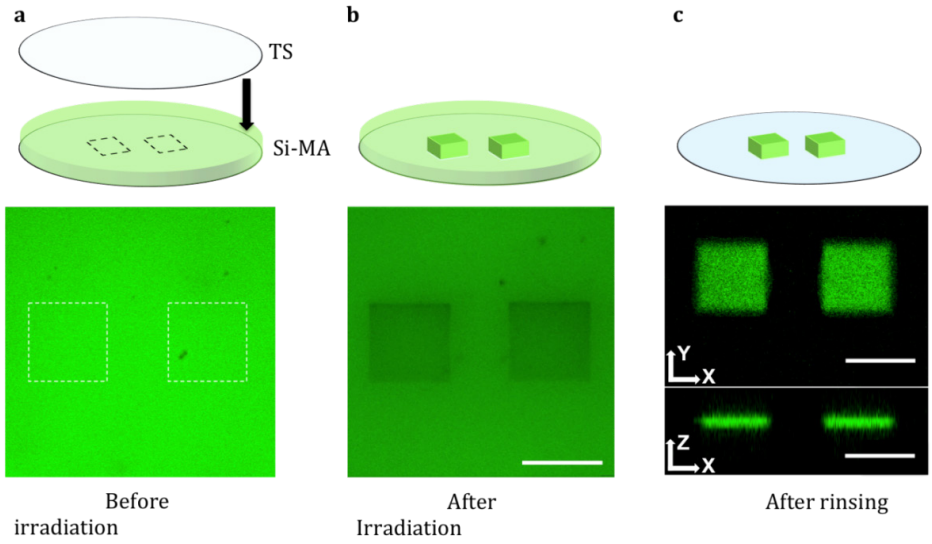

Figure S2. Experimental procedure for direct Dex-MA10 hydrogel writing with CLSM. a) Top: aqueous solution of Dex-MA10 (5 wt%), LAP (0.5 wt%), and Dex-FL (0.02 wt%) intercalated between a Si-MA slide and a plastic cover slide. Bottom: two squared illumination profiles, designated with dashed lines. b) Top: hydrogel is formed selectively in illuminated areas. Bottom: illuminated areas are slightly bleached compared to the surrounding solution due to illumination at 405 nm. c) Top: after rinsing the glass slide with water covalently bound hydrogel objects remain. Bottom: fluorescence confocal image of obtained hydrogel objects, scale bars 200 µm.

Experimental conditions using 10× objective

Experiments were performed as described above, settings: frame 1024 × 1024, pixel size: 0.83 × 0.83 µm, pixel dwell: 0.64 µs, laser-diode power 100%. Averaging (number times an area was illuminated) was adjusted to control total illumination time to study hydrogel formation. Figure S3 shows the effect of averaging once (S3a) twice (S3b), and four times (S3c), corresponding to illumination times of 0.93 µs/µm^2, 1.86 µs/µm^2, 3.71 µs/µm^2 respectively. Under applied experimental conditions an illumination time of 3.71 µs/µm^2 was found to be optimal for hydrogel fabrication.

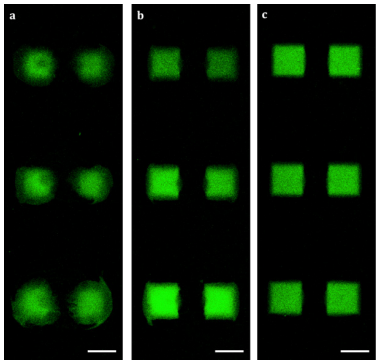

Figure S3. Fluorescence confocal images of hydrogel objects obtained by illumination times of a) 0.93 µs/µm^2 b, 1.86 µs/µm^2 c, 3.71 µs/µm^2. Experimental settings: illumination through 10× objective, frame 1024 × 1024, pixel size: 0.83 x 0.83 µm, pixel dwell: 0.64 µs, laser-diode power 100%.

Experimental conditions using 40× objective

Experiments were performed as described above, settings: frame 1024 × 1024, 0.21 × 0.21 µm, pixel dwell: 0.64 µs, averaging: 2, exposure time: 4.36 µs/µm^2. In these experiments the power of the laser-diode was adjusted to study hydrogel formation. Figure S4 shows the effect of illumination using a laser power of 2.4 %, 10 %, 50 %, and 100 %. Laser-diode power of 2.4% did not lead to well-defined hydrogel object (S4a), increasing the power to 10% led to fabrication of well-defined hydrogel objects (S4b). Applying even higher laser power of 50 and 100% led to significant hydrogel formation outside of the desired areas and significant bleaching of illuminated areas, see S4c and S4d respectively. Under applied experimental conditions illumination time of 4.36 µs/µm^2, using a laser-diode power of 10% was found to be optimal for hydrogel fabrication.

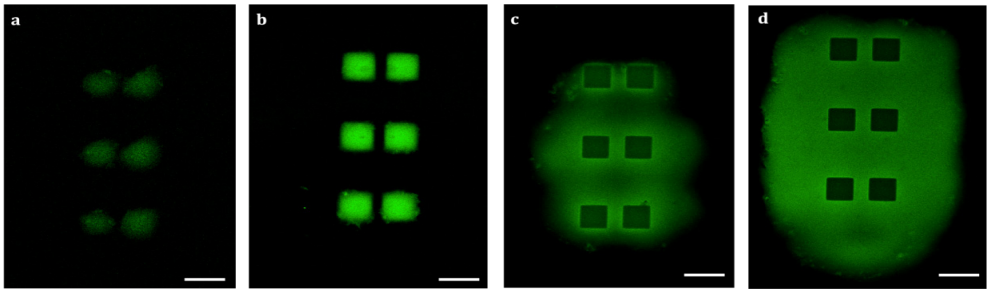

Figure S4. Fluorescence confocal images of hydrogel objects obtained by illumination with different laser-diode power of 2.4% a, 10% b, 50% c, 100% d. Experimental settings: illumination through 40× objective, pixel size: 0.21 × 0.21 µm, pixel dwell: 0.64 µs, averaging: 2, exposure time: 4.36 µs/µm^2.

Patterning resolution

The smallest feature size obtainable was determined by applying an illumination profile of an extended triangle measuring the size of the smallest feature of the hydrogel that was arbitrarily well-defined. It was found that feature sizes down to 50 µm and 15 µm could easily be obtained with 10× and 40× objectives respectively see Figures S5 and S6.

Resolutions limits of CLSM hydrogel writing was determined using an illumination profile consisting of two separated rectangular areas (dashed rectangles in Figure S7 and S8 for illumination through a 10× and 40× objective respectively) and controlling the spacing between them. Experimental parameters used are as described above. It was found that illumination through a 10× objective successfully led to the formation of two individual hydrogel objects using a spacing of 100, 60, 45, and 35 µm while a spacing of 25 µm led to the merging of the two hydrogel objects, see Figure S7. By applying the same methodology using a 40× objective it was found that spacing of 40, 25, and 15 µm successfully led to the formation of two individual hydrogel objects while 10 µm led to merging, see Figure S8. Based on these results the resolution was found to be 35 µm and 15 µm for 10× and 40× objectives respectively.

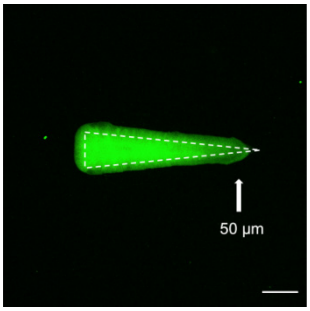

Figure S5. Fluorescence confocal images of hydrogel triangle obtained by illumination of area indicated by white dashed line (height: 100 µm, length: 500 µm) through 10× objective, smallest well-defined feature is determined to be approximately 50 µm scale bar 100 µm.

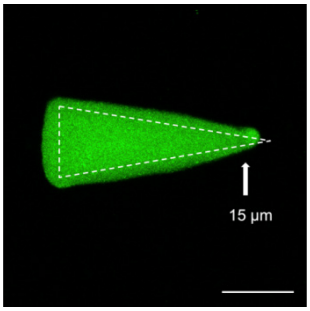

Figure S6. Fluorescence confocal images of hydrogel triangle obtained by illumination of area indicated by white dashed line (height: 50 µm, length: 360 µm) through 40× objective, smallest well-defined feature is determined to be approximately 15 µm, scale bar 50 µm.

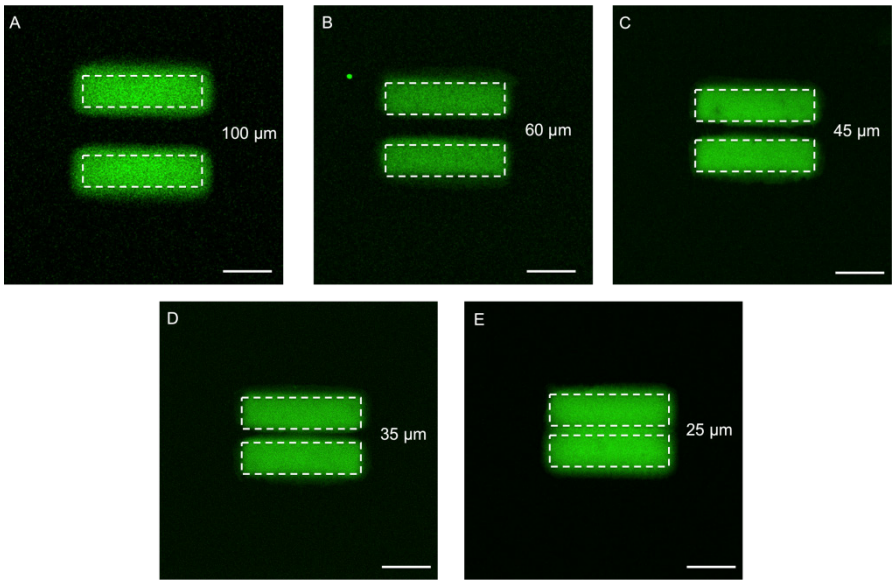

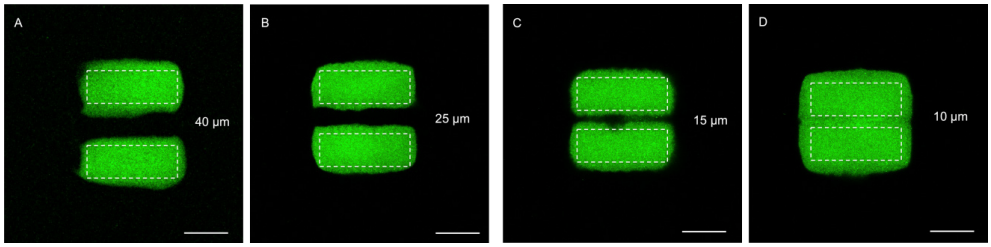

Figure S8. Fluorescence confocal images of hydrogel objects obtained by illumination of two rectangular areas (white dashed line 80 × 30 µm) with various spacing, 40 µm a, 25 µm b, 15 µm c, 10 µm d. Scale bars 50 µm.

Hydrogel shape analysis

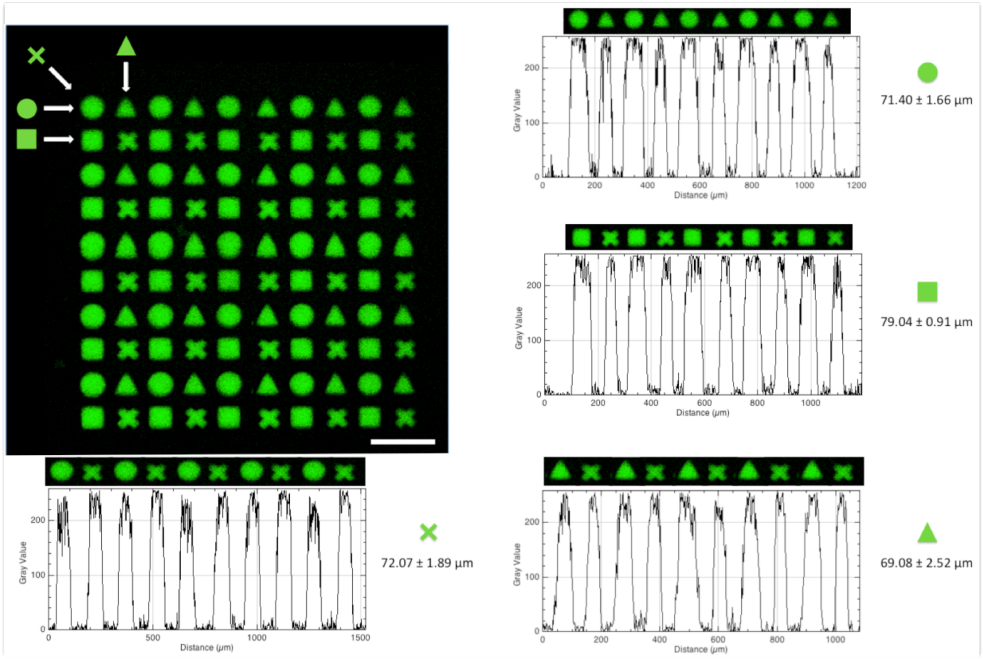

Figure S9. Hydrogel shape analysis of a 5 × 5 tile containing four different objects a circle, square, triangle, and a cross. The analysis shows that the objects were well defined and could be prepared in a reproducible manner. Arrows in figure show the directionality in which the object sizes were determined, circle: 71.40 ± 1.66 µm, square: 79.04 ± 0.91 µm, cross: 72.07 ± 1.89 µm, triangle 69.08 ± 2.52 µm. Scale bar 200 µm. CLSM image was obtained using standard fluorescein imaging conditions. Scale bar 200 µm.

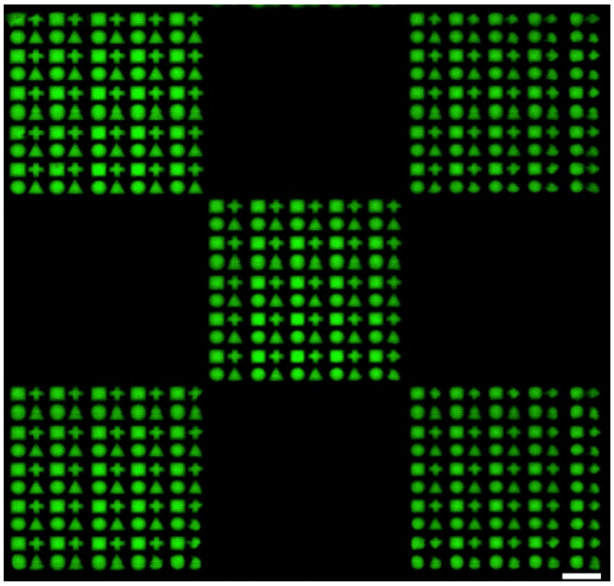

Figure S10. Fluorescence CLSM image of a checkerboard consisting of 5 tiles of 100 hydrogel objects each (circles, squares, triangles, and crosses) fabricated fully automatic. Scale bar 200 µm.

Micro-particle embedding, experimental conditions using 10× objective

Illumination experiments were performed as described above, using the following experimental settings: frame 1024 × 1024, pixel size: 0.83 × 0.83 µm, pixel dwell: 1.27 µs, laser-diode power: 100%, averaging: 4. Circular illumination profiles of 100-200 µm were applied surrounding the micro-particles of interest. After illumination the plastic cover slide was carefully remove and the sample was rinsed with water (4 times) and imaged with confocal microscope, see figure S11.

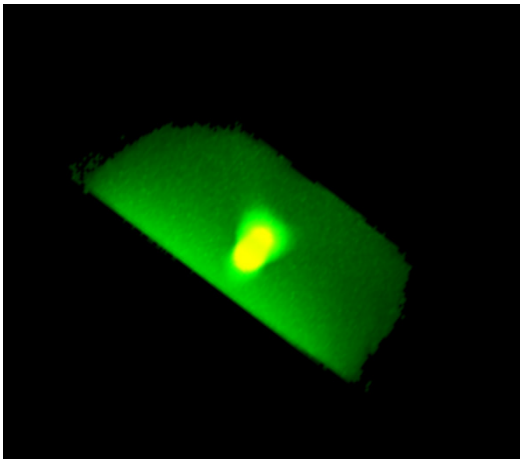

Figure S11. Three-dimensional confocal image of a green fluorescent micro-particle 25 µm embedded in a 200 µm hydrogel.

Cell lines, co-culture and viability assay

The cell lines used in this study were A549 human lung carcinoma cells and NIH/3T3 mouse embryonic fibroblasts both obtained from the American Type Culture Collection (ATCC, USA). The A549 cells were cultured in Dulbecco's modified Eagle's medium (DMEM) supplemented with 10% Fetal Bovine Serum (FBS) and 0.5% (v/v) penicillin-streptomycin. NIH/3T3 fibroblasts were cultured in DMEM supplemented with 10% Newborn Calf Serum (NCS) and 0.5% (v/v) penicillin-streptomycin. For the experimental studies, cell cultures were prepared from frozen stock vials and seeded in 25 cm^2 culture bottles (Cellstar, Greigner Bio-One). Cells were incubated under standard cell culture conditions (37°C, 5% CO_2 atmosphere and water-saturated 95% air) and maintained until sub-confluence was reached (70-80%).

For the co-culture assays, NIH/3T3 cells were seeded in 35 mm glass-bottom petri dishes (In Vitro Scientific) and allowed to adhere for 24 h. Then, adherent NIH/3T3 cells were labelled with a CellTracker™ Green 5-chloromethylfluorescein diacetate solution (Molecular Probes, C7025) at a concentration of 10 µM in serum-free medium for 45 minutes at 37°C. Cells were then washed twice with Dulbecco's Phosphate-Buffered Saline (DPBS, Gibco) and covered with fresh culture medium. Simultaneously, A549 cells were labelled in suspension with the CellTracker™ Red CMTPX probe (Molecular Probes, C34552) at a concentration of 10 µM in serum-free medium for 30 minutes at 37°C. A549 cells were washed twice with cell culture medium and CellTracker™-loaded A549 cells in suspension were added to the petri dishes containing the green labeled NIH/3T3 cells to obtain simultaneously co-culture of green NIH/3T3 cells and red A549 cells. Experiments were performed on the following day to

allow the attachment of the A549 cells.

Cell selection, embedding and isolation

After obtaining co-cultures of CellTracker™ Green-loaded NIH/3T3 cells and CellTracker™ Red-loaded A549 cells in glass-bottom petri dishes, the medium was removed and cells were washed twice with PBS (1X). Then, a Dex-MA10 solution (5 wt%) prepared in PBS with Dex-FITC (0.02 wt%) was added to form a thin layer on top of the cells and cells were imaged by confocal microscopy using a 10x objective. A digital mask was drawn around the selected cells and illumination was performed following the procedures described above and optimized experimental settings: frame 1024 × 1024, pixel size: 0.83 × 0.83 µm, pixel dwell: 1.27 µs, laser-diode power: 100%, averaging: 4. After formation of the hydrogels, the cells were washed 2 times with PBS (1X) and Trypsin-EDTA solution (0.25%) was added and incubated at 37°C for 5 minutes. The detached cells were washed twice with PBS (1X) and DPBS was added. The selected cells embedded in the hydrogels and imaged. Cell release was performed by the addition of 50 µL Dextranase (dilution factor of 1000) at room temperature, degradation times were found to be approximately 10-15 minutes.

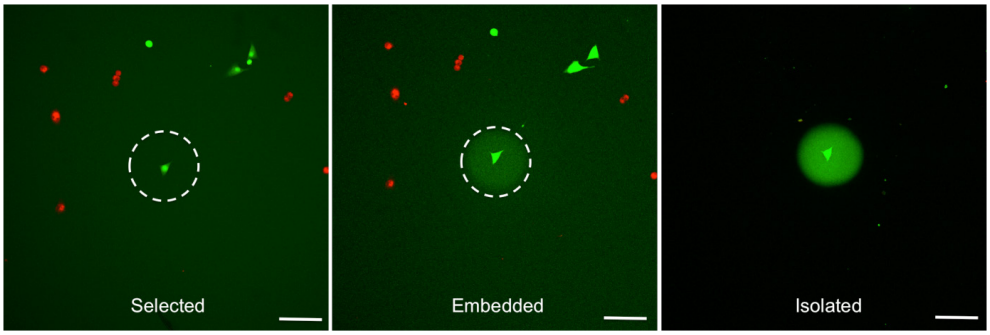

Figure S12. Fluorescence confocal images of an isolation experiment of a single NIH/3T3 cell from a heterogeneous sample. Left, single cell is selected and a circular illumination profile is applied. Middle, cell is successfully embedded in hydrogel. Right, After trypsinization unwanted cells were suspended and washed away. Scale bars 100 µm.

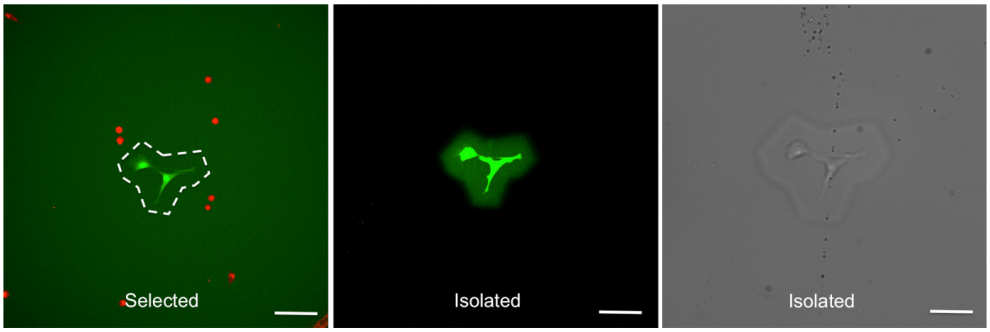

Figure S13. Fluorescence confocal and transmission microscope images of an isolation experiment of a pair of NIH/3T3 cells from a heterogeneous sample. Left, pair of cells is selected and a matching illumination profile is applied. Middle and right, CLSM and transmission images of embedded cells that are successfully isolated after trypsinization removing of unwanted cells. Scale bars 100 µm.

Chapter 5

Microfluidic shrinking of aqueous droplets for continuous production of micron-sized particles*

Abstract

Versatile and controlled production of micro-particles in a range of sizes within a single microfluidic device is often challenging in traditional droplet microfluidics. Here, we present a microfluidic platform for shrinking of aqueous droplets applied to production of polymeric micro-hydrogels. Continuous on-chip shrinking was achieved by controlled extraction of water into the surrounding immiscible 1-octanol phase. Adjusting the initial polymer concentration within the droplet phase allowed us to produce particles of a controlled range of sizes within a single device geometry. Additionally, the method developed here represents a way to produce identical multi-phase aqueous droplets, which can be further exploited for structuring and compartmentalization of hydrogel particles.

*Manuscript in preparation

Introduction

Micro-hydrogels are micro-particles (0.1-100 μm in diameter) generally consisting of a water-swollen cross-linked polymer network.[1] In recent years, they found many applications in fields ranging from food and cosmetics to oil recovery and controlled drug delivery.[2] Due to this growing interest, many micro-hydrogel production methods have been developed, among which droplet microfluidics is one of the most promising and versatile.

Droplet microfluidics is an efficient tool for producing various polymeric micro-particles, offering high degree of control over their composition, size and dispersity. By controlling the formation of aqueous droplets containing pre-gel solution (monomers, cross-linkable polymers, etc.), droplet microfluidics allows precisely controlling the size, and sometimes even shape, of the desired microgels.[3] Commonly, droplet microfluidics allows producing particles in the size range of 5-500 μm, but a single device design is usually not able to span such broad range. This leads to the necessity of using different chip architectures for every specific narrow particle size range.

One potential way to address this problem is to use controlled on-chip shrinking of droplets formed by dilute solutions. Such strategy allows tuning the size of produced particles by simply changing the initial composition of the droplets, thus expanding the size range attainable with a single device geometry. Droplet shrinking is achieved either through evaporation of the droplet-forming phase or through its controlled extraction by the carrying fluid. Recently, several studies have explored the application of both shrinking approaches for microfluidics-based concentration of extremely dilute analytes, thus greatly improving their limits of detection.[4–8] Kojima *et al* have employed similar concept to study polymer phase-separation in aqueous micro-droplets.[9] Some initial attempts to produce polymeric micro-particles using microfluidic extraction of partially water-soluble organic phase by aqueous flow have also been demonstrated.[10–12] Further extending this concept for production of alginate-based micro-hydrogels, several groups have exploited limited solubility of water in dimethylcarbonate and 1-undecanol (oil phase).[13,14] However, continuous production of such hydrogel particles, while at the same time being able to adjust their size, still remains to be challenging.

Here we present a method for controlled dehydration of droplets composed of dilute aqueous polymer solutions by exploiting partial water solubility in 1-octanol (carrier phase), eventually leading to the formation of dry polymeric micro-spheres, which upon cross-linking followed by rehydration are transformed into microgels. By adjusting initial polymer concentration in the droplet phase we could tune the final size of produced particles without the need of re-designing required microfluidic device. Additionally, we could achieve up to a 60000-fold decrease of droplet volume, allowing us to produce sub-10 micrometer particles starting from ~100 μm droplets. Finally, our approach allows controlling the dehydration rate by changing the initial water content in the continuous phase, thus offering the means to potentially tune the size and microstructure of produced particles.

Results

To achieve controlled shrinking of aqueous droplets in this work we exploited limited solubility of water (~4% v/v) in a continuous phase formed by 1-octanol. Octanol was selected due to its low solubility in water and good compatibility with poly(dimethylsiloxane) (PDMS), allowing to perform dehydration experiments in cheap and easy-to-make PDMS microfluidic devices. As a model hydrophilic solute for production of microparticles we have chosen

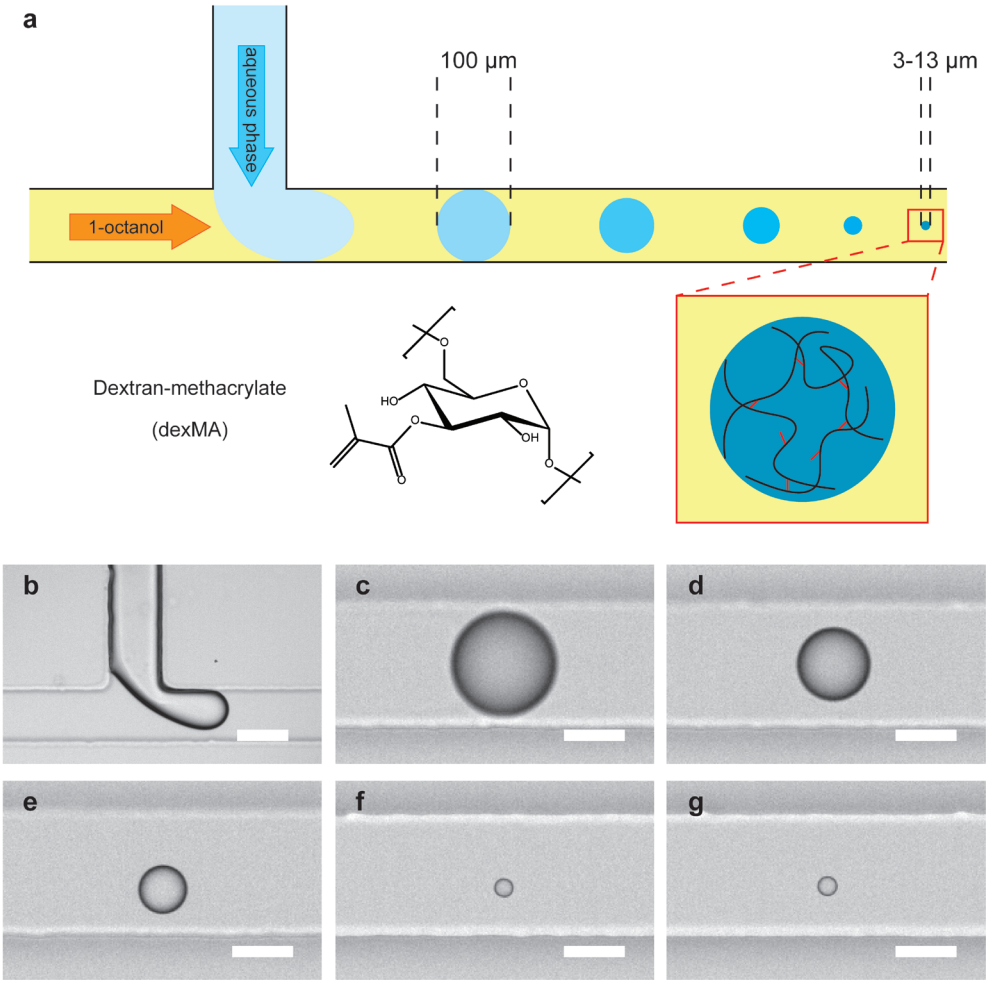

Figure 1. Schematic representation of the Droplet dehydration strategy for production of dextran particles (**a**). Bright-field micrographs of microfluidic droplet shrinking chip in operation: droplet formation at a T-junction (**b**), droplets at 7.5 cm (**c**), 17.5cm (**d**), 22.5 cm (**e**), 32.5 cm (**f**), 100 cm (**g**). Initial C_{dexMA} = 0.1%, $Q_{octanol}$ = 2.0 µl/min, $Q_{aqueous}$ = 0.02 µl/min, scale bars (b) 100 µm, (c-g) 50 µm.

dextran, a natural linear polysaccharide. Its insolubility in alcohols ensures the formation of solid particles, whereas ease of its chemical modification offers a variety of approaches for particle cross-linking.

Once the droplets of dilute aqueous dextran solution are produced within the flow of dry 1-octanol, they travel through the channels while water is slowly extracted out of the droplets and into the continuous phase (**Figure 1**). From thermodynamic point of view, extraction of water should stop once chemical potentials of all components in both phases reach equilibrium. In order to produce dextran micro-particles, we have deliberately chosen high volume ratio between octanol and water phases (Q_{oct} /Q_{aq} = 100/1), thus ensuring complete dissolution of aqueous droplets, resulting in the formation of dehydrated dextran microspheres. Even though in these conditions we expect water to be fully extracted out of aqueous droplets, certain negligible amount of it may remain bound by dextran. For simplicity, we refer to

dextran micro-spheres produced by our method as dry.

For reliable generation of the droplets and observation of their shrinking we have designed a T-junction microfluidic device with rectangular 100x100 μm channels and a total channel length of 140 cm. Microfluidic devices were fabricated out of PDMS as described previously[15], bonded to PDMS-coated glass slides (25×75 mm) with 125 μm inner diameter (ID) PEEK tubing inlets secured using epoxide-based adhesive. Simple T-junction geometry allowed us to easily generate "plug-like"/cylindrical droplets of 100×100×170 μm, which were then further monitored downstream. The large length of the device channel allowed us to explore a range of dehydration conditions and to observe the shrinking of generated droplets over the whole length of the device.

To characterize the dehydration process, we monitored the change of droplet size depending on the distance travelled within the chip with initial dextran concentrations ranging from 10^{-4} to 0.1% and compared the obtained profiles with shrinkage of droplets containing no dextran. As can be seen from the **Figure 2**, in all cases droplets shrank at nearly identical rates regardless of initial polymer content, indicating that the initial water extraction was unaffected by presence of dextran. However, while pure water droplets shrunk with a constant rate and eventually fully dissolved, polymer-containing droplets, as they approached their final size, displayed a deviation of the rate of diameter change from a linear trend. Droplets reached their final size within 70-80 seconds on-chip and remained unchanged for the rest of the length of the microfluidic device, indicating the formation of fully dried dextran particles. This observation is further supported by the fact that V_0/V_{final} for most of the studied dextran concentrations correlated well to the expected final particle size (**Figure 2b**), assuming that the density of produced micro-spheres remains fairly close to 1.2 g/ml as estimated for 50% w/w solutions of dextran[16].

The final size of produced particles decreased with decreasing the initial dextran concentration. In view of plug-like, nearly cylindrical shape of initial droplets, to simplify the comparison with the size of spherical particles formed at later shrinking stages, we treated them as spherical droplets of equal volume, translating to a diameter of ~137 μm. By varying dextran concentration from 10^{-4} to 0.5% we were able to produce particles ranging from 3.4 to 13.3 μm, thus achieving up to 60000-fold decrease in droplet volume. Initially,

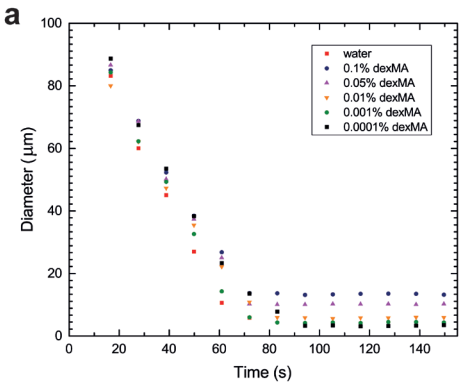

b

C_{dexMA}, %	Shrinking rate, μm/s	Final size, μm	V_0/V_{final}
0	1.6	-	-
0.0001	1.4	3.4	$64.8 \cdot 10^3$
0.001	1.5	4.4	$29.9 \cdot 10^3$
0.01	1.3	6	$11.8 \cdot 10^3$
0.05	1.4	10.3	$2.3 \cdot 10^3$
0.1	1.3	13.3	$1.1 \cdot 10^3$

Figure 2. (**a**) Shrinking rates for droplets with several initial dextran concentrations. (**b**) Summary of observed dehydration rates and minimal obtainable particle sizes at different initial dextran concentrations. All data was collected for Q_{oct} = 2.0 μl/min, Q_{aq} = 0.02 μl/min.

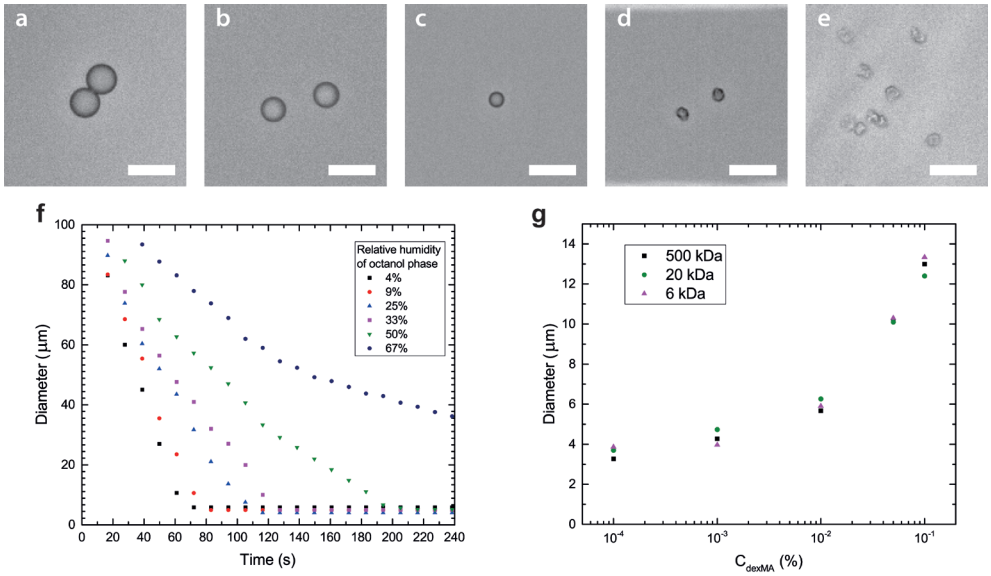

Figure 3. (**a-e**) Bright-field micrographs of particles (in octanol) produced from droplets with different initial dextran concentrations: (**a**) 0.1%, (**b**) 0.05%, (**c**) 0.01%, (**d**) 0.001% and (**e**) 0.0001%. Scale bars 20 µm. (**f**) Controlling the dehydration speed by adjusting the saturation of the continuous phase with water (C_{dexMA} = 0.01%). (**g**) Final droplet/particle size vs. the initial concentration of dextrans of different molecular weights. All data was collected for Q_{oct} = 2.0 µl/min, Q_{aq} = 0.02 µl/min.

for concentration range between 0.1% w/w and 0.01% w/w, for tenfold decrease of starting polymer concentration we observed approximately twofold decrease in particle diameter, which corresponds to the expected change of diameter of a sphere upon a tenfold change of its volume.

However, for dextran solutions below 0.01% w/w significantly smaller change in particle diameters was observed (**Figure 3a-e**). Upon closer examination we observed that the shape of particles produced from highly dilute dextran solutions has deviated from spherical and resembled that of deflated balloons, implying that particles possessed skin-like outer shell and a hollow core (**Figure 3d-e**). This morphology suggests that due to the fast extraction of water, diffusion of dissolved polymer was not fast enough to keep up with the shrinking of the droplet interface, thus leading to accumulation of the polymer at the interface. Polymer accumulation results in the formation of a solid polymeric crust before completion of the shrinking process, thus leading to production of buckled and crumpled hollow particles. Even though we have only observed serious particle deformation for particles produced from droplets with very low initial dextran concentrations, we suspect a similar effect to be present in the larger particles as well, but instead of crumpling resulting in a gentle density gradient within a spherical solid micro-particle. In other words, the severity of final particle deformation may be connected to the droplet diameter at which skin formation begins to take place, and to the speed at which droplet surface is decreasing.

In order to investigate achievable degree of control over droplet shrinking rate, we have followed the dehydration of aqueous droplets using octanol phases with different initial water content. To be able to adjust the humidity of octanol flow on-demand, we tuned the composition of octanol-phase by mixing flows of dry and water-saturated octanol in a desired

proportion. By simply adjusting the ratio of volumetric flowrates of these octanol flows before combining them on-chip we could tune the relative humidity of resulting octanol flow in the range from 4 to 96%. **Figure 2c** displays the dehydration profiles of aqueous droplets containing 0.01% dexMA recorded in a single device by online control of the water content of the continuous octanol phase. With the increase of the octanol flow humidity we observed a gradual decrease in the shrinking rate and eventual deviation from the initially observed linear trend (**Figure 3f**). Despite this decrease in the shrinking rate we could still observe droplets reaching the same final size values as in fully dry octanol, suggesting that slower droplet dehydration did not significantly affect the final particle composition. Moreover, based on water solubility and Q_{oct}/Q_{aq} ratio, water extraction should proceed to completion up to a relative octanol humidity of 75%, however, in a current design of the microfluidic device we could only observe formation of such small particles up to a relative octanol humidity of 50% due to the insufficient length of micro-channels. Overall, online control of humidity of the octanol flow grants access to a wide range of shrinking rates, thus allowing to adjust the experimental conditions as required.

Next, we investigated the influence of polymer diffusion coefficient on obtainable particle size and shape by dehydrating the droplets containing dextrans with molecular weights of 6, 20 and 500 kDa, thus varying the diffusion coefficient of dissolved polymers from ~70 $\mu m^2/s$ to ~9 $\mu m^2/s$ (**Figure 3g**). By doing so, we aimed to estimate the ratio of diffusive and evaporative transport rates in our dehydration process and thus better control the morphology of produced particles. However, upon varying the initial concentration of above-mentioned dextrans we have observed identical trends in final particle size for all three studied molecular weights. This finding indicates that the shrinking process in our method is so fast that even nearly eightfold increase in diffusive transport of dissolved dextran did not significantly affect the size and morphology of produced particles, resulting in crumpled hollow micro-spheres even for low molecular weight dextran. Nevertheless, we envision that a careful selection of initial dextran concentration and appropriate dehydration rate may enable additional way to control the morphology of generated particles.

To render produced particles stable for their subsequent transfer into aqueous environment, we have incorporated a photo-cross-linking step into the method. To this end we have employed previously described dextran-methacrylate (dexMA)[17] in combination with a water-soluble photoinitiator (Irgacure 2959) and on-chip UV curing. To maintain a sufficient concentration of the initiator in the aqueous droplet phase we introduced the initiator in excess into the continuous octanol phase. Since we determined the octanol/water partitioning coefficient of Irgacure 2959 to be 3.73:1, introducing it at concentration of 15 mg/ml into the octanol-phase ensured that due to the partitioning aqueous phase would contain ~4 mg/ml of initiator at all times during dehydration process. Droplets shrunken in these conditions, were then subjected to irradiation with UV light (300-400nm, peak intensity @365nm) using 110W mercury vapour light source. Irradiation has been performed at the position in the device where droplets would first reach their expected final size. After passing through the irradiation area droplets further travelled through the chip (~5 min) and after being collected off-chip, resulting suspension was subjected to 7 ethanol washing/centrifugation cycles to ensure the removal of residual photoinitiator and the octanol phase. In order to test the efficiency of cross-linking, 20 µl of particle suspension in ethanol was drop-casted onto a glass coverslip, and once ethanol has evaporated deionized water was introduced (**Figure 4**). The observed particles swelled from 13 µm in ethanol to ~16 µm in water, and showed no signs of dissolution even after 5 days of observation, indicating successful photo-polymerization.

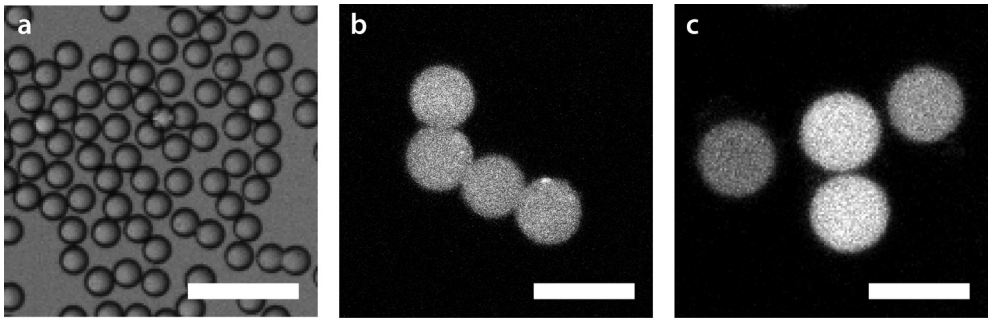

Figure 4. Cross-linked hydrogel particles produced from droplets with initial dexMA concentration of 0.1%: (**a**) bright-field micrograph of particles as collected in octanol; (**b**) CLSM micrograph of particles in octanol; (**c**) CLSM micrograph of cross-inked particles re-suspended in water (after 3 hours). Scale bars (a) 50 μm, (b-c) 20 μm.

The dehydration approach described in this work does not only provide one with the means to shrink and concentrate droplets, but also represents a method for precisely controlling the formation of multi-phase droplets/particles. To illustrate this possibility we have applied our approach to aqueous multi-phase systems (AMPS) – aqueous solutions of polymers that form distinct immiscible aqueous phases above certain polymer concentrations. Traditionally, to produce two- and three-phase droplets from AMPS using microfluidics, one would have to design the device geometry to precisely control the volume fractions of each of the aqueous phases. However, such approach while being efficient, still leads to a certain degree of variability of composition between multi-phase droplets due to the albeit small but ever-present size polydispersity of produced phase-forming droplets. Application of the droplet shrinkage approach to extremely dilute mixtures of phase-separating polymers offers a powerful alternative way of producing such droplets. Since generated droplets are initially homogeneous, they have identical composition and phase-separate into multiple compartments only further downstream as the polymer concentration increases due to the droplet dehydration. To demonstrate this potential application, we continuously generated two- and three-phase droplets formed by polyethylene glycol (PEG) –dextran and PEG – Ficoll – dextran AMPS (**Figure 5**).

In the first case, illustrated in **Figure 5(I)**, droplets produced from a homogeneous mixture of PEG and dextran (0.5%w/w of each polymer) were subjected to dehydration, leading to shrinkage and increase of polymer concentration, eventually resulting in phase-separation and formation of two-phase aqueous droplets. Dextran-phase was stained with dextran-FITC, which allowed us to establish its position as a core-phase of produced two-phase droplets using epifluorescence microscopy (not shown). Droplets displayed in **Figure 5 (I a-d)** were still in the liquid state, however, due to polymer concentration gradient induced by water extraction that was described above, we expect phases of these droplets to be out of thermodynamic equilibrium, unless the dehydration process is stopped. Further shrinkage of these two-phase droplets led to formation of solid particles with varying morphologies (not shown here), and this approach has to be further investigated and optimized for production of compartmentalized polymeric particles. Moreover, we believe that microfluidic shrinkage-induced phase-separation can be optimized to use for construction of accurate phase-diagrams for ATPS formed by expensive polymers since it allows using extremely low quantities of materials. However, it is worth noting that the droplet structures observed here are out of equilibrium, and thus data derived from their observation cannot be directly used for estimating any AMPS phase-equilibrium parameters.

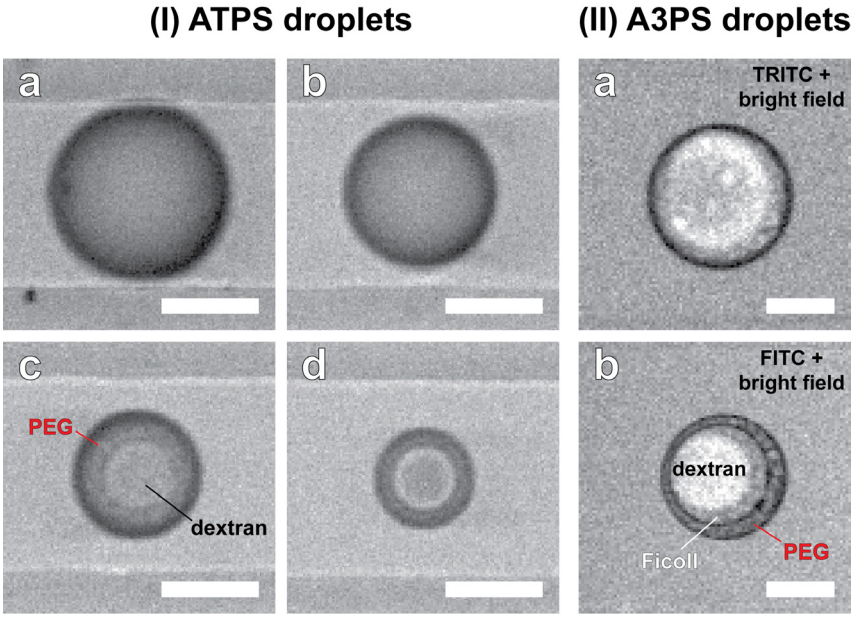

Figure 5. Bright-field micrographs of multi-phase droplets prepared by microfluidic dehydration of dilute aqueous two- and three-phase systems. (**I**) Different stages of dehydration of droplets containing PEG (10kDa) and dextran (500kDa) at 1/1 weight ratio illustrated by micrographs at 50 (**I a**), 100 (**I b**), 110 (**I c**) and 160 mm (**I d**) within the microfluidic device. Scale bars 50 μm. (**II**) Composite bright-field and wide-field fluorescence micrographs of phase-separated droplets containing PEG (10kDa), Ficoll 400 and dextran (500kDa) with Ficoll and dextran phases respectively labelled with TRITC and FITC fluorescent dyes: (**II a**) Ficoll-TRITC channel, (**II b**) dextran-FITC channel. Scale bars 25 μm.

Similarly, three-phase aqueous droplets were produced from a homogeneous mixture of PEG, dextran and Ficoll (0.5% w/w of each polymer) which phase-separated upon shrinkage. To determine the location of corresponding polymer-rich phases we stained them with fluorescently labelled dextran-FITC and Ficoll-TRITC as illustrated in **Figure 4 (II)**. Positioning of the phases gives an insight into the balance of interfacial tensions in the system, indicating that the PEG-rich phase is most hydrophobic and thus has most favourable interaction with the outer octanol phase. Interestingly, Ficoll-phase in a three-phase system displays intermediate behaviour and is situated between PEG outer shell and dextran-rich core. Potentially, engineering the composition of initial droplets in this droplet shrinking approach could allow exploiting aqueous polymer phase-separation for designing compartmentalized microparticles with identical content and thus extremely similar architectures. Greater flexibility in choosing volume ratio of the compartments compared to conventional multi-phase droplet production strategies makes further exploration of this approach highly interesting.

The scope of the droplet shrinking approach described here could potentially be widened even further, with an outlook of production of sub-micron polymeric particles using regular microfluidic devices. In order to investigate this avenue we have designed a flow-focusing microfluidic chip for production of smaller initial droplets. In this geometry, channel dimensions were 100x100 μm with ~70 cm total length and the nozzle of 25×6 μm, allowing continuously and consistently generating aqueous droplets of 35-45 μm in diameter at ~25Hz

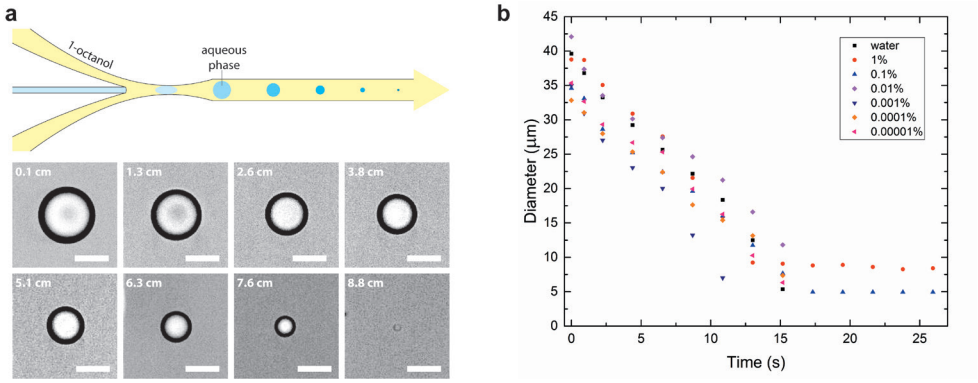

Figure 6. (**a**) Schematics of the alternative design of the dehydration microfluidic device and series of experimental micrographs illustrating the shrinking of 0.01% dexMA solution droplet as it travels through the chip. (**b**) Dependence of droplet diameter on time spent on-chip for various initial dexMA concentrations. $Q_{octanol}$ = 2.0 µl/min, $Q_{aqueous}$ = 30 nl/min. Scalebars 25 µm.

within octanol flow. **Figure 6** summarizes the dehydration profiles of droplets containing varying initial dextran concentrations, which correlated well to the trends observed for larger droplets. Similarly as in the above-described experiments in a larger microfluidic device, droplets reached a stable final size, even though it could only be accurately measured with light microscopy for dextran concentrations of 1 and 0.1%, being 7.0 and 3.6 µm respectively. Also with these experiments, the measured final sizes corresponded well to the estimated diameter of dry dextran micro-spheres, e.g. for 1% dextran droplets, estimated final particle density of ~1.2 g/ml and measured volumetric shrinking ratio of 125, final particles are expected to be water-free. Importantly, the produced particles appeared to have a spherical shape without any visible signs of crumpling or collapsing, however the effect observed for larger particles may still be present here for particles produced with higher shrinking ratios, thus requiring additional investigation. To test this hypothesis, we have attempted characterize the size and morphology of produced particles using scanning electron microscopy (SEM). Unfortunately, it was only possible to visualize the largest particles (d = 7 µm), while smaller particles appeared to be destroyed during repeated steps of washing/centrifugation necessary to remove the octanol-phase in which they were dispersed after formation. Therefore, the procedure of particle isolation and purification needs be further optimized. Nevertheless, these experiments highlight the potential of our technique to produce micron-sized particles of several diameters while using a single device. Our future work will focus on further development of the described method with a goal of producing structured sub-micron particles.

Conclusions and outlook

In conclusion, we have developed a microfluidic approach for generation and controlled shrinking of aqueous droplets by extracting the water into a partially miscible continuous octanol phase. Our method allows controlling the size of polymeric microparticles produced in a single device by simply adjusting initial polymer concentration within original droplets. Additionally, by tuning the relative humidity of the octanol phase we could adjust the shrinking rate of the droplets on-demand, which represents an additional degree of control over particle production process. Moreover, by using dilute solutions of phase-separating polymers, we could generate and observe multi-phase all-aqueous droplets, which can be

potentially applied for producing compartmentalized or non-spherical micro-hydrogels. Finally, droplet shrinking approach may also be employed for microfluidic production of sub-micron particles, or even exploited to trigger chemical or enzymatic reactions sensitive to concentration change.

Despite the progress we have recently made in applying the concept of droplet shrinking to several analytical and formulation challenges, this area of research remains largely unexplored. Advances in design of dehydration system we describe in this chapter give better understanding of the processes but also point out the challenges associated with applying this technique to particle production, which could not be addressed during this PhD project due to the limited time.

First of all, alternative methods of polymer cross-linking should be investigated, since direct photo-initiation is seriously affected by partitioning of the initiator and can be ineffective for quickly moving particles, thus requiring even higher initiator concentrations. Such situation, in its turn, may lead to accumulation of initiator degradation by-products inside the devices resulting in their clogging. One potentially suitable alternative method to consider, would be exploiting the shrinking to start the cross-linking, for instance, by employing a chemical/enzymatic reaction that can be drastically sped up by increase in reagents' concentration, or employing polymers that would physically cross-link upon reaching certain concentration.

Additionally, influence of dehydration speed and flow velocities on obtained particle morphology should be further investigated, as well as particle collection and octanol removal procedures need to be further optimized. Due to relatively low number of produced particles washing/centrifugation procedures used in this work may have led to substantial losses of material. To maximize the recovery of generated microgels, ultrafiltration techniques with compatible membranes may be used. Such approach would also minimize the potential mechanical damage of the particles because of lower required centrifugation speeds.

Materials and methods

Materials

All reagents were used as received. Dextran-FITC (500 kDa), 1-octanol (ACS reagent), water (ACS reagent, for ultratrace analysis), glycidyl methacrylate, 4-dimethylaminopyridine (DMAP), and 2-hydroxy-4'-(2-hydroxyethoxy)-2-methyl-propiophenone (Irgacure® 2959) were purchased from Sigma-Aldrich (Steinheim, Germany). Dextrans (MW = 6, 20, 500 kDa) were purchased from Alfa-Aesar (Karlsruhe, Germany).

Preparation of cross-linkable dextran

Methacrylate modified dextran was prepared according to previously described procedure.17 In short, 10 g of dextran, 1 mg of dextran-FITC and 2 g DMAP were dissolved in 100 mL DMSO, followed by addition of glycidyl methacrylate. After stirring at 30°C for 24 hours, pH of the mixture was adjusted to 7 by the addition of a 1M HCl solution and diluted with 100 mL of water. Subsequently, the reaction mixture was extensively dialyzed against demineralized water at 5°C over a period of 10 days after which it was freeze-dried yielding Dex-MA as white flakes. Degree of substitution (DS) was determined to be 10% using ^{1}H-NMR.

Chip fabrication

The devices were fabricated by replica molding in PDMS (Dow Corning, Sylgard 184 elastomer kit) using SU-8 patterned silicon wafer as a master mold following previously

described procedure.15 Channels were sealed by bonding such PDMS replicas to PDMS-coated microscopy glass slides (25×75 mm). To ensure the hydrophobic recovery of PDMS surfaces, bonded devices were further heated to 70°C for 12 hours and stored at room temperature.

Setup

All microfluidic experiments were performed on an Axio Observer A1 inverted microscope (Zeiss) and imaged using a Zyla 5.5 sCMOS camera (Andor) at 100 fps. The microscope was equipped with an EC-Plan Neofluar objective (20×, 0.5 NA) and Mercury-arc light source (HXP 120V, 120 W), which was used with a band pass filter 300-400 nm (peak intensity at 365 nm, Zeiss, filter set 02) to initiate the cross-linking of the droplets.

Preparation of fluids

Dry octanol was prepared by the addition of activated 3.5 Å molecular sieves to commercially obtained octanol. Water-saturated octanol was prepared by equilibrating octanol with water for 1 day, and separating the top phase with a syringe. Intermediate degrees of octanol saturation with water were achieved by simply mixing dry and wet octanol stock in desired proportions. Dextran was dissolved in ultrapure water to result in 1% stock solution. All other concentrations were achieved by diluting 1% stock solution with water. In order to cross-link dexMA particles octanol phase was saturated with Irgacure 2959.

All solutions were filtered through 0.45 μm PTFE syringe filters (Sartorius, MicroSart) prior to injection into the chip using 50 and 500 μl glass syringes (Hamilton, Gastight 1700) and individual syringe pumps (Harvard Apparatus, 11 PicoPlus).

Microfluidic experiments

All flowrates were initially set to relatively high values (2-3 μl/min) in order to flush out air from the channels, and afterwards adjusted to normal operating values ($Q_{octanol}$ = 2 μl/min, $Q_{aqueous}$ = 0.02 μl/min) and flows were stabilized for approximately 30 minutes before the start data collection. In case of online control of octanol humidity, two separate flows of dry and wet octanol were combined into a single flow using a T-shaped connector prior to injection on the chip, while keeping total octanol phase flowrate constant.

Particle isolation and characterization

Particle dispersions in octanol were collected into 1.5 ml Eppendorf tubes. To characterize the final size of the particles aliquots of such dispersions were sandwiched between glass coverslips No. 1.5 (170 μm) and imaged using inverted microscope in brigh-field and fluorescence modes.

References

(1) Baah, D.; Floyd-Smith, T. Microfluidics for Particle Synthesis from Photocrosslinkable Materials. *Microfluid. Nanofluidics* **2014**, *17* (3), 431–455.

(2) Kawaguchi, H. Micro Hydrogels: Preparation, Properties, and Applications. *J. Oleo Sci.* **2013**, *62* (11), 865–871.

(3) Dressler, O. J.; Maceiczyk, R. M.; Chang, S.-I.; deMello, A. J. Droplet-Based Microfluidics. *J.*

Biomol. Screen. **2014**, *19* (4), 483–496.

(4) Bajpayee, A.; Edd, J. F.; Chang, A.; Toner, M. Concentration of Glycerol in Aqueous Microdroplets by Selective Removal of Water. *Anal. Chem.* **2010**, *82* (4), 1288–1291.

(5) Ji, J.; Nie, L.; Li, Y.; Yang, P.; Liu, B. Simultaneous Online Enrichment and Identification of Trace Species Based on Microfluidic Droplets. *Anal. Chem.* **2013**, *85* (20), 9617–9622.

(6) Fukuyama, M.; Hibara, A. Microfluidic Selective Concentration of Microdroplet Contents by Spontaneous Emulsification. *Anal. Chem.* **2015**, *87* (7), 3562–3565.

(7) Wu, T.; Hirata, K.; Suzuki, H.; Xiang, R.; Tang, Z.; Yomo, T. Shrunk to Femtolitre: Tuning High-Throughput Monodisperse Water-in-Oil Droplet Arrays for Ultra-Small Micro-Reactors. *Appl. Phys. Lett.* **2012**, *101* (7), 74108.

(8) He, M.; Sun, C.; Chiu, D. T.; Mingyan He; Chenhang Sun, A.; Chiu*, D. T. Concentrating Solutes and Nanoparticles within Individual Aqueous Microdroplets. *Anal. Chem.* **2004**, *76* (5), 1222–1227.

(9) Kojima, T.; Takayama, S. Microscale Determination of Aqueous Two Phase System Binodals by Droplet Dehydration in Oil. *Anal. Chem.* **2013**, *85* (10), 5213–5218.

(10) He, Y.; Battat, S.; Fan, J.; Abbaspourrad, A.; Weitz, D. A. Preparation of Microparticles through Co-Flowing of Partially Miscible Liquids. *Chem. Eng. J.* **2017**, *320*, 144–150.

(11) Ono, T.; Yamada, M.; Suzuki, Y.; Taniguchi, T.; Seki, M.; Mou, C. L.; Weitz, D. A.; Chu, L. Y.; Gitlin, I.; Whitesides, G. M.; et al. One-Step Synthesis of Spherical/nonspherical Polymeric Microparticles Using Non-Equilibrium Microfluidic Droplets. *RSC Adv.* **2014**, *4* (26), 13557.

(12) Jeong, J.; Um, E.; Park, J.-K.; Kim, M. W.; Du, J.; O'Reilly, R. K.; Yang, S. M.; Guo, F.; Kiraly, B.; Mao, X.; et al. One-Step Preparation of Magnetic Janus Particles Using Controlled Phase Separation of Polymer Blends and Nanoparticles. *RSC Adv.* **2013**, *3* (29), 11801.

(13) Sugaya, S.; Yamada, M.; Hori, A.; Seki, M. Microfluidic Production of Single Micrometer-Sized Hydrogel Beads Utilizing Droplet Dissolution in a Polar Solvent. *Biomicrofluidics* **2013**, *7* (5), 54120.

(14) Pittermannová, A.; Ruberová, Z.; Zadražil, A.; Bremond, N.; Bibette, J.; Štěpánek, F. Microfluidic Fabrication of Composite Hydrogel Microparticles in the Size Range of Blood Cells. *RSC Adv.* **2016**, *6* (105), 103532–103540.

(15) McDonald, J. C.; Duffy, D. C.; Anderson, J. R.; Chiu, D. T.; Wu, H.; Schueller, O. J. A.; Whitesides, G. M. Fabrication of Microfluidic Systems in Poly(dimethylsiloxane). *Electrophoresis* **2000**, *21* (1), 27–40.

(16) Totlani, K. A. Microfluidic Synthesis of All Aqueous Core Shell Particles for Drug Delivery Applications, Delft University of Technology, MSc thesis, 2015.

(17) van Dijk-Wolthuis, W. N. E.; Franssen, O.; Talsma, H.; van Steenbergen, M. J.; Kettenes-van den Bosch, J. J.; Hennink, W. E. Synthesis, Characterization, and Polymerization of Glycidyl Methacrylate Derivatized Dextran. *Macromolecules* **1995**, *28* (18), 6317–6322.

Summary

Growing importance of hydrogels in various areas of human life has led to increasing need in controlling their properties, which is generally achieved by adjusting hydrogels shape and microstructure. Even though standard microfabrication and microstructuring techniques can be currently applied in hydrogel research, the variety of properties of hydrogel materials makes it difficult to employ any of these techniques universally. Furthermore, to produce hydrogel structures complex enough to mimic biological tissues, several structuring and microfabrication approaches on various length scales would need to be combined. The complexity and diversity of problems associated with such processes raises a whole set of multidisciplinary challenges. This doctoral dissertation explores novel approaches to structuring and fabrication of polymeric and supramolecular hydrogels by combining modern microfabrication techniques with molecular self-assembly and/or exploiting mutual incompatibility of certain hydrophilic polymers.

Chapter 1 introduces the main types and properties of hydrogels followed by a brief review of the literature on their microfabrication and structuring. Additionally, chapter 1 summarizes the challenges of existing techniques and outlines the goals of this doctoral project.

Chapter 2 describes a method for continuous microfluidic production of hydrogel capsules with a hydrogel shell and a liquid core from an all-aqueous double emulsion. While most previous work on water-in-water emulsions focused on active droplet formation, here double emulsion droplets were spontaneously generated at a three-dimensional flow-focusing junction through the break-up of a double jet formed by immiscible aqueous solutions of polyethylene glycol and cross-linkable dextrans. The capsules obtained with this method displayed excellent stability in a variety of harsh conditions, as well as good permeability to polar solutes.

Chapter 3 presents a general method for compartmentalizing supramolecular hydrogels with water-in-water emulsions. By forming the low-molecular-weight hydrogel throughout all phases of all-aqueous emulsions, we created distinct, micro-compartmentalized materials. This structuring approach offers control over the composition of each type of the compartments by directing the partitioning of objects to be encapsulated. Moreover, our method allows for barrier-less, dynamic exchange of even large hydrophilic solutes between separate aqueous compartments.

In chapter 4, we report a flexible method for direct fabrication of hydrogel objects by controlling illumination of confocal laser-scanning microscope. We were able to semi-automatically produce large arrays of identical microscopic hydrogel objects without the need of employing pre-designed photomasks. To further illustrate the versatility of the approach, we applied this technique to single-cell isolation. We selectively captured the cells of interest by encasing them into a polymeric hydrogel, removed the unwanted cells and subsequently released of isolated cells by enzymatic hydrogel degradation. Isolated cells displayed excellent viability thus offering an opportunity for their further analysis or cultivation.

Chapter 5 deals with the development of a microfluidic platform for shrinking of aqueous

droplets applied to production of polymeric micro-particles. Continuous on-chip shrinking was achieved by controlled extraction of water into the surrounding immiscible 1-octanol phase. Adjusting the initial polymer concentration within the droplet phase allowed us to produce particles of a controlled range of sizes within a single microfluidic device. Additionally, the method developed here represents a way to produce identical multi-phase aqueous droplets, which can be further exploited for structuring and compartmentalization of hydrogel particles.

In conclusion, this doctoral dissertation presents several novel methods for hydrogel structuring and fabrication, that were developed by combining modern microfabrication techniques and/or molecular self-assembly. Due to the importance of controlling properties of hydrogels by adjusting their size, shape and structure, we envision the content of this dissertation to make an impact on future design of biomedically relevant hydrogel-based materials.

Sammenvatting

Het toenemende belang van hydrogels in verscheidene gebieden van het menselijk leven heeft geleid tot een toenemende behoefde in het controleren van hun eigenschappen, wat in het algemeen bereikt wordt door de vorm en microstructuur van de hydrogel aan te passen. Hoewel standaard microfabricatie- en microstructuurtechnieken tegenwoordig toegepast kunnen worden in hydrogelonderzoek, maakt de verscheidenheid van hydrogelmaterialen het moeilijk om één van deze technieken universeel te gebruiken. Bovendien, om hydrogelstructuren complex genoeg te produceren dat biologische weefsels nagebootst kunnen worden, moeten verschillende structurerings- en microfabricatiebenaderingen op allerlei lengteschalen worden gecombineerd. De complexiteit en verscheidenheid van problemen behorend tot zulke processen wekt een hele set van multidisciplinaire uitdagingen op. Dit proefschrift onderzoekt nieuwe benaderingen om polymeergebaseerde en supramoleculaire hydrogels te structureren en fabriceren door moderne microfabricatietechnieken te combineren met moleculaire zelfassemblage en/of het verkennen van wederzijdse incompatibiliteit van bepaalde hydrofiele polymeren.

Hoofdstuk 1 introduceert de voornaamste soorten en eigenschappen van hydrogels gevolgd door een kort overzicht van de literatuur over hun microfabricatie en structurering. Verder vat hoofdstuk 1 de uitdagingen van de bestaande technieken samen en zet het de doelen van dit promotieonderzoek uit.

Hoofdstuk 2 beschrijft een methode voor continue microfluïdische productie van hydrogelcapsules, met een schil van hydrogel en een vloeibare kern, van een geheel waterige dubbele emulsie. Hoewel de meeste van de vorige onderzoeken over water-in-wateremulsies gefocust zijn op actieve druppelvorming, werden hier dubbele emulsiedruppels spontaan gegenereerd op het driedimensionale stroomgefocuste knooppunt door de breking van een dubbele straal gevormd door onmengbare waterige oplossingen van polyethyleenglycol en crosslinkbare dexranen. De capsules gevormd door deze methode laten uitstekende stabiliteit zien in verscheidene zware omstandigheden, evenals een goede permeabiliteit tot polaire opgeloste stoffen.

Hoofdstuk 3 presenteert een algemene methode voor het compartmentaliseren van supramoleculaire hydrogels met water-in-wateremulsies. Door het vormen van een laag-moleculair-gewichthydrogel door alle fases van geheel waterige emulsies, hebben we onderscheidende microgecompartmentaliseerde materialen gemaakt. Deze structureringsbenadering geeft controle over de compositie van elk soort gedeelte door het leiden van de verdeling van objecten die moeten worden ingekapseld. Bovendien staat onze methode ook barrièreloze, dynamische uitwisseling toe tussen grote hydrofiele opgeloste stoffen tussen verschillende waterige gedeeltes.

In hoofdstuk 4 rapporteren we een flexibele methode voor het direct fabriceren van hydrogelobjecten door het licht van de confocale-laser-scan-microscoop te controleren. We zijn in staat om grote reeksen identieke microscopische hydrogelobjecten halfautomatisch te produceren zonder dat we een vooraf ontworpen fotomasker nodig hebben. Om verder de

veelzijdigheid van de methode te laten zien, hebben we deze techniek toegepast op de isolatie van afzonderlijke cellen. We vingen selectief interessante cellen door ze in te kapselen met een polymeerhydrogel, verwijderden de ongewenste cellen en lieten vervolgens de geïsoleerde cellen vrij door enzymatische hydrogeldegradatie. Geïsoleerde cellen lieten uitstekende levensvatbaarheid zien, dus geven een mogelijkheid voor hun verdere analyse of teelt.

Hoofdstuk 5 behandelt de ontwikkeling van een microfluïdisch platform voor het krimpen van waterige druppels toegepast op de productie van polymeermicrodeeltjes. Onafgebroken krimpen op een chip was bereikt door de extractie van water in de nabijgelegen onmengbare 1-octanolfase te controleren. Door het aanpassen van de initiële polymeerconcentratie in de druppelfase kunnen we deeltjes produceren met een gecontroleerde groottedistributie in één enkel microfluïdica apparaat. Bovendien geeft deze ontwikkelde methode een manier om identieke multifase waterige druppels te produceren, die verder uitgebuit kunnen worden voor structurering en compartmentalisatie van hydrogeldeeltjes.

Ter conclusie, dit proefschrift presenteert verscheidene nieuwe methodes voor het structureren en fabriceren van hydrogels, die zijn ontwikkeld door moderne microfabricatietechnieken en moleculaire zelfassemblage te combineren. Door het belang van het controleren van de hydrogeleigenschappen door het aanpassen van hun grootte, vorm en structuur, stellen we ons voor dat de inhoud van dit proefschrift een impact heeft op toekomstig ontwerp van biomedische relevante hydrogelgebaseerde materialen.

About the author

Serhii Mytnyk

born on 17 September 1989 in Cherkasy, Ukraine

2006-2010	B.Sc. in Organic Chemistry, with Honors *Taras Shevchenko National University of Kyiv, Ukraine*
2010-2012	M.Sc. in Organic Chemistry, with Honors *Taras Shevchenko National University of Kyiv, Ukraine*
2012	M.Sc. research project *Laboratory of Coordination Chemistry, CNRS, Toulouse, France*
2012-2013	Synthetic chemist *Spectrum Info Ltd., Kyiv, Ukraine*
2013-2019	PhD in Chemical Engineering *Delft University of Technology, Delft, the Netherlands*
2017-2019	Postdoctoral researcher *Delft University of Technology, Delft, the Netherlands*

List of publications

1. Q. Liu, M. Zhao, S. Mytnyk, B. Klemm, K. Zhang, D. Yan, E. Mendes, J. van Esch, *Angew. Chem. Int. Ed.*, **2018**, *In press*.

2. K. Zhang, A. Aranja, H. Chen, S. Mytnyk, Y. Wang, S. Oldenhof, J. van Esch, E. Mendes, *RSC Adv.*, **2018**, *8*, 21777-21785.

3. M. De Puit, J. van Esch, S. Oldenhof, S. Mytnyk, Hydrogel micro-patterning for embedding purposes, *WO2018097715*, **2018**.

4. S. Mytnyk, A. Olive, F. Versluis, J. Poolman, E. Mendes, R. Eelkema, J. van Esch, *Angew. Chem. Int. Ed.*, **2017**, *56*, 14923.

5. M. Lovrak, W. Hendriksen, C. Maity, S. Mytnyk, V. van Steijn, R. Eelkema, J. van Esch, *Nat. Commun.*, **2017**, *8*, 15317.

6. W. Noteborn, D. Zwagerman, V. Saez-Talens, C. Maity, L. van der Mee, J. Poolman, S. Mytnyk, J. van Esch, A. Kros, R. Eelkema, R. Kieltyka, *Adv. Mater.*, **2017**, *29*, 1603769.

7. S. Mytnyk, I. Ziemecka, A. Olive, J.W. van der Meer, K. Totlani, S. Oldenhof, M. Kreutzer, V. van Steijn, J. van Esch, *RSC Adv.*, **2017**, *7*, 11331-11337.

8. F. Versluis, D. van Elsland, S. Mytnyk, D. Perrier, F. Trausel, J. Poolman, C. Maity, V. le Sage, S. van Kasteren, J. van Esch, R. Eelkema, *J. Am. Chem. Soc.*, **2016**, *138*, 8670-8673.

9. A. Mityuk, S. Kolodych, S. Mytnyk, Yu. Dmytriv, D. Volochnyuk, P. Mykhailiuk, A. Tolmachev, *Synthesis*, **2010**, *16*, 2767-2770.

Acknowledgements

Navigating through an open-ended doctoral project can sometimes be as hard as exploring an unknown planet in a galaxy far-far away. Of course, neither of the endeavors would have ever led to a happy ending if not for support and help from all the people involved in both expeditions. As my journey through an exciting and daunting world of aqueous multi-phase systems has come to an end, I would like to express my gratitude to everyone who helped me on my way to obtaining my PhD degree.

Jan, I am extermely grateful for the opportunity to be a part of a multi-disciplinary SMARTNET project, and even though it took me somewhat longer than planned, I enjoyed it most of the way. Thank you for all your guidance and advice.

Eduardo, your optimistic view of the world together with your passion in polymer physics made a lot of our meetings very fun. And even though I did not pursue polymer physics path during my PhD, our discussions have made an impact on the way I see ATPS and science in general.

Volkert, I thank you for introducing me into the wonderful world of microfluidics and for being my unofficial PhD co-supervisor. Your always-positive attitude and attention to smallest details have inspired me to try deciphering the mysteries of all-aqueous microfluidics. Moreover, thank you for the great opportunity to participate in a challenging applied postdoctoral project while working on the last stage of my thesis.

Ger, working with you has taught me a lot about physical chemistry and how creative approach to viewing a complex problem can completely change the way to solving it. Thanks for organizing those wonderful winter schools in Han-sur-Lesse and good luck in your future projects!

Stephen, thanks for all the polymer-related advice and lots of success with your future science-meets-art projects.

Rienk, even though we have not worked much together directly, I will remember our lunch dicsussions about things ranging from supramolecular chemistry to European politics.

Also, I would like to thank my thesis committee for taking the time to evaluate it and participate in the defense ceremony.

Similarly to how no exploratory expedition can be successful without a team of skilled engineers, my PhD could not have been completed without the help from ASM support staff. *Lars*, I appreciate a lot your role in day-to-day operation of the synthesis lab and especially your help in setting up the GPC set-up. Also, thanks for all the fun we had while editing those PhD movies together! *Marcel*, thanks for all of your advice on how to deal with all kinds of equipment and for all the fun chemistry and travelling related stories. Good luck with your chemistry show! *Ben*, if not for your knowledge on how and where to perform a specific measurement, I think half of ASM PhD's would have taken at least another extra year before graduating. Thanks a lot! Louw, thank you for keeping the labs running and for arranging such great ASM labs in the new building. *Duco*, thanks for all the SEM measurements and for the philosophical discussions during the lunchtime. *Veby*, thanks for all your help with arranging the meetings and dealing with the numerous forms.

Furthermore, I would like to acknowledge people who I have been lucky to work with during my time at TU Delft.

Matija, I am happy to have worked and partied with you. I still have no idea how you can be incredibly organized in one sense and extremely chaotic in another, but it is simply a part of your charm! All of our shared fun moments at the conferences, SMARTNET meetings and numerous parties have made my PhD a lot more enjoyable. Thanks!

Tomasz, we have found a lot in common and I enjoyed all of our coffee breaks and board game nights at your place. Your insatiable drive for new hobbies has turned out to be contagious within the group, and even I tried a few myself. Keep it up and best of luck to you in your future career!

Roman, we had a lot of great times whether partying with Matija and Alex, or having our usual coffee breaks in the old building. Hope you'll stay as cheerful and as positive!

Alex, thanks for being my day-to-day mentor in the beginning of my PhD. Without your guidance in matters of confocal microscopy and of how the department works, I wouldn't have gone this far. And of course thanks for all the great evenings we had over a couple of beers at 't Klooster!

Sander, your innovative ideas and commercial talent have inspired me to work smarter, not harder. I wish you great success at NFI!

Dainius, thanks for all the advice about reality of PhD life at the end of your project. I learned a lot from you and I hope you are enjoying your new career path.

Wouter, thanks for your guidance and advice both scientific and regarding practicalities in the lab.

Simge, I will always remember the atmosphere you created in the old ASM lab and I am grateful for all your advice on a variety of synthetic procedures. And for those epic music battles you used to have with Jos :)

Elena, your energy have brightened the lab during day and your flan have made so many of our coffee breaks soooo much better.

Emma, thanks for your openness and positivity. Good luck with finishing your thesis and lots of patience with even more challenging task of bringing up your beautiful girls.

Jos, your jokes, both appropriate ones and not-so-much, have been a huge part of why I enjoyed working in ASM.

Cansel, I hope that even despite those never-ending column chromatographies you will manage to stay as bright and positive as always.

Frank, I will remember our chess battles and all of your advice on writing.

Fanny, always cheerful and curious. Stay that way and enjoy what you do!

Susan, your seriousness and patience will help you to achieve whatever you desire.

Vasu, such a talented singer in a chemistry lab. Your positivity is contagious!

Vincent, hot chocolate + spectra processing + hearthstone streams = awesome office times ;) Good luck with your car racing!

Kai, those occasional Friday drinks that you joined in the old building have been quite fun. Success in your future career!

Qian, I wish you to get those articles you need to go back to a lot warmer climate very-very soon :)

Benjamin and Tobias, thanks for organizing so many ASM dinners! *Benjamin*, I enjoyed our discussions, confocal-related and otherwise. Good luck with all your entrepreneurial ideas!

Chandan, *Karolis*, *Piotr* and *Saida*, it was a pleasure working with you, all the best!

Yiming, *Bowen*, *Fan* and *Michelle*, it was nice meeting you. I wish you success in your research!

To my SMARTNET colleagues, *Ana Catarina*, *Inês*, *Iván*, *Jorge*, *Kars*, *Laura*, *Marco*, *Maria*, *Nishant*, *Philip* and *Vânia*, I will really miss our joint meetings and parties that followed, since they were some of the best times I have had during my PhD.

Additionally, I would like to acknowledge my new colleagues from PPE group.

Kartik, you were one of my first MSc students and now you are finishing your PhD. Time flies, but persevere and you will make it!

Dayinta, thanks for sharing your experiences while going through the same troubles I had: doing a postdoc and PhD at the same time. Have fun at your new job!

Maulik, thanks for being a great office mate. I hope you will finish your PhD in time.

Shaurya, as the most senior PhD of PPE you are now responsible for the others, so keep it up! ;)

Dominik, sometimes our lunch discussion went way too far off track, but they were always fun. Good luck with your Ultimate Frisbee!

Erik, *Aswin*, *Afshin* and *Hamid* it was a pleasure working with you, and I wish you all the best.

Наостанок, я хочу подякувати моїм мамі та брату за їхню віру в мене. Та найважливіше, я би не зміг здолати всіх труднощів PhD без моєї коханої дружини, яка завжди була поруч. Щиро дякую тобі за твою турботу та підтримку, моє сонце!